Antenna Design for Ultra Wideband Radio

by

Johnna Powell

B.S., Electrical Engineering
New Mexico State University, 2001

SUBMITTED TO THE DEPARTMENT OF ELECTRICAL ENGINEERING IN PARTIAL FULFILLMENT OF THE REQUIREMENTS FOR THE DEGREE OF

MASTER OF SCIENCE IN ELECTRICAL ENGINEERING

AT THE

MASSACHUSETTS INSTITUTE OF TECHNOLOGY

May 7, 2004

Signature of Author . . . . . .
Department of Electrical Engineering and Computer Science
May 7, 2001

Certified by . . . . . .
Anantha P. Chandrakasan
Professor of Electrical Engineering and Computer Science
Thesis Supervisor

Accepted by . . . . . .
Arthur C. Smith
Chairman, Department Committee on Graduate Students

Antenna Design for Ultra Wideband Radio

by

Johnna Powell

Submitted to the Department of Electrical Engineering
on May 7, 2004 in Partial Fulfillment of the
Requirements for the Degree of
Master of Science in Electrical Engineering

ABSTRACT

The recent allocation of the 3.1-10.6 GHz spectrum by the Federal Communications Commission (FCC) for Ultra Wideband (UWB) radio applications has presented a myriad of exciting opportunities and challenges for design in the communications arena, including antenna design. Ultra Wideband Radio requires operating bandwidths up to greater than 100% of the center frequency. Successful transmission and reception of an Ultra Wideband pulse that occupies the entire 3.1-10.6 GHz spectrum require an antenna that has linear phase, low dispersion and VSWR ≤ 2 throughout the entire band. Linear phase and low dispersion ensure low values of group delay, which is imperative for transmitting and receiving a pulse with minimal distortion. VSWR ≤ 2 is required for proper impedance matching throughout the band, ensuring at least 90% total power radiation. Compatibility with an integrated circuit also requires an unobtrusive, electrically small design. The focus of this thesis is to develop an antenna for the UWB 3.1-10.6 GHz band that achieves a physically compact, planar profile, sufficient impedance bandwidth, high radiation pattern and near omnidirectional radiation pattern.

Thesis Supervisor: Anantha P. Chandrakasan
Title: Professor of Electrical Engineering

ACKNOWLEDGEMENTS

First and foremost, I would like to thank my advisor, Anantha Chandrakasan, for the opportunity to work on this project, and also for his support and confidence in my work. His patience and encouragement were invaluable to me throughout the course of this research. He pushed me to perform to the best of my abilities and gave me opportunities and exposure I never would have had if I had not joined his group. For that, I am extremely grateful. I would also like to thank the entire UWB group including Raul Blazquez, Fred Lee, David Wentzloff, Brian Ginsburg, and former student Puneet Newaskar, for their questions, suggestions, help and support. Especially I would like to thank Raul and Fred for their many suggestions and much warranted help. Fred initially proposed the need for a differential antenna, which made my investigation much more interesting. Raul was always helpful, no matter when asked. His kind and caring qualities were much appreciated.

In addition, I would also like to thank Professor David Staelin for connecting me with Lincoln Laboratory in order to perform my very necessary chamber measurements. My results were enhanced greatly with the chamber results. He also provided a great amount of insight and advice.

I would also like to thank David Bruno at Lincoln Laboratory, who conducted our radiation experiments in the anechoic chambers. Dr. Catherine Keller and Alan Fenn were also very helpful at Lincoln Laboratory, and instrumental in connecting me with the right people.

I am grateful to many helpful people at Intel, including Evan Green, who spent a great deal of time helping me on the discrete UWB system and providing helpful advice. Alan Waltho and Jeff Schiffer provided antenna insight, and I sincerely appreciate all of the useful discussions we had.

Antenna fabrication was made much easier with the help of Sam Lefian and Nathan Ickes, who helped with generating gerber files; Michael Garcia-Webb of the Bioinstrumentation Laboratory, who helped with the fabrication of the spiral antenna with the PCB milling router; and Chip Vaughan of the Laboratory for Manufacturing and Productivity, who provided access to the Omax waterjet, which enabled a clean circular cut of the spiral antennas.

One cannot attribute success only to work-related help. I thank, from the bottom of my heart, those who have supported me throughout these two years at MIT through their true friendship and thoughtfulness. My family has been an incredible pillar of support including my wonderful parents, Barbara and Richard, and my beautiful star athlete sister Chelsea Powell, who will never let you have a dull moment. My parents each had their own special way of making my life great, and I would not change a thing. I would not be who I am if it weren't for my family, and I am so proud of them. This includes all of us- Dan, thank God you taught me about wine- one of my new passions; Betty, who's taught me to dance from the time I was five- tap, jazz and Latin ballroom; Dina, you are the goddess of cosmetology and I will never trust anyone with my hair the way I trust you; Brad, a good hearted guy who's down to earth and sensitive; Rachel, a bona fide biotechnoloist; Luke, a true gym freak; Matt, a talented Magna Cum Laude artist; Melissa, our new sister-in-law who is our most welcomed new addition to the family; and Eric, who will probably own his own ski resort someday- now you're all my family, and I love you all. My best friend Lucie Fisher, whom I have known for my whole life minus 8 months or so (I crawled up to her at the university swimming pool- yes Lucie, it was me, and now we have a written account!), talked me into going to MIT so we could be closer to each other. I have enjoyed every trip to NYC I have taken to see her since I got here. Lucie will truly be a friend for life.

People at MIT have also been a great source of comfort, including Julia Cline, who has been such a great person to have around the lab. I will miss our coffee breaks, talks and walks.

She has a true life perspective; she is a secure person who is grounded and friendly, thoughtful and sincere. Julia, I will truly miss you and wish you all the best! Frank Honore has been a great "next door neighbor", as it were. I enjoyed coming into lab to find him working at all hours, from early morning until late at night, and sharing conversations about marathons and other random topics. Margaret Flaherty helped me immensely, from keeping me on track with packing slips and receipts to making sure I got all of my reimbursements as fast as possible. She surprised me the very first day I entered lab by her warmth and pleasantness, which I was not expecting after having been semi-acclimated to the Boston attitude. Every member of "ananthagroup" has added their own flare of contribution to the culture of the lab, to make it a productive and fun place. Thanks to everyone in ananthagroup.

I'd also like to thank Debb Hodges-Pabon, who does such a great job every year convincing the new admits to come to MIT. She is a burst of energy, joy and humor. MTL would not be the same without her. Karen Gonzalez-Valentin Gettings, who was the very first person to call me and inform me of my acceptance to MIT- you've really put things into perspective for me, and I appreciate just how sweet and genuine you are.

My grad residence, Sidney Pacific, was made much more pleasant by the camaraderie of the Sidney Pacific officers. Working with them made my living environment so much more enjoyable. Thanks again to Michael Garcia-Webb for helping me get through the first semester, which was the hardest. I appreciated the shoulder to lean on.

I'd like to thank Chip Vaughan for his much valued friendship, for training and running the marathon with me, and for helping me in every way imaginable just by being who he is. Chip, you're amazing.

Finally NMSU. My alma mater. My best memories. Great profs, great students, great friends. Thank you so much Dr. Russ Jedlicka, for giving me a great undergraduate research project, teaching me about antennas and making me laugh. David Brumit, thanks for being a great research buddy. Dr. Steve Castillo, Dr. Javin Taylor, Dr. Satish Ranade, Dr. Prasad, Dr. Stohaj, Dr. Bill McCarthy, Rich Turietta, and everyone I may have missed- thanks for being great teachers and mentors.

CONTENTS

FIGURES

CHAPTER

1

INTRODUCTION

Ultra Wideband Radio (UWB) is a potentially revolutionary approach to wireless communication in that it transmits and receives pulse based waveforms compressed in time rather than sinusoidal waveforms compressed in frequency. This is contrary to the traditional convention of transmitting over a very narrow bandwidth of frequency, typical of standard narrowband systems such as 802.11a, b, and Bluetooth. This enables transmission over a wide swath of frequencies such that a very low power spectral density can be successfully received.

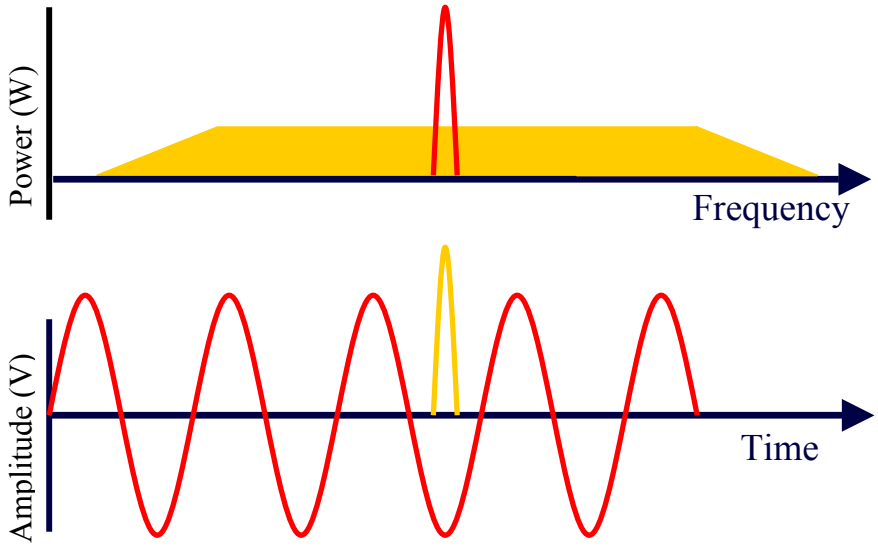

Figure 1. Diagram explanation illustrating the equivalence of a pulse based waveform compressed in time to a signal of very wide bandwidth in the frequency domain.

Figure 1 illustrates the equivalence of a narrowband pulse in the time domain to a signal of very wide bandwidth in the frequency domain. Also, it shows the equivalence of a

sinusoidal signal (essentially expanded in time) to a very narrow pulse in the frequency domain.

In February 2004, the FCC allocated the 3.1-10.6 GHz spectrum for unlicensed use [1]. This enabled the use and marketing of products which incorporate UWB technology. Since the allocation of the UWB frequency band, a great deal of interest has generated in industry.

The UWB spectral mask, depicted in Figure 2, was defined to allow a spectral density of -41.3 dBm/MHz throughout the UWB frequency band. Operation at such a wide bandwidth entails lower power that enables peaceful coexistence with narrowband systems. These specifications presented a myriad of opportunities and challenges to designers in a wide variety of fields including RF and circuit design, system design and antenna design.

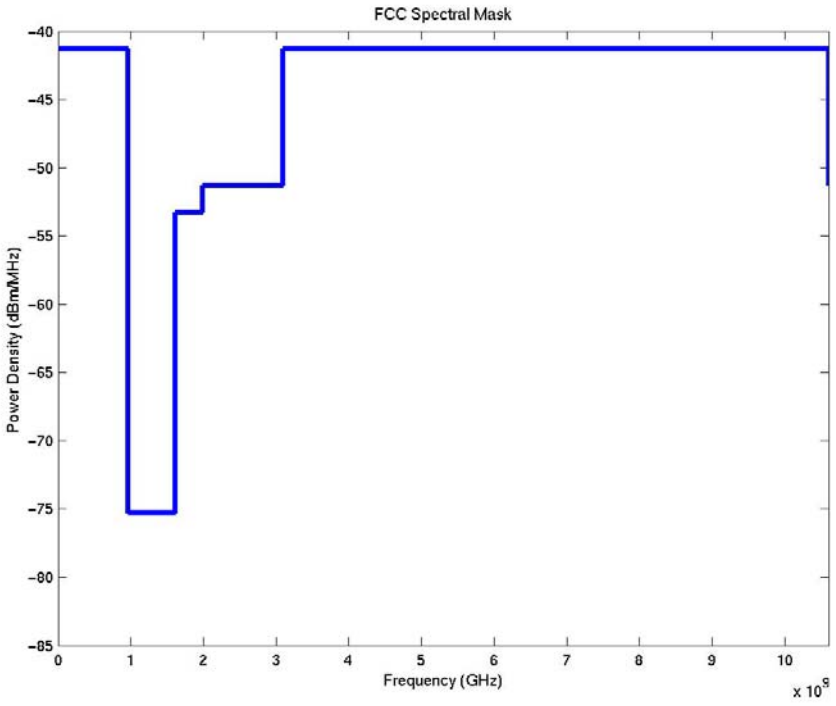

Figure 2. FCC Spectral Mask for indoor unlicensed UWB transmission. [1].

Ultra Wideband is defined as any communication technology that occupies greater than 500 MHz of bandwidth, or greater than 25% of the operating center frequency. Most narrowband systems occupy less than 10% of the center frequency bandwidth, and are transmitted at far greater power levels. For example, if a radio system is to use the entire UWB spectrum from 3.1-10.6 GHz, and center about almost any frequency within that band, the bandwidth used would have to be greater than 100% of the center frequency in order to span the entire UWB frequency range. By contrast, the 802.11b radio system centers about 2.4 GHz with an operating bandwidth of 80 MHz. This communication system occupies a bandwidth of only 1% of the center frequency.

1.1 Motivation for Ultra Wideband Antenna Design

UWB has had a substantial effect on antenna design. Given that antenna research for most narrowband systems is relatively mature, coupled with the fact that the antenna has been a fundamental challenge of the UWB radio system, UWB has piqued a surge of interest in antenna design by providing new challenges and opportunities for antenna designers. The main challenge in UWB antenna design is achieving the wide impedance bandwidth while still maintaining high radiation efficiency. Spanning 7.5 GHz, almost a decade of frequency, this bandwidth goes beyond the typical definition of a wideband antenna. UWB antennas are typically required to attain a bandwidth, which reaches greater than 100% of the center frequency to ensure a sufficient impedance match is attained throughout the band such that a power loss less than 10% due to reflections occurs at the antenna terminals.

Aside from attaining a sufficient impedance bandwidth, linear phase is also required for optimal wave reception, which corresponds to near constant group delay. This minimizes pulse distortion during transmission. Also, high radiation efficiency is required especially for UWB applications. Since the transmit power is so low (below the noise floor), power loss due to dielectrics and conductor losses must be minimized. Typically, antennas sold commercially achieve efficiencies of 50-60% due to lossy dielectrics. A power loss of 50% is not acceptable for UWB since the receive end architecture already

must be exceptionally sensitive to receive a UWB signal. Extra losses could compromise the functionality of the system. The physical constraints require compatibility with portable electronic devices and integrated circuits. As such, a small and compact antenna is required. A planar antenna is also desirable.

Given that there are several additional constraints and challenges for the design of a UWB system antenna, motivation for antenna design is clear.

1.2 Thesis Contribution and Overview

This thesis will first present a comprehensive background of the fundamental antenna parameters that should be considered in designing any antenna, narrowband or UWB. The key differences and considerations for UWB antenna design are also discussed in depth as several antennas are presented with these considerations in mind. A discrete system implementation is also discussed, in order to provide a method for which a comparison of several antennas can be made against a benchmark UWB antenna. The discrete system also provides insight into the operation of a UWB system. Time domain considerations are addressed, as well as frequency considerations including impedance matching, phase and group delay.

Several UWB antennas will be presented which were designed, simulated, tested and characterized at MIT, including a spiral equiangular slot patch antenna, a circular disc monopole, variations of a diamond dipole, and differential and single ended elliptical monopole antennas. A few of the antennas were also fabricated at MIT. Specifications such as physical profile, radiation efficiency, impedance bandwidth, phase, group delay, radiation pattern, beamwidth, gain and directivity will all be considered as various tradeoffs are discussed.

While these antenna designs and results are presented, explanation will be provided to encourage intuitive insight into how the antennas work, and why they achieve wide

bandwidth. Precious few references have contributed to an intuitive understanding of why certain antenna topologies achieve wide bandwidth.

CHAPTER

2

BACKGROUND

2.1 History of UWB

While Ultra Wideband technology may represent a revolutionary approach to wireless communication at present, it certainly is not a new concept. The first UWB radio, by definition, was the pulse-based Spark Gap radio, developed by Guglielmo Marconi in the late 1800's. This radio system was used for several decades to transmit Morse code through the airwaves. However, by 1924, Spark Gap radios were forbidden in most applications due to their strong emissions and interference to narrowband (continuous wave) radio systems, which were developed in the early 1900's. [2, 3].

By the early 1960's, increased interest in time domain electromagnetics by MIT's Lincoln Laboratory and Sperry Research Center [3] surged the development of the sampling oscilloscope by Hewlett-Packard in 1962. This enabled the analysis of the impulse response of microwave networks, and catalyzed methods for subnanosecond pulse generation. A significant research effort also was conducted by antenna designers, including Rumsey and Dyson [4, 5], who were developing logarithmic spiral antennas, and Ross, who applied impulse measurement techniques to the design of wideband, radiating antenna elements [6]. With these antenna advances, the potential for using impulse based transmission for radar and communications became clear.

Through the late 1980's, UWB technology was referred to as baseband, carrier-free or impulse technology, as the term "ultra wideband" was not used until 1989 by the U.S.

Department of Defense. Until the recent FCC allocation of the UWB spectrum for unlicensed use, all UWB applications were permissible only under a special license.

For the nearly 40 year period from 1960-1999, over 200 papers were published in accredited IEEE journals, and more than 100 patents were issued on topics related to ultra wideband technology [7]. The interest seems to be growing exponentially now, precipitated by the FCC allocation in 2002 of the UWB spectrum, with several researchers exploring RF design, circuit design, system design and antenna design, all related to UWB applications. Several business ventures have started with the hope of creating the first marketable UWB chipset, enabling revolutionary high-speed, short range data transfers and higher quality of services to the user.

2.2 Antenna Requirements and Specifications

In order to understand the challenges that UWB provides to antenna designers, a comprehensive background outlining several characterizing antenna parameters will be presented. Next, a clear description of the challenging requirements that UWB imposes with regard to these fundamental antenna parameters will be presented. Several parameters have been defined in order to characterize antennas and determine optimal applications. One very useful reference is the IEEE Standard Definitions of Terms for Antennas [8].

Several factors are considered in the simulation, design and testing of an antenna, and most of these metrics are described in 2.2.1, Fundamental Antenna Parameters. These parameters must be fully defined and explained before a thorough understanding of antenna requirements for a particular application can be achieved.

2.2.1 Fundamental Antenna Parameters

Among the most fundamental antenna parameters are impedance bandwidth, radiation pattern, directivity, efficiency and gain. Other characterizing parameters that will be discussed are half-power beamwidth, polarization and range. All of the aforementioned

antenna parameters are necessary to fully characterize an antenna and determine whether an antenna is optimized for a certain application.

2.2.1.1 Impedance Bandwidth

Impedance bandwidth indicates the bandwidth for which the antenna is sufficiently matched to its input transmission line such that 10% or less of the incident signal is lost due to reflections. Impedance bandwidth measurements include the characterization of the Voltage Standing Wave Ratio (VSWR) and return loss throughout the band of interest. VSWR and return loss are both dependent on the measurement of the reflection coefficient Γ. Γ is defined as ratio of the reflected wave Vo^- to the incident wave Vo^+ at a transmission line load as shown in Figure 3. Transmission Line Model, and can be calculated by equation 1. [9, 10, 11]:

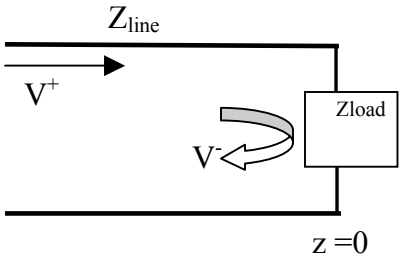

Figure 3. Transmission Line Model

$$\Gamma = \frac{Vo-}{Vo+} = \frac{Zline - Zload}{Zline + Zload} \qquad \text{Equation 1}$$

Z_{line} and Z_{load} are the transmission line impedance and the load (antenna) impedance, respectively. The voltage and current through the transmission line as a function of the distance from the load, z, are given as follows:

$$V(z) = Vo^{+}e^{-j\beta z} + Vo^{-}e^{j\beta z} = Vo^{+}(e^{-j\beta z} + \Gamma e^{j\beta z}) \quad \text{Equation 2}$$

$$I(z) = 1/Z_o\,(Vo^{+}e^{-j\beta z} - Vo^{-}e^{j\beta z}) = Vo^{+}/Z_o\,(e^{-j\beta z} - \Gamma e^{j\beta z}) \quad \text{Equation 3}$$

Where $\beta = 2\pi/\lambda$.

The reflection coefficient Γ is equivalent to the S_{11} parameter of the scattering matrix. A perfect impedance match would be indicated by $\Gamma = 0$. The worst impedance match is given by $\Gamma = -1$ or 1, corresponding to a load impedance of a short or an open.

Power reflected at the terminals of the antenna is the main concern related to impedance matching. Time-average power flow is usually measured along a transmission line to determine the net average power delivered to the load. The average incident power is given by:

$$P^{i}_{ave} = \frac{|Vo+|^2}{2Zo} \quad \text{Equation 4}$$

The reflected power is proportional to the incident power by a multiplicative factor of $|\Gamma|^2$, as follows:

$$P^{r}_{ave} = -|\Gamma|^2\,\frac{|Vo+|^2}{2Zo} \quad \text{Equation 5}$$

The net average power delivered to the load, then, is the sum of the average incident and average reflected power:

$$P_{ave} = \frac{|Vo+|^2}{2Zo}\,[1-|\Gamma|^2] \quad \text{Equation 6}$$

Since power delivered to the load is proportional to $(1-|\Gamma|^2)$, an acceptable value of Γ that enables only 10% reflected power can be calculated. This result is $\Gamma = 0.3162$.

When a load is not perfectly matched to the transmission line, reflections at the load cause a negative traveling wave to propagate down the transmission line. Ultimately, this creates unwanted standing waves in the transmission line. VSWR measures the ratio of the amplitudes of the maximum standing wave to the minimum standing wave, and can be calculated by the equation below:

$$\text{VSWR} = \frac{V_{\max}}{V_{\min}} = \frac{1+|\Gamma|}{1-|\Gamma|} \qquad \text{Equation 7}$$

The typically desired value of VSWR to indicate a good impedance match is 2.0 or less. This VSWR limit is derived from the value of Γ calculated above.

Return loss is another measure of impedance match quality, also dependent on the value of Γ, or S_{11}. Antenna return loss is calculated by the following equation:

$$\text{Return Loss} = -10\log|S_{11}|^2, \text{ or } -20\log(|\Gamma|). \qquad \text{Equation 8}$$

A good impedance match is indicated by a return loss greater than 10 dB. A summary of desired antenna impedance parameters include $\Gamma<0.3162$, VSWR<2, and Return Loss > 10 dB.

2.2.1.2 Radiation Pattern

One of the most common descriptors of an antenna is its radiation pattern. Radiation pattern can easily indicate an application for which an antenna will be used. For example, cell phone use would necessitate a nearly omnidirectional antenna, as the user's location is not known. Therefore, radiation power should be spread out uniformly around the user for optimal reception. However, for satellite applications, a highly directive antenna would be desired such that the majority of radiated power is directed to a specific, known location. According to the IEEE Standard Definitions of Terms for Antennas [8], an antenna radiation pattern (or antenna pattern) is defined as follows:

"a mathematical function or a graphical representation of the radiation properties of the antenna as a function of space coordinates. In most cases, the radiation pattern is determined in the far-field region and is represented as a function of the directional coordinates. Radiation properties include power flux density, radiation intensity, field strength, directivity phase or polarization."

Three dimensional radiation patterns are measured on a spherical coordinate system indicating relative strength of radiation power in the far field sphere surrounding the antenna. On the spherical coordinate system, the x-z plane (θ measurement where φ=0°) usually indicates the elevation plane, while the x-y plane (φ measurement where θ=90°) indicates the azimuth plane. Typically, the elevation plane will contain the electric-field vector (E-plane) and the direction of maximum radiation, and the azimuth plane will contain the magnetic-field vector (H-Plane) and the direction of maximum radiation. A two-dimensional radiation pattern is plotted on a polar plot with varying φ or θ for a fixed value of θ or φ, respectively. Figure 4 illustrates a half-wave dipole and its three-dimensional radiation pattern. The gain is expressed in dBi, which means that the gain is referred to an isotropic radiator. Figure 5 illustrates the two dimensional radiation patterns for varying θ at φ=0°, and varying φ at θ=90°, respectively. It can be seen quite

clearly in Figure 4 that the maximum radiation power occurs along the θ=90° plane, or for any varying φ in the azimuth plane. The nulls in the radiation pattern occur at the ends of the dipole along the z-axis (or at θ=0° and 180°). By inspection, the two dimensional polar plots clearly show these characteristics, as well. Figure 5 shows the radiation pattern of the antenna as the value in the azimuth plane is held constant and the elevation plane (θ) is varied (left), and to the right, it shows the radiation pattern of the antenna as the value in the elevation plane is held constant (in the direction of maximum radiation, θ=90°) as φ varies, and no distinction in the radiation pattern is discernable.

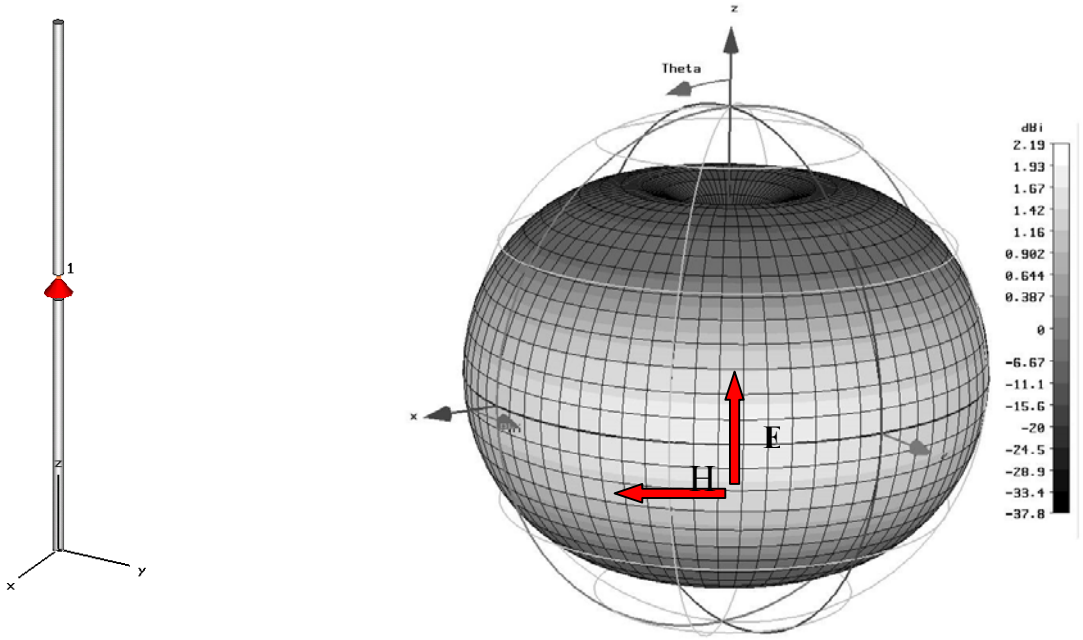

Figure 4: Dipole Model for Simulation and simulated 3D radiation pattern. Modeled in CST Microwave Studio

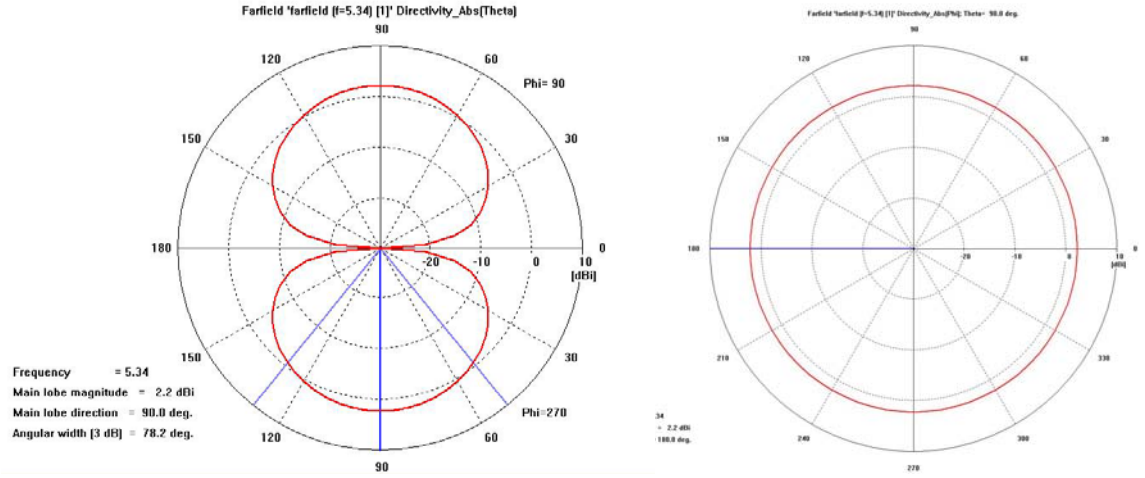

Figure 5. Two dimensional radiation plot for half-wave dipole: Varying θ, φ = 0° (left) and Two dimensional radiation plot for half-wave dipole: Varying ϕ, θ = 0° (right)

While many two-dimensional radiation patterns are required for a fully complete picture of the three-dimensional radiation pattern, the two most important measurements are the E-plane and H-plane patterns. The E-plane is the plane containing the electric field vector and direction of maximum radiation, and the H-plane is the plane containing the magnetic field vector and direction of maximum radiation. While Figure 5 shows simply two "cuts" of the antenna radiation pattern, the three-dimensional pattern can clearly be inferred from these two-dimensional illustrations.

The patterns and model in Figure 4 and Figure 5 illustrate the radiation characteristics of a half-wavelength dipole, which is virtually considered an omnidirectional radiator. The only true omnidirectional radiator is that of an isotropic source, which exists only in theory. The IEEE Standard Definitions of Terms for Antennas defines an isotropic radiator as "a hypothetical lossless antenna having equal radiation in all directions." A true omnidirectional source would have no nulls in its radiation pattern, and therefore have a directivity measurement of 0 dBi. However, since no source in nature is truly isotropic, a directive antenna typically refers to an antenna that is more directive than the half-wave dipole of the figures above.

An example of a directive antenna is the Computer Simulation Technology (CST) Microwave Studio Horn antenna illustrated in Figure 6, along with its three-dimensional radiation pattern. This shows clearly the direction of maximum radiation that lies along $\theta = 0°$, and no back radiation (or back lobes). Since this radiation pattern is simulated in an ideal environment with an infinite ground plane, no back lobe radiation has been simulated. The only lobes observable are the maximum radiation lobe and the smaller side lobes. However, in a realistic measurement conducted with a finite sized ground plane, back lobe radiation would be observed in which radiation would escape to the back of the ground plane. This simulation model suffices, however, to illustrate the radiation characteristics of a directive antenna versus the virtually omnidirectional half-wave dipole of in Figure 4 and Figure 5.

Figure 7 shows the principal E-plane and H-plane measurements of the horn antenna, clearly illustrating the characteristics indicated in the three-dimensional radiation plot. The leftmost illustration of Figure 7 holds φ constant while varying θ, while the plot on the right holds θ constant while varying φ. A pronounced difference in the directivity of maximum radiation is clearly apparent.

2.2.1.3 Half Power Beam Width (HPBW)

Half power beamwidth (HPBW) is defined as the angular distance from the center of the main beam to the point at which the radiation power is reduced by 3 dB. This measurement is taken at two points from the center of the main beam such that this angular distance is centered about the main beam. This measurement is clearly indicated in the two dimensional plot simulations of Figure 5 and Figure 7, labeled as “Angular width (3dB)”. This measurement is useful in order to describe the radiation pattern of an antenna and to indicate how directive it is.

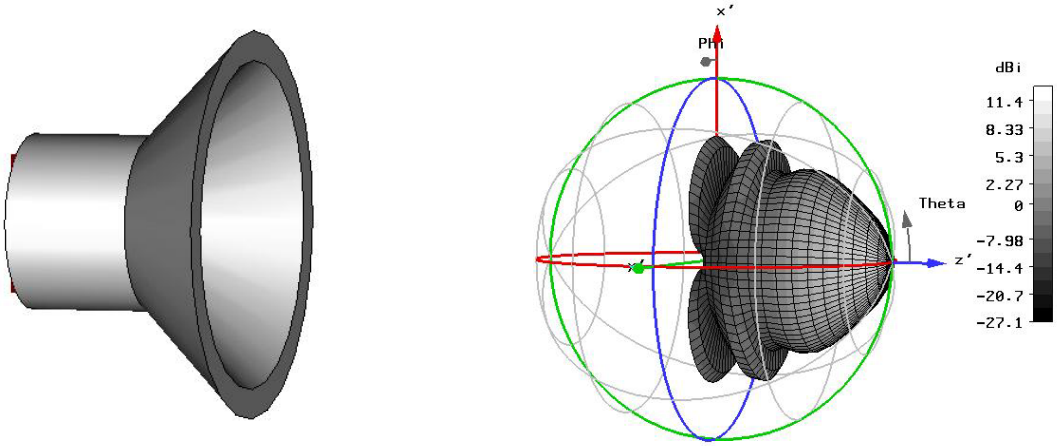

Figure 6. CST Microwave Studio model of horn antenna and simulated 3D radiation pattern.

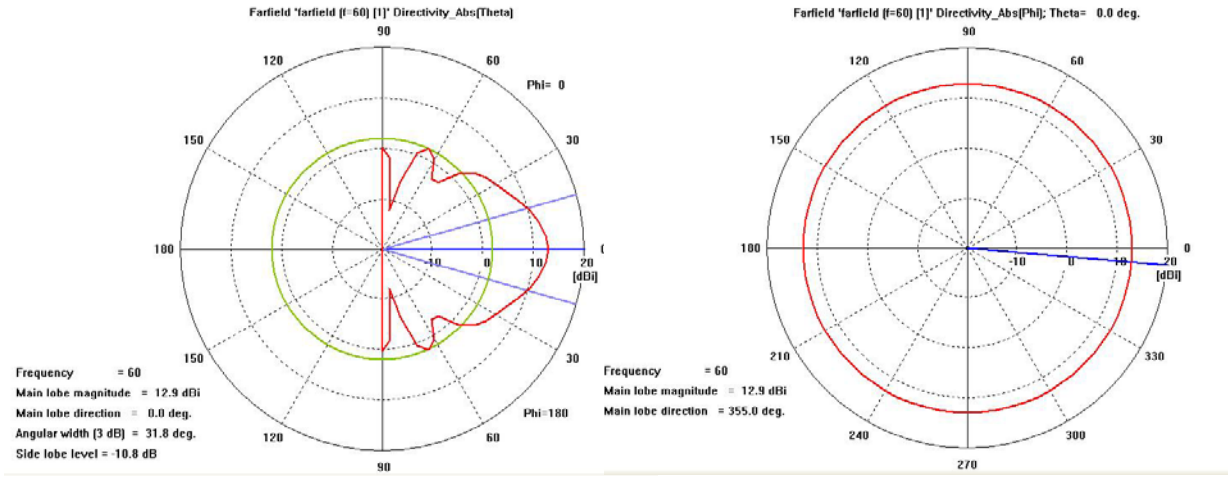

Figure 7. CST MW Studio simulated radiation pattern. Varying θ, ϕ=0° (left). Varying ϕ, θ = 0° (right).

2.2.1.4 Directivity

According to [8], the directivity of an antenna is defined as "the ratio of the radiation intensity in a given direction from the antenna to the radiation intensity averaged over all directions. The average radiation intensity is equal to the total power radiated by the antenna divided by 4π." Directivity is more thoroughly understood theoretically when an explanation of radiation power density, radiation intensity and beam solid angle are given. References [9-11] should be referred to for more thorough explanation.

The average radiation power density is expressed as follows:

$S_{av} = \frac{1}{2} \mathrm{Re}[\vec{E} \times \vec{H}^*]$ (W/m^2) Equation 9

Since $\mathbf{S_{av}}$ is the average power density, the total power intercepted by a closed surface can be obtained by integrating the normal component of the average power density over the entire closed surface. Then, the total radiated power is given by the following expression:

$$P_{rad} = P_{av} = \frac{1}{2} \oiint_S \mathrm{Re}(\vec{E} \times \vec{H}^*) \bullet ds = \oiint_S S_{rad} \bullet ds$$ Equation 10

Radiation intensity is defined by the IEEE Standard Definitions of Terms for Antennas as "the power radiated from an antenna per unit solid angle." The radiation intensity is simply the average radiation density, $\mathbf{S_{rad}}$, scaled by the square product of the distance, r. This is also a far field approximation, and is given by:

$U = r^2 S_{rad}$ Equation 11

Where U = radiation intensity (W/unit solid angle) and $\mathbf{S_{rad}}$ = radiation density (W/m^2).

The total radiated power, P_{rad}, can be then be found by integrating the radiation intensity over the solid angle of 4π steradians, given as:

$$P_{rad} = \oiint_{\Omega} U d\Omega = \int_0^{2\pi}\int_0^{\pi} U \sin\theta d\theta d\phi \qquad \text{Equation 12}$$

$$P_{rad} = \oiint_{\Omega} U_o d\Omega = U_o \oiint_{\Omega} d\Omega = 4\pi U_o \qquad \text{Equation 13}$$

Where $d\Omega$ is the element of solid angle of a sphere, measured in steradians. A steradian is defined as "a unit of measure equal to the solid angle subtended at the center of a sphere by an area on the surface of the sphere that is equal to the radius squared." Integration of $d\Omega$ over a spherical area as shown in the equation above yields 4π steradians. Another way to consider the steradian measurement is to consider a radian measurement: The circumference of a circle is $2\pi r$, and there are $(2\pi r/r)$ radians in a circle. The area of a sphere is $4\pi r^2$, and there are $4\pi r^2/r^2$ steradians in a sphere.

The beam solid angle is defined as the subtended area through the sphere divided by r^2:

$$d\Omega = \frac{dA}{r^2} = \sin\theta d\theta d\phi \qquad \text{Equation 14}$$

Given the above theoretical and mathematical explanations of radiation power density, radiation intensity and beam solid angle, a more complete understanding of antenna directivity can be achieved. Directivity is defined mathematically as:

$$D = \frac{U}{U_o} = \frac{4\pi U}{P_{rad}} \text{ (dimensionless)} \qquad \text{Equation 15}$$

Simply stated, antenna directivity is a measure of the ratio of the radiation intensity in a given direction to the radiation intensity that would be output from an isotropic source.

2.2.1.5 Efficiency

The antenna efficiency takes into consideration the ohmic losses of the antenna through the dielectric material and the reflective losses at the input terminals. Reflection efficiency and radiation efficiency are both taken into account to define total antenna efficiency. Reflection efficiency, or impedance mismatch efficiency, is directly related to the S_{11} parameter (Γ). Reflection efficiency is indicated by e_r, and is defined mathematically as follows:

$$e_r = (1-|\Gamma|^2) = \text{reflection efficiency} \qquad \text{Equation 16}$$

The radiation efficiency takes into account the conduction efficiency and dielectric efficiency, and is usually determined experimentally with several measurements in an anechoic chamber. Radiation efficiency is determined by the ratio of the radiated power, P_{rad} to the input power at the terminals of the antenna, P_{in}:

$$e_{rad} = \frac{P_{rad}}{P_{in}} = \text{radiation efficiency} \qquad \text{Equation 17}$$

Total efficiency is simply the product of the radiation efficiency and the reflection efficiency. Reasonable values for total antenna efficiency are within the range of 60% - 90%, although several commercial antennas achieve only about 50-60% due to inexpensive, lossy dielectric materials such as FR4.

2.2.1.6 Gain

The antenna gain measurement is linearly related to the directivity measurement through the antenna radiation efficiency. According to [8], the antenna absolute gain is "the ratio of the intensity, in a given direction, to the radiation intensity that would be obtained if

the power accepted by the antenna were radiated isotropically." Antenna gain is defined mathematically as follows:

$$G = e_{rad}D = 4\pi \frac{U(\theta,\phi)}{P_{in}} \qquad \text{(dimensionless)} \qquad \text{Equation 18}$$

Also, if the direction of the gain measurement is not indicated, the direction of maximum gain is assumed. The gain measurement is referred to the power at the input terminals rather than the radiated power, so it tends to be a more thorough measurement, which reflects the losses in the antenna structure.

Gain measurement is typically misunderstood in terms of determining the quality of an antenna. A common misconception is that the higher the gain, the better the antenna. This is only true if the application requires a highly directive antenna. Since gain is linearly proportional to directivity, the gain measurement is a direct indication of how directive the antenna is (provided the antenna has adequate radiation efficiency).

2.2.1.7 Polarization

Antenna polarization indicates the polarization of the radiated wave of the antenna in the far-field region. The polarization of a radiated wave is the property of an electromagnetic wave describing the time varying direction and relative magnitude of the electric-field vector at a fixed location in space, and the sense in which it is traced, as observed along the direction of propagation [8]. Typically, this is measured in the direction of maximum radiation. There are three classifications of antenna polarization: linear, circular and elliptical. Circular and linear polarization are special cases of elliptical polarization. Typically, antennas will exhibit elliptical polarization to some extent. Polarization is

indicated by the electric field vector of an antenna oriented in space as a function of time. Should the vector follow a line, the wave is linearly polarized. If it follows a circle, it is circularly polarized (either with a left hand sense or right hand sense). Any other orientation is said to represent an elliptically polarized wave. Aside from the type of polarization, two main factors are taken into consideration when considering polarization of an antenna: Axial ratio and polarization mismatch loss, which can be referenced in [9-11].

2.2.2 UWB Antenna Requirements

All of the fundamental parameters described in the previous section must be considered in designing antennas for any radio application, including Ultra Wideband. However, there are additional challenges for Ultra Wideband. By definition, an Ultra Wideband antenna must be operable over the entire 3.1-10.6 GHz frequency range. Therefore, the UWB antenna must achieve almost a decade of impedance bandwidth, spanning 7.5 GHz. Another consideration that must be taken into account is group delay. Group delay is given by the derivative of the unwrapped phase of an antenna. If the phase is linear throughout the frequency range, the group delay will be constant for the frequency range. This is an important characteristic because it helps to indicate how well a UWB pulse will be transmitted and to what degree it may be distorted or dispersed. It is also a parameter that is not typically considered for narrowband antenna design because linear phase is naturally achieved for narrowband resonance. This will be discussed in greater detail in section 3.2.

Radiation pattern and radiation efficiency are also significant characteristics that must be taken into account in antenna design. A nearly omnidirectional radiation pattern is desirable in that it enables freedom in the receiver and transmitter location. This implies maximizing the half power beamwidth and minimizing directivity and gain. Conductor and dielectric losses should be minimized in order to maximize radiation efficiency. Low

loss dielectric must be used in order to maximize radiation efficiency. High radiation efficiency is imperative for an ultra wideband antenna because the transmit power spectral density is excessively low. Therefore, any excessive losses incurred by the antenna could potentially compromise the functionality of the system.

In this research, the primary application focuses on integrated circuits for portable electronic applications. Therefore, the antenna is required to be physically compact and low profile, preferably planar. Several topologies will be evaluated and presented, considering tradeoffs between each design.

For specific IC radio applications in this research, the UWB antenna requirements can be summarized in the following table:

VSWR Bandwidth	3.1 – 10.6 GHz
Radiation Efficiency	High (>70%)
Phase	Nearly linear; constant group delay
Radiation Pattern	Omnidirectional
Directivity and Gain	Low
Half Power Beamwidth	Wide (> 60 °)
Physical Profile	Small, Compact, Planar

2.3 Current and Previous Research

While narrowband antenna research has reached a certain level of maturity, it is important to briefly describe antennas and their applications in traditional narrowband design. Following traditional narrowband design, techniques for achieving broader bandwidth are introduced in this section, and several antenna topologies are considered. Finally, Rumsey's theory of frequency independence relating to spiral antenna design is detailed and discussed.

2.3.1 Traditional Narrowband Design

Thin dipoles and microstrip patch antennas are commonly used and are quite effective for narrowband operation. For instance, dipoles are known to virtually everyone because of their common use in cell phones, televisions and automobiles. The main reason for their ubiquitous nature is that they exhibit nearly omnidirectional radiation patterns, making transmit and receive capabilities viable for almost all locations. An example of a dipole antenna and its radiation pattern were already cited in 2.2.1.2.

Microstrip patch antennas are generally used for aircraft, spacecraft, and even cellular communication. They can easily be designed for resonance and a desired polarization at a particular center frequency with a bandwidth of about 1% of that center frequency. In that range, return loss values of approximately 20-30 dB are achievable, with gains of approximately 2-4 dB, depending on the frequency of operation. Microstrip patch antennas are low-profile, conformable, and inexpensive to fabricate out of printed circuit board material. Figure 8 illustrates a typical microstrip patch antenna and its two-dimensional radiation pattern.

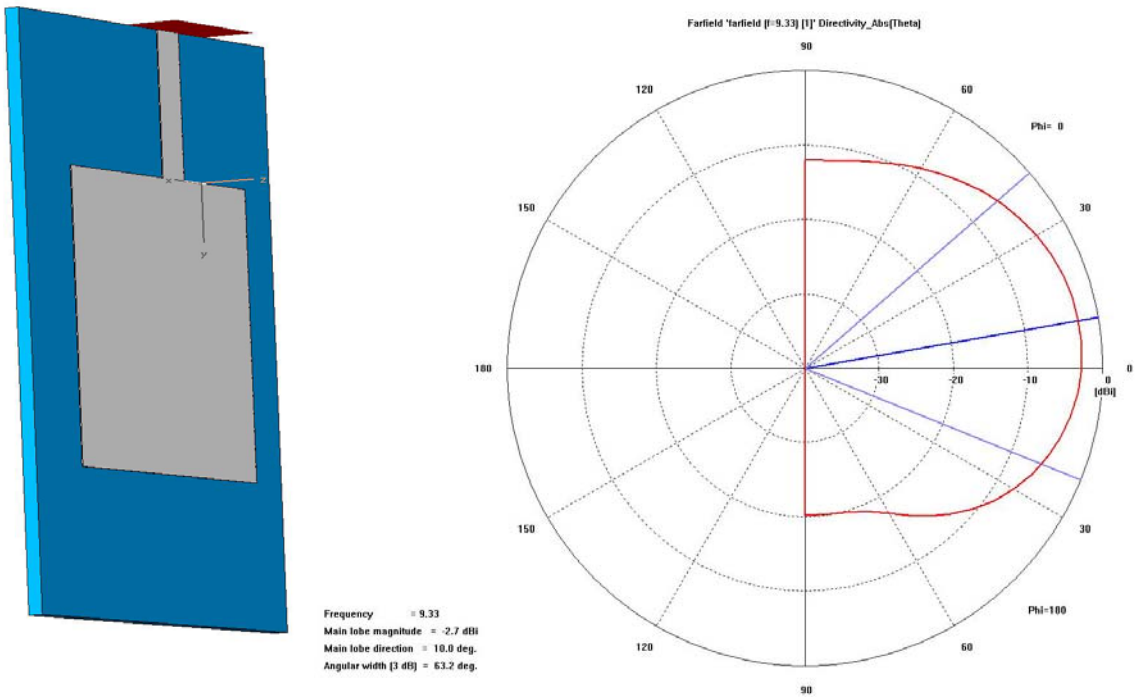

Figure 8. Typical microstrip patch configuration and its two dimensional radiation pattern. Modeled in CST Microwave Studio.

The caveat to these typical antenna designs is that they are narrowband in nature. Thin dipoles and microstrip patches exhibit reactances that converge to zero when the antenna appears as a half-wavelength transmission line to the incoming signal. Their geometry is therefore frequency dependent. However, traditional narrowband communication systems require bandwidths of several MHz for a GHz center frequency, rendering the narrowband nature of these types of antennas no substantial problem.

As mentioned previously, Ultra Wideband Radio is unique to narrowband communication systems in that it utilizes the entire 3.1-10.6 GHz band recently allocated by the FCC. UWB requires an antenna that operates sufficiently throughout the entire frequency band, such that the pulse is not distorted or dispersed during transmission and reception. Correlation schemes depend on the predictability of the pulse-shaping effects of the antenna, and as such, it is optimal to minimize pulse distortion effects.

2.3.2 Achieving Broader Bandwidths

There are many methods for broadening the bandwidth of antennas. For instance, it is well known that thickening a dipole leads to a broader bandwidth. An intuitive explanation for this follows from the fact that most of the electromagnetic energy is stored within a few wire radii of a thin dipole. Therefore, the fields are most intense around the wire radius and can be approximated by a TEM transmission line model, which corresponds to high Q resonance. However, as the dipole wire radius becomes thicker, the TEM transmission line model approximation breaks down and we achieve a lower Q resonance. Bandwidths versus length to diameter (l/d) ratios of antennas have been documented. [9,10]. For example, an antenna with a ratio l/d =5000 has an acceptable bandwidth of about 3%, which is a small fraction of the center frequency. An antenna of the same length but with a ratio l/d =260 has a bandwidth of about 30%. [9] This would correspond to a bandwidth of approximately 2.0 GHz for a center frequency of 6.5 GHz, which is still not sufficient for the entire UWB bandwidth of 7.5 GHz.

There are also several known antenna topologies that are said to achieve broadband characteristics, such as the horn antenna, biconical antenna, helix antenna and bowtie antenna. An illustration of a horn antenna has been presented in Figure 6. Illustrations of a bicone and helical antenna are shown in Figure 9.

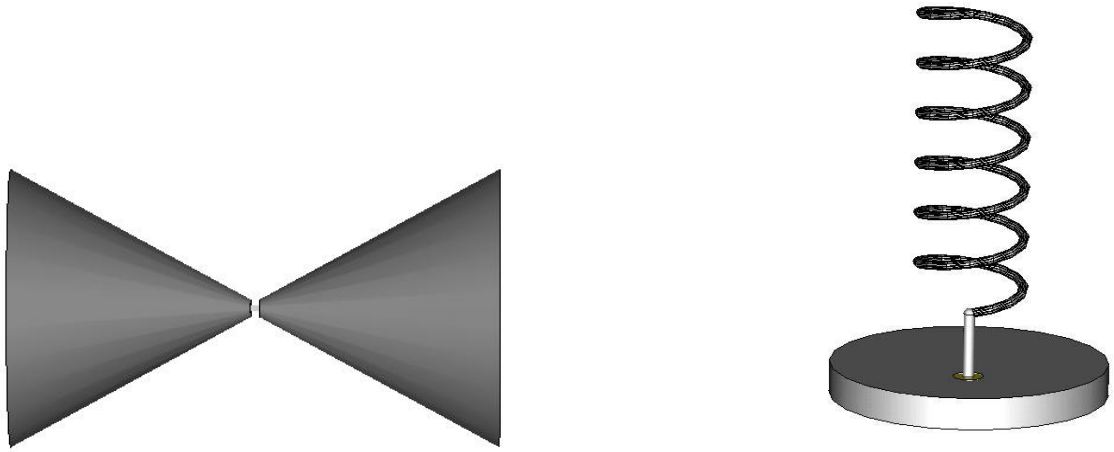

Figure 9. Illustrations of a biconical antenna (left) and a helical antenna (right). Models from CST Microwave Studio.

While the horn, bicone and helix antenna certainly have been proven to have excellent broadband characteristics, even for the FCC allocated UWB range, they are large, non-planar and physically obtrusive, therefore ruling them out as a possibility for use with small UWB integrated electronics. However, several topologies are worth consideration. One example of a thick dipole in the form of a planar biconical antenna is the bow-tie antenna, illustrated in Figure 10.

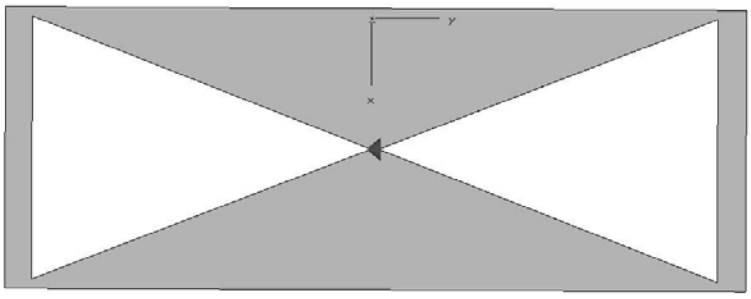

Figure 10. Illustration of a bow-tie antenna configuration. Designed in CST Microwave Studio.

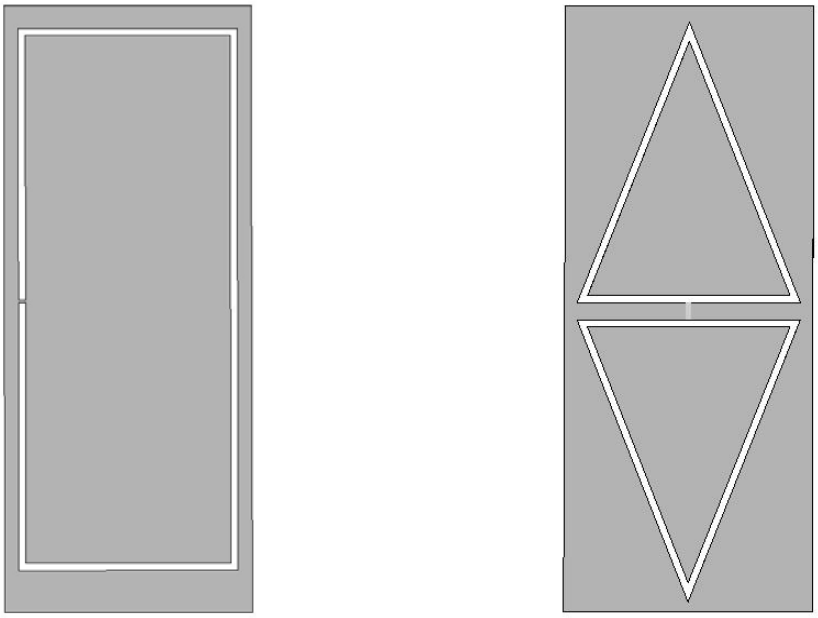

Figure 11. Rectangular loop antenna model (left) [9,10,13] and diamond dipole antenna model (right) [12].

There are also certain polygonal configurations of the thin-wire dipole that lead to broader bandwidths, such as the triangular loop antenna proposed by Time Domain Corporation ("Diamond Dipole") [12] and the rectangular loop antenna ("Large Current Radiator") proposed by several groups as an impulse antenna [13]. Figure 11 shows embodiments of these geometrical configurations.

Intuitively, the broadband characteristics of these loop antennas is easiest to understand by inspecting their current distribution. Analyzing these dipoles as TEM transmission lines leads to the recognition that there are sharp current nulls at each edge, which creates low current standing wave ratios (SWR) even at antiresonant frequencies. The antiresonant frequencies that will see low standing wave ratios are geometrically determined. .

While these planar topologies can achieve broader bandwidths than the typical narrowband dipole or microstrip patch antenna, their frequency ranges are not broad enough to cover the 3.1-10.6 GHz band. Input reactances will cause nonlinear phase throughout the band, thereby creating distortion in the transmitted and received pulses.

2.3.3 Achieving Frequency Independence

One antenna design proposal suggests that there is a method for meeting the requirements of very wide impedance bandwidth, which uses Babinet's Equivalence Principle of duality and complementarity. [14]

Babinet's Equivalence Principle states that the product of the input impedances of two planar complementary antennas is one-quarter of the square of the characteristic impedance of the free space: $Z_1Z_2=\eta^2/4$.

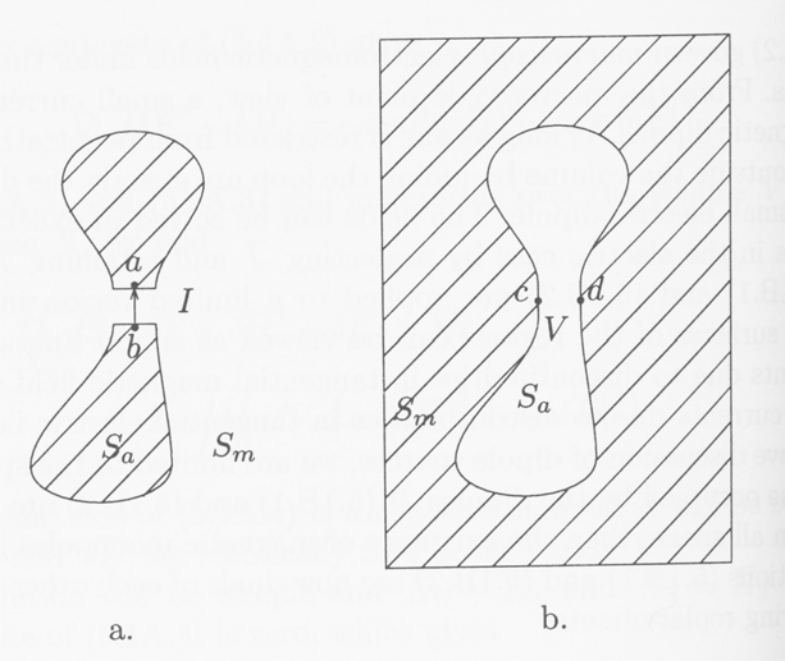

Figure 12. Complementary antennas illustrating Babinet's Equivalence Principle [14]

Illustrated in Figure 12, antenna A is the complement of antenna B. By Babinet's Equivalence Principle, it can be empirically and theoretically proven that $Z_AZ_B = \eta^2/4$. This principle can be used to achieve impedance matching throughout frequency, such

that $Z_A = Z_B = \eta/2$ for all frequencies. This idea was first introduced by Rumsey, who proved frequency independence for an antenna whose geometry could be described solely as a function of angles in its spherical coordinate system. The following introduces Rumsey's theoretical proof for this possibility [4]:

Assuming an antenna in spherical coordinate geometry (r, θ, φ) has both terminals infinitely close to the origin and each is symmetrically disposed along the $\theta=0, \pi$ axes, we begin by describing its surface by the curve:

$$r=F(\theta, \varphi) \qquad \text{Equation 19}$$

where r represents the distance along the surface. Supposing the antenna must be scaled in size to a frequency K times lower than the original frequency, the antenna size would necessarily be scaled by K times greater. Thus, the new antenna surface would be described by

$$r' = KF(\theta, \varphi) \qquad \text{Equation 20}$$

Surfaces r and r' are identical in electrical dimensions, and congruence can be established by rotating the first antenna by an angle C so that

$$KF(\theta, \varphi) = F(\theta, \varphi + C) \qquad \text{Equation 21}$$

Essentially, this means that r = r' if we move r through φ in the xy-plane at angle C. It should be noted that physical congruence implies that the original antenna would behave the same at both frequencies corresponding to φ and $(\varphi + C)$. However, the radiation pattern would be rotated azimuthally through angle C with frequency. Because C depends on K and not θ or φ, its shape will be unaltered through its rotation. Thus, the impedance and radiation pattern will be frequency independent.

Following this proof is a derivation in order to obtain functional representation of $F(\theta,\varphi)$ by differentiating each side of the above equation with respect to C and φ, and equating, which yields

$$(dK/dC)F(\theta,\varphi) = K\partial F(\theta,\varphi)/\partial\varphi \qquad \text{Equation 22}$$

$$1/K\ (dK/dC) = (1/r)\ \partial r/\partial\varphi \qquad \text{Equation 23}$$

This leads to the general solution for the surface $r = F(\theta,\varphi)$ of the antenna:

$$r = F(\theta,\varphi) = e^{a\varphi}f(\theta) \quad \text{where } a = 1/K\ (dK/dC) \qquad \text{Equation 24}$$

Thus, for any antenna to exhibit frequency independence, its surface must be described by the above equation. This geometry reflects a function of angles, independent of wavelength. Assuming the antenna has physical congruence, the infinite antenna pattern will behave the same at frequencies of any wavelength.

Babinet's Principle of Equivalence and Rumsey's theory of frequency independent geometry come together in the spiral slot antenna. This spiral curve can be derived by letting $f'(\theta) = A\delta(\pi/2 - \theta)$, where A is constant and δ is the three dimensional Dirac delta function (defined in Electromagnetic waves, [14]). Letting $\theta = \pi/2$, $r = Ae^{a(\varphi-\varphi 0)}$, where $A = r_o e^{-a\varphi 0}$. Further derivation leads to the representation of r in wavelengths, $r_\lambda = Ae^{a(\varphi-\varphi 1)}$, where $\varphi_1 = (\ln\lambda)/a$.

The expression of r in wavelengths shows it is evident that changing the wavelength is equivalent to varying φ, which results in nothing more than a pure rotation of the infinite structure pattern. 1/a is the rate of expansion of the spiral. [9]

CHAPTER

3

DISCRETE PROTOTYPE

3.1 UWB Discrete System Implementation

The question to be asked is whether a degree of frequency independence, or at least "ultra" wide bandwidth might be achieved in the UWB system antenna design in order to substantially minimize or eliminate pulse distortion from a transmit to receive system. Preliminary observations of pulse-shaping effects were made on a UWB discrete system. This system was modeled after a design initially made at Intel Labs. EMCO double-ridged waveguide horn antennas with operable ranges of 1-18 GHz were used to transmit the pulses, and were used as benchmark antennas by which other antennas could be compared against. The transmitter block diagram is shown in Figure 18.

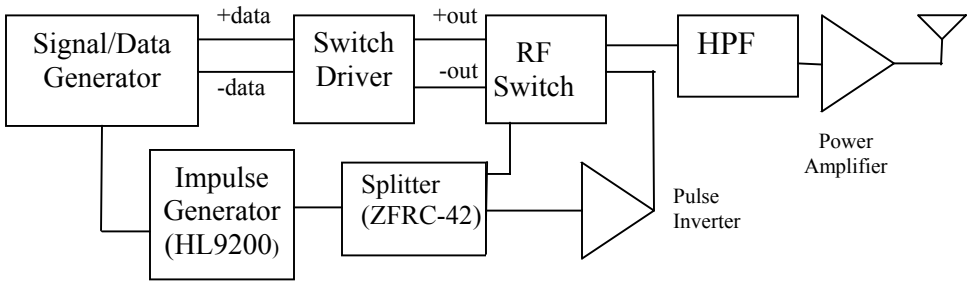

Figure 13. Transmit Block Diagram [15].

This system utilizes a clock and data generator, which provides a 50 MHz clock and data synchronized with the clock. This corresponds to a pulse repetition rate (prf) of 20ns. Although a clock of 50 MHz was used for this system, a very wide range of clock frequencies could have been used for this analysis. The frequency of 50 MHz was chosen because the pulse repetition rate was long enough to resolve multipath echoes. The clock is fed to an impulse generator, which generates sub-nanosecond pulses on the order of 200ps wide. The impulse generator is split into positive and negative pulses via a power splitter and pulse inverter. The positive and negative pulses are then input to an RF switch. The RF switch is driven by a switch driver circuit, which provides a -5V drive voltage depending on the data it receives. Thus, the RF switch produces positive and negative pulses at its output depending on the data that the RF switch driver receives. The switch output is then fed to an LNA, which amplifies the signal to be transmitted via the transmit antenna. The EMCO transmit and receive antennas are operable from 1-18 GHz such that distortion is minimized. Figure 19 shows the transmit system implementation.

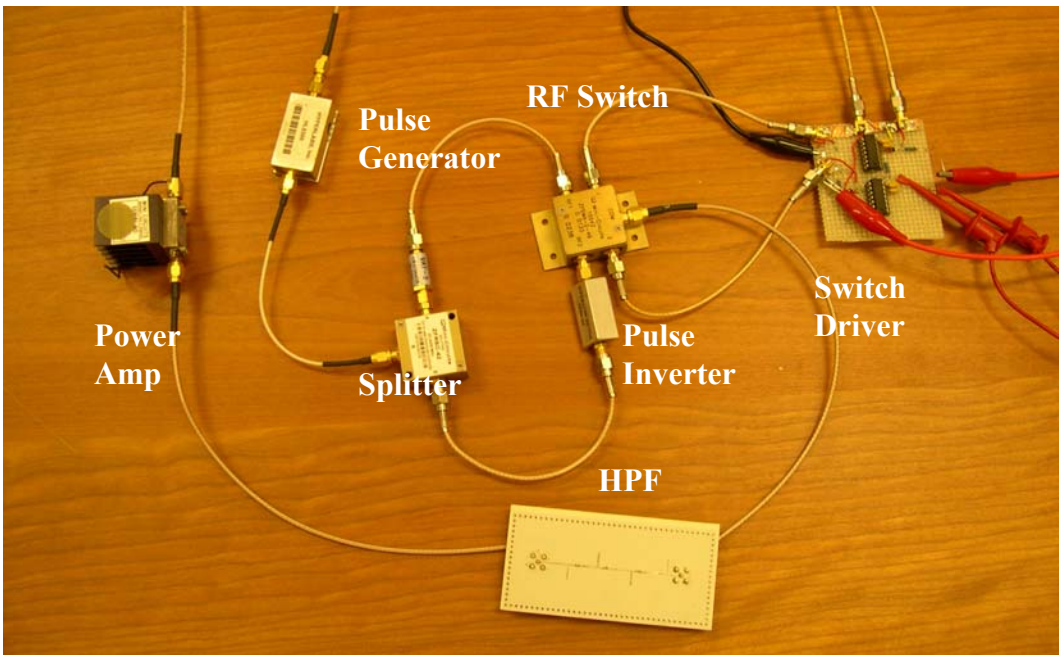

Figure 14. UWB Discrete Transmitter Implementation based on design from Intel [15].

3.2 Antenna Measurements and Time Domain Results

The impulse generator used in this system is an HL9200 from Hyperlabs. Powered by a 9V battery and excited by a 2V amplitude waveform, this pulse generator produces an output pulse approximately 200ps in width. Noise at the tail end of the impulse generator is present, but fortunately is substantially attenuated. After several trials with different cables, connectors, pulse repetition rates and clock voltage levels, the noise remained present, indicating that it is most likely inherent in the pulse generator. Figure 20 shows the time domain measurement of the output of the impulse generator and the filtered pulse on the TDS 8000 oscilloscope, 500ps/div and 30 mV/div.

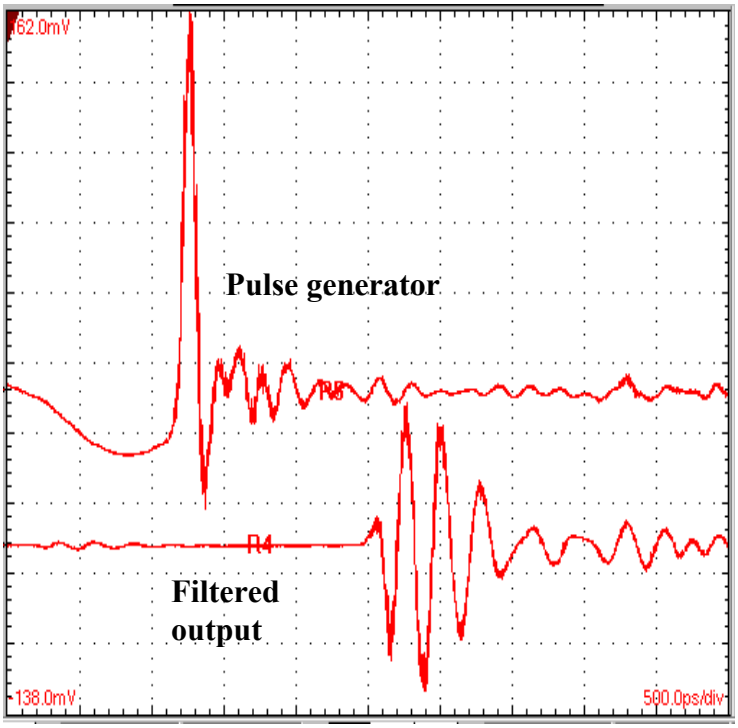

Figure 15. Output pulse from impulse generator (top) and pulse output from high pass filter.

The top waveform of Figure 15 illustrates the output directly at the output of the impulse generator. The pulse information is very narrow, but has a wide, low frequency depression before the pulse. This depression is inherent in the impulse generator which was provided by Hyperlabs, and is caused by the step recovery diode which generates the

impulse. This impulse is generated by driving the diode first in conduction, and then switching the operation to reverse bias. The quick switch in bias causes the very short pulse, but the negative depression is required in order to generate the pulse. Fortunately, the depression is a very low frequency component and is easily filtered by the high pass filter.

The waveform at the bottom of Figure 20 exhibits characteristics of a 3.1-10.6 GHz pulse after high pass filtering with a PCB filter designed on Rogers 4003 material at Intel Labs. This filter has a 3dB frequency of 3.0 GHz and a maximum passband ripple of 6.5 dB. The stopband is suppressed by approximately -45 dB. The S21 plot of this high pass filter is shown in Figure 21.

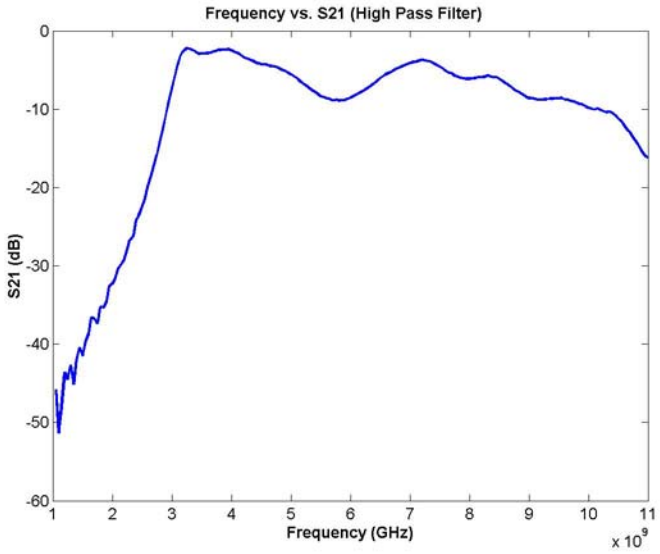

Figure 16. S21 plot of high pass filter used in discrete UWB system implementation.

One clearly important consideration to take into account is whether the transmitted pulse fits within the FCC spectral mask for indoor communication. In order to test this, the transmit waveform at the output of the power amplifier was attenuated by 20 dB attenuators and measured on the TDS oscilloscope. The attenuation accounted for

sensitivity of the oscilloscope to the voltage levels, and to avoid clipping. This waveform was exported and analyzed with a matlab script that performed an FFT with averaging and windowing to correct for amplitude error. This script is included in Appendix A.

Figure 22 illustrates the power spectrum of the transmitted pulse, taken at the output of the 20 dB attenuator attached to the output terminals of the power amplifier. An additional 20 dB was added linearly to this vector to account for the extra 20 dB of attenuation. Therefore, the plot of Figure 22 illustrates the power spectrum of the transmitted pulse taken effectively at the output of the power amplifier.

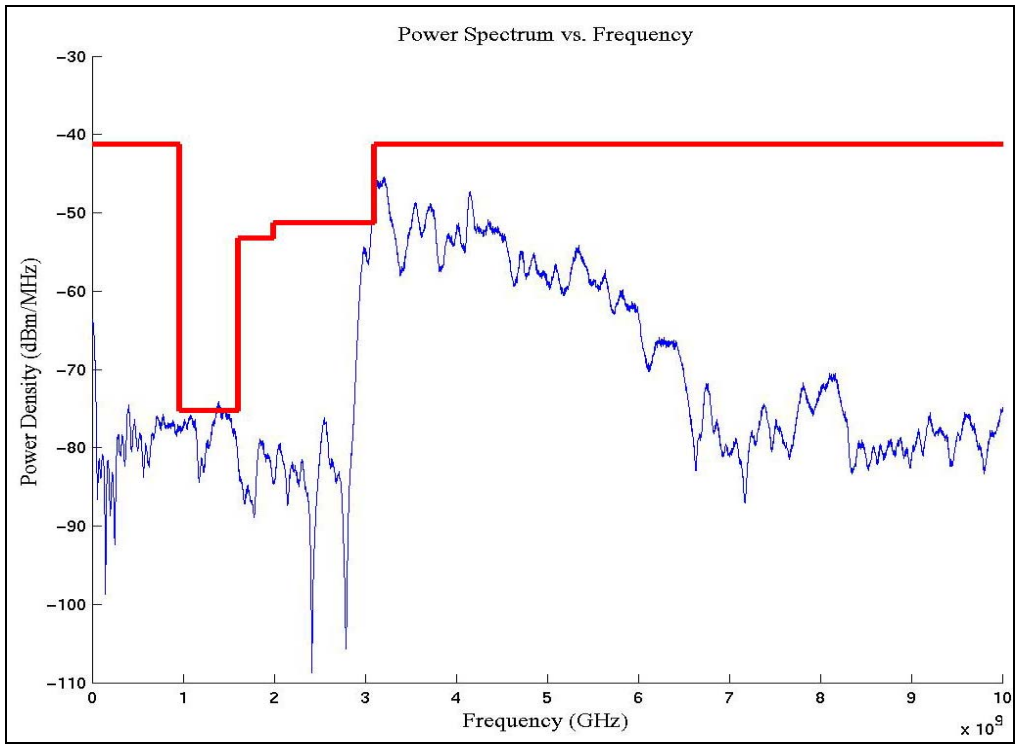

Figure 17. Power spectrum of the transmitted pulse plotted against the FCC spectral mask.

Observation of the power spectrum indicates that the power peaks from 3.1 GHz through 6 GHz and tapers down from 7 – 10 GHz. The maximum energy output by the impulse generator rolls off at about 6 GHz, and this is indicated in the power spectrum. The power spectrum exhibits noise, and this noise is also exhibited in the time domain pulse.

In analyzing this discrete system from the perspective of antenna analysis, it is important to study the characteristics of the benchmark horn antenna. Figure 18 illustrates the commercial double ridged waveguide horn antenna used initially in the discrete UWB system. This antenna was chosen because it is a known standard for wideband applications. Rated for an operating range of 1-18 GHz, horizontal polarization and an average gain of approximately 10 dBi throughout the UWB frequency range, this antenna is optimal for transmitting and receiving wideband pulses.

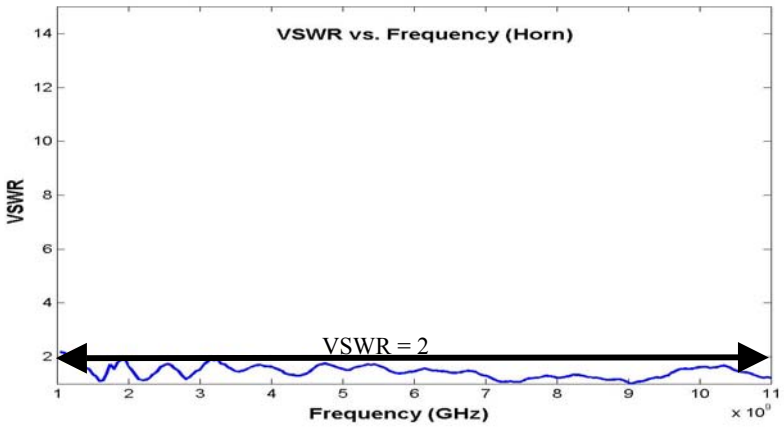

Figure 18. Top: Double Ridged Waveguide Horn Antenna (Photo courtesy ETS Lindgren, Inc.) Bottom: VSWR vs. Frequency for the Double Ridged Waveguide Horn Antenna.

The impedance bandwidth, phase, group delay and qualitative time domain impulse reception were tested and verified on this antenna to establish a standard by which other

antennas will be measured against. Figure 18 also illustrates the VSWR vs. Frequency for 1.0 to 11.0 GHz, indicating an excellent impedance match.

Figure 18 indicates that the VSWR impedance bandwidth for the UWB horn antenna is sufficient for the entire UWB frequency range, as the VSWR value is less than 2 for 3.1-10.6 GHz. As described in section 2.2.1.1, this corresponds to a power loss of less than 10% at the antenna terminals due to impedance mismatch. This is also indicated by a return loss of greater than 10 dB, or $10\log(S11)^2 < -10$. The return loss plot is shown in Figure 19, and also indicates more clearly the points of resonance at 7 GHz, 9 GHz and 1-3 GHz.

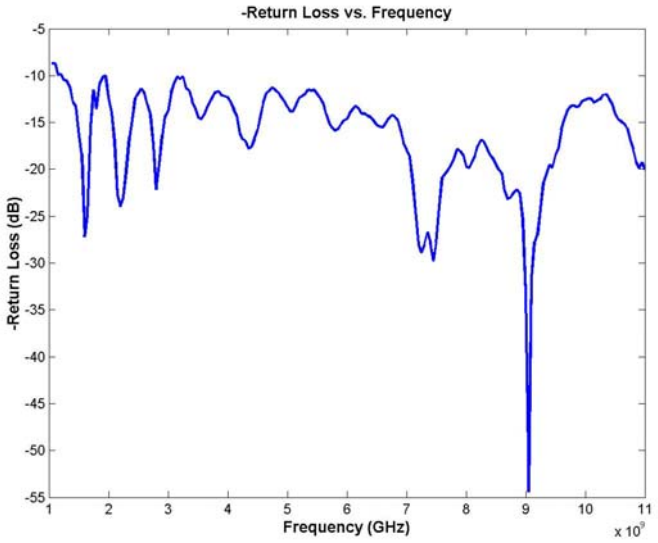

Figure 19. Return Loss vs. Frequency for Double Ridged Waveguide Horn Antenna.

Return loss is, again, another method of indicating impedance bandwidth, which is one of the fundamental parameters used to characterize an antenna. For consistency, subsequent impedance plots will be plotted in terms of VSWR.

Another important metric is the phase of the horn antenna. Given that there are modes throughout the frequency band that are more resonant than others, a phase shift is expected, and therefore, perfectly linear phase is not entirely attainable for this frequency

bandwidth. To minimize group delay, which is the derivative of the unwrapped phase of the antenna, the ideal impedance plot would contain no strong resonances (ie., appear as flat as possible throughout the frequency band, but still attain a good impedance match). This would also be correlated with constant gain throughout the frequency range. Figure 26 illustrates the phase for the waveguide horn antenna, which shows distinct nonlinear characteristics at the most resonant points. The sharp nulls in the return loss plot correspond to the frequencies that attain the highest resonances, which also correspond to the points at which the VSWR is closest to 1. These points indicate a near perfect match to 50 Ω.

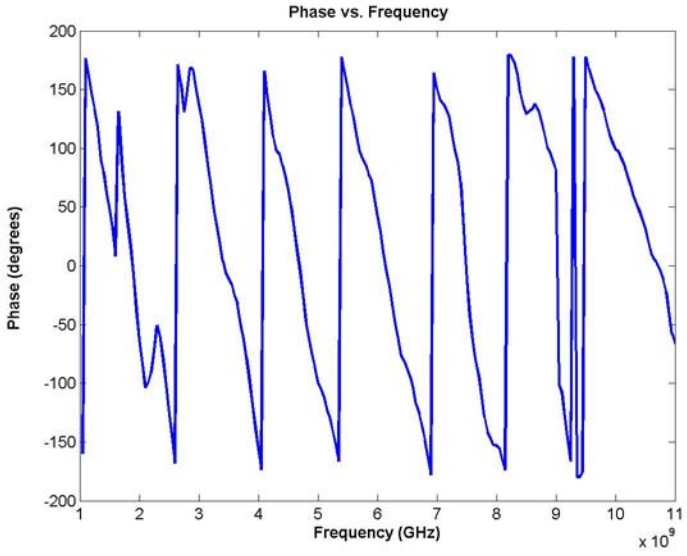

Figure 20. Phase vs. Frequency for Horn Antenna.

Figure 21 illustrates the group delay vs. frequency plot. As indicated by the phase plot, the group delay is not ideally constant. However, the plot seems to converge to an average group delay value of approximately 1ns with relatively few deviations compared to that which would be observed for a characteristically narrowband antenna. The frequency results for the horn antenna will be compared with several other wideband topologies as well as a narrowband wire antenna in order to see the relative differences in impedance matching, phase and group delay.

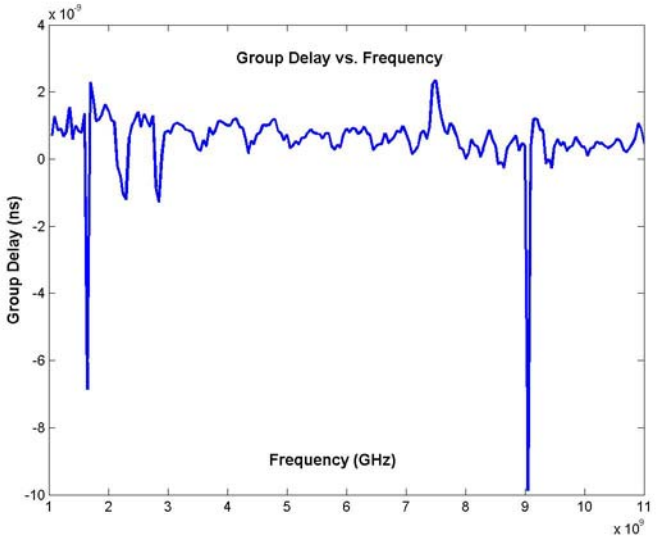

Figure 21. Group Delay vs. Frequency for Horn Antenna.

Group delay and linear phase are not overarching concerns in most *narrowband* antenna specifications because, by definition, the band of resonance in a narrowband antenna is the governed by frequency at which the antenna input impedance achieves a *linear* phase shift of 180°. This indicates LC resonance and real input impedance. Therefore, the narrowband frequency range that typically spans 100-200 MHz would naturally exhibit linear phase and constant group delay at resonance. Ultra Wideband provides a deviation from this concept in that resonance is not desired unless it is consistently resonant throughout the bandwidth. The higher Q value the antenna achieves (and higher level of resonance), typically the less bandwidth it exhibits. Therefore, the distinct 180° phase shift is not desired throughout the band in that high resonant points provide deviations in the group delay and phase plots.

The most significant results observed from this discrete system were the waveforms directly transmitted and received by the antennas. While many groups involved in UWB design observed various pulse shaping effects on the UWB pulse by the antenna including differentiation and other forms of distortion, no such effects were observed on our discrete system [16]. In fact, there were very few distortion effects observed.

Figure 28 shows the UWB pulse measured directly at the output of the transmit LNA superimposed on the waveform measured at the receive antenna terminals. It should be mentioned that the transmit pulse is attenuated by 30 dB in order to protect the input channels of the TDS 8000 oscilloscope receiver, which allow a maximum voltage wave amplitude of ± 2 V peak to peak.

As indicated by Figure 28, there are very few distortion effects from the transmit pulse to receive pulse. The conclusion that can be drawn from this is that the EMCO double-ridged waveguide horn antennas are certainly sufficient for guiding a pulse through a channel with little or no distortion of the pulse. The nonlinearity in the antenna phase and inconsistencies in the group delay observed in Figures 26 and 27 were not significant enough to have a pronounced effect on the UWB pulse.

One important point to consider is whether UWB OFDM (orthogonal frequency division multiplexing) systems would consider similar linearity issues for pulse transmission. These systems typically transmit pulses with approximately 500 MHz of bandwidth, in several "sub-bands" throughout the UWB range. This is most certainly the case, regardless of the bandwidth of the signal. Non-distortion in signal transmission and reception by an antenna is always desired; however, this is most often assumed in narrowband systems. For narrowband resonance, linear phase is easily achieved because, by definition, at resonance there is a linear 180° phase shift.

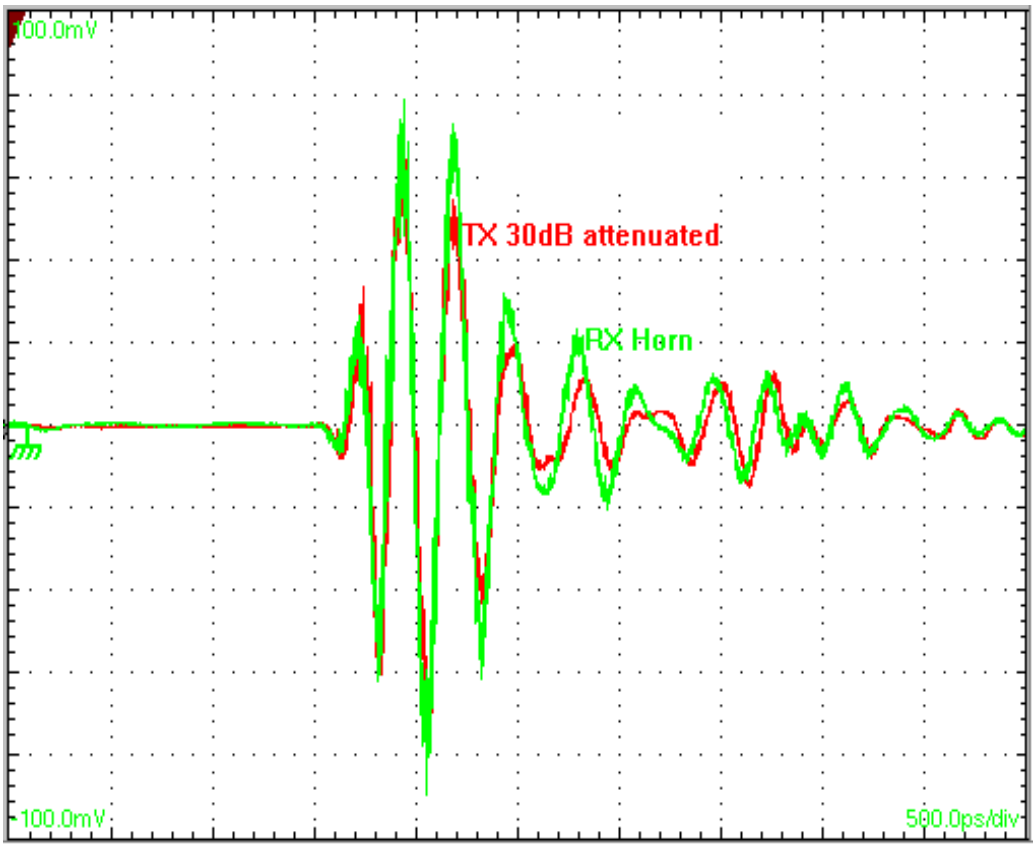

Figure 22. Transmitted Pulse (Red) Superimposed on Received Pulse (Green). Measured directly at antenna terminals.

Undoubtedly, the properties of gain and directivity, and hence, radiation pattern, would differ considerably between a horn antenna and a small planar antenna. In contrast to a horn antenna, the power radiated by a near omnidirectional antenna is not localized in any particular direction. Therefore, smaller gain and directivity would be expected. Gain and directivity specifications depend on the application for which the antenna is being used. Generally, a horn antenna or other highly directive antenna would only be used if the receiver location is known, or if multiple antennas are used. This research considers mainly the applications in which an omnidirectional antenna would be necessary, in that the location of the receiver is not known.

Regardless of the gain and directivity differences between the horn antenna and a small planar wideband antenna, this research suggests that it is possible to achieve similar time domain pulse reception characteristics. Although incident power levels of received time

domain pulses will not be comparable for line of sight (LOS) measurements, pulse shaping characteristics can certainly be compared between both antennas. Qualitative comparisons can be made with time domain results of transmission vs. reception pulses, and quantitative comparisons can be made with frequency domain results including impedance bandwidth, phase and group delay, and also anechoic chamber results including radiation pattern, directivity and gain.

CHAPTER

4

ANTENNA DESIGNS, SIMULATIONS AND RESULTS

In choosing an antenna topology for UWB design, several factors must be taken into account including physical profile, compatibility, impedance bandwidth, radiation efficiency, directivity and radiation pattern. In this research, several antennas were designed, simulated, fabricated, tested and characterized. Tradeoffs including strengths and weaknesses regarding the UWB required parameters were analyzed in each antenna. Among the antennas that will be presented in this research are the equiangular spiral slot patch antenna, the diamond dipole, the circular disc monopole, and differential and single ended tapered clearance elliptical monopole antennas. Some antennas that were simulated but not fabricated include the bowtie antenna configuration (which is a planar version of the biconical antenna described in chapter 2) a rectangular loop antenna and an elliptical dipole. These will also be briefly presented.

4.1 Equiangular Spiral Slot Patch Antenna

Babinet's Equivalence Principle and Rumsey's first discovery of frequency independence were described in 2.3.3. The spiral topology has long been known to achieve broadband impedance matching [4, 5], as first introduced by Rumsey's theory of frequency independent geometry. A significant amount of research has been conducted on the spiral antenna topology since Rumsey's first discovery; however, the recent allocation of the UWB spectrum by the FCC has piqued new interest in this antenna area [17,18,19]. Key motivation for this research includes compact size, low profile and low pulse

distortion upon transmission and reception. Several spiral antenna topologies have been explored and published in other works, including the Archimedes spiral antenna, the circular spiral antenna and the equiangular spiral antenna [20]. The equiangular spiral slot antenna was found empirically to have the best matching characteristics for a broad bandwidth [9]. Therefore, this is the topology that was initially chosen in this research to be a main contender as a wideband UWB antenna that would be compatible with portable electronic devices.

The spiral was constructed by the equation $\rho = \rho_o e^{a(\theta-\theta_o)}$, where ρ and ρ_o are the radial distance and initial radial distance for each arm of the spiral, respectively; θ and θ_o represent the angular position and initial angular position, respectively, and a is the expansion rate. The spiral was designed with an expansion rate of 0.38, initial inner radius of 1.5mm, total arm length of 6cm, outer radius of 2.25cm and arm slot ratio of 0.65. The total arm length was chosen for optimization of polarization and impedance bandwidth for the lower end frequency, while the slot ratio, outer radius and inner radius were also optimized for bandwidth through simulation. When the spiral arm length equals approximately one wavelength, the impedance begins to match the feedline and the radiated wave achieves circular polarization (CP), which is desirable for optimal reception [9,10]. The chosen spiral arm length theoretically enables CP and impedance matching at 1.6 GHz and higher. While this is certainly effective for UWB operation, size reduction can still be employed for a smaller profile and higher frequency cutoff.

Figure 13 shows a spiral slot patch antenna designed and simulated with Remcom's XFDTD software [21].

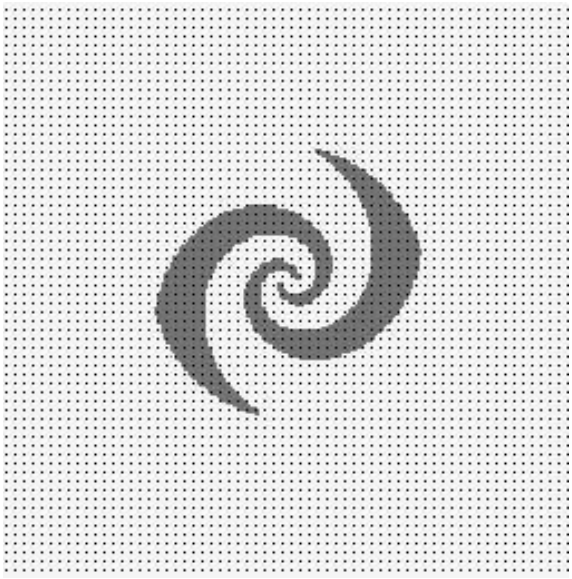

Figure 23. Spiral Slot Antenna Design. Remcom XFDTD simulation model.

It is easy to note that, by inspection, this antenna is self-complementary in that the metal spiral arms are similar to the free-space spiral arms cut out from the metal sheet. This antenna exhibits a differential feed at its center through the ground plane. By Babinet's Equivalence Principle, $Z_1Z_2 = \frac{\eta^2}{4}$, and $Z_1 = Z_2 = \frac{\eta}{2}$ Ω for all frequency. Extensive simulations have been run using a variety of dielectric constant values. While the spiral slot antenna generally matches to 188.5 Ω, increasing the relative dielectric constant value ε_r allows for adjustment of the matching impedance. This can be understood by noting the relationship $\eta = \sqrt{\frac{\mu}{\varepsilon_o \varepsilon_r}}$. By setting the dielectric constant value to10, an impedance match of approximately 59 Ω can be achieved. PCB manufacturers do not typically offer boards with dielectric constants larger than 10.

The design shown in Figure 23 has an outer radius of 2.25cm, making the total diameter of the slot approximately 4.5 cm, conformable with communications electronics. As mentioned previously, the reason for this physical dimension requirement is that the total arm length should approximately equal the value of the largest operating wavelength [9]

cross reference other spiral papers. With a value of 6 cm for the total arm length and a dielectric constant of 9.8, the corresponding lowest operable frequency is 1.6 GHz, suggesting that some size reduction is possible to achieve a lower operable frequency of 3.1 GHz. However, a more optimal impedance match is achieved for the higher frequencies than for the frequencies close to the lowest operable frequency. This can be observed in Figure 24, which illustrates the simulated imaginary and real antenna input impedance. For increasing frequency, the imaginary impedance converges to zero, while the real impedance converges to 50 Ω. A possible explanation for this phenomenon is that as frequencies increase, the electrical distance between the antenna element and the ground plane also increases, which limits the destructive ground effects, which tend to cancel out the radiation of the antenna. Figure 25 and Figure 26 show the return loss and VSWR simulation results, respectively, indicating that the desired specifications of Return Loss ≥ 10 dB and VSWR ≤ 2.0 have been achieved for the UWB bandwidth.

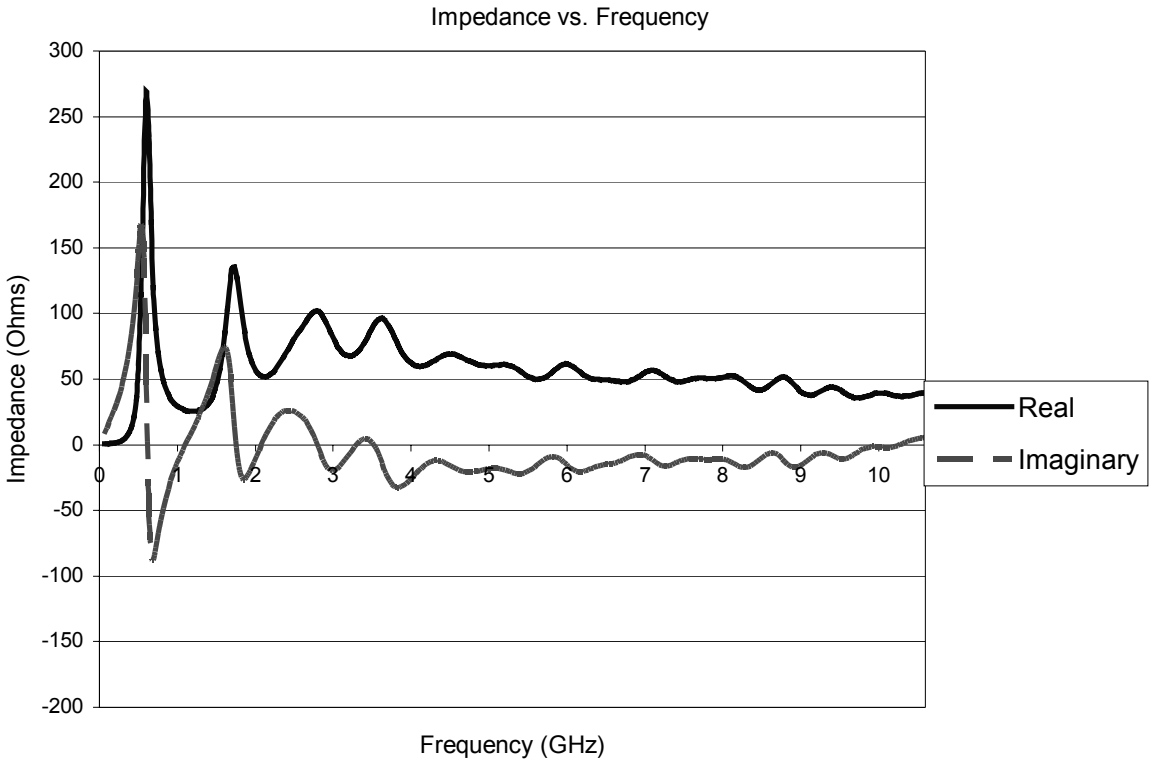

Figure 24. Input Impedance vs. Frequency. Results from XFDTD Simulation.

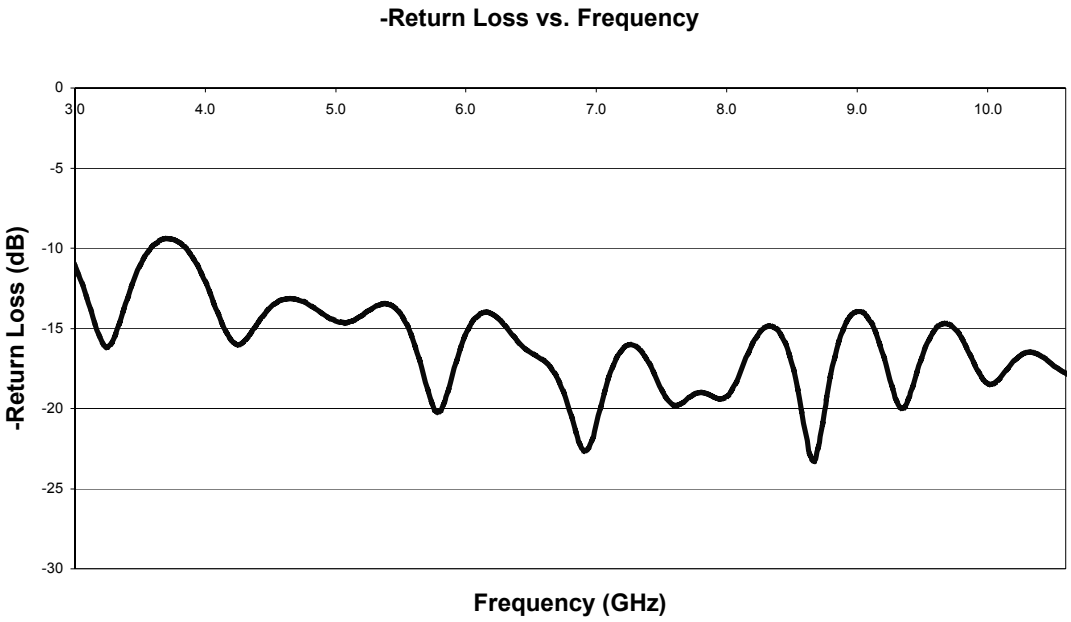

Figure 25. S11 (Return Loss) vs. Frequency. Results from XFDTD Simulation.

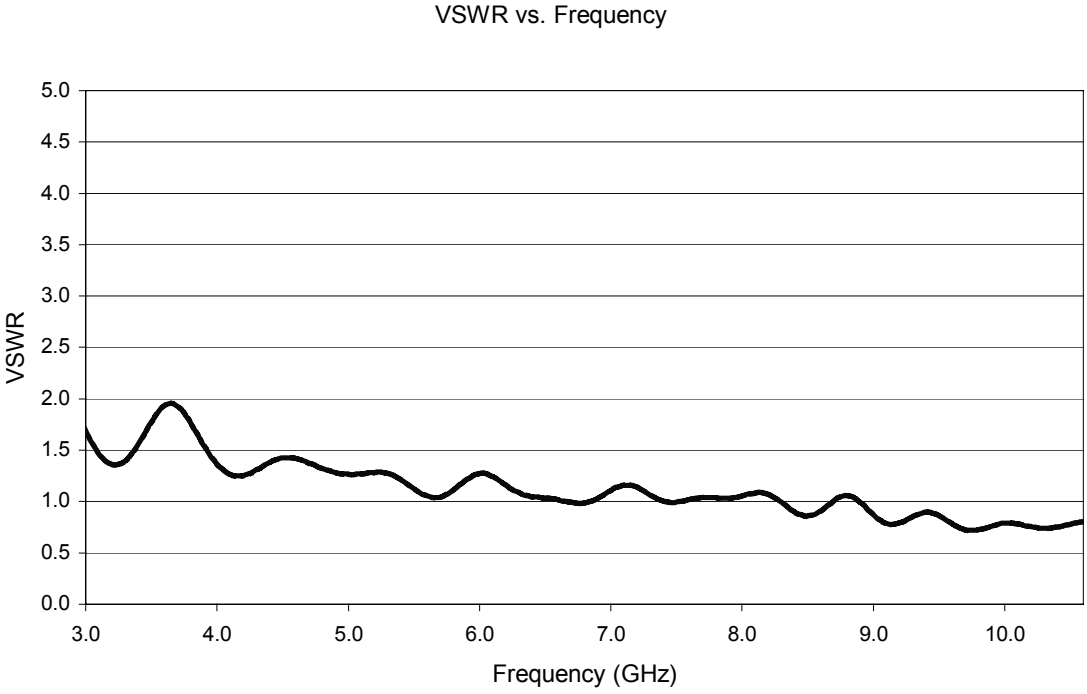

Figure 26. VSWR vs. Frequency. Results from XFDTD Simulation.

Simulations of this design have shown promising results with regard to meeting the UWB impedance bandwidth specification.

Next, as shown in Figure 27, a prototype of this antenna was fabricated on Rogers TMM10i material at MIT with a PCB milling router of 0.010" tolerance. The circular pattern cutout of the Rogers material was machined by an Omax waterjet, which uses a high pressure stream of water and garnet abrasive to cut through material.

Figure 27. Fabricated Equiangular Spiral Slot Patch Antenna. 2.5 cm radius, 0.5 cm thickness.

The distinguishing factor about this antenna is that it was designed with a bottom ground plane to make it conformable to portable electronic devices (PEDs), which require a ground plane for physical design compatibility. Spiral designs are typically two terminal devices with a large cavity to absorb back radiation, which makes them non-planar and physically non-conformal. Spiral antennas are not typically designed with a ground plane because image currents cancel the antenna's radiated waves and therefore limit the antenna bandwidth. However, thorough simulation with various dielectric constant values and dielectric thickness has yielded a successful simulated design for the spiral of Figure 23, printed on a Rogers TMM 10i board material with e_r=9.8 and thickness =

0.200” above a ground plane. Thinner dielectric material was found to degrade the antenna bandwidth performance, as the ground plane distance approached a limit that was too close, and therefore became destructive.

The key to this spiral design is that it is low profile and conformable to some small electronic devices. As mentioned previously, spirals typically incorporate an absorptive back cavity, which significantly thickens the size of the antenna and decreases its efficiency. They also incorporate a balun feed, which increases design complexity and can harm the radiation pattern. In this design, neither an absorptive cavity nor a balun is used. A balanced feed is achieved with an MMCX to SMA connector with positive and negative terminals each attached to the feed point of a spiral arm.

Upon initial investigation of impedance bandwidth results on a network analyzer, it was found that the impedance bandwidth was significantly impaired due to reflections at the ends of the spiral arms that were unaccounted for in the XFDTD simulation. The reflections traveled from the ends of the spiral arms back toward the feed at the antenna terminals and were re-reflected. The result was a narrowband antenna with reflections accounting for a great deal of noise in the VSWR measurement. This effect has been noted in prior research [22]. .Resistive paint and 3mm thick foam absorber was placed around the circumference of the antenna and at the ends of the spiral arms. The resistive termination enabled a wideband impedance match, which absorbed current spikes that would have otherwise reflected toward the feed terminals. The radiation pattern was also improved, as the reflections are not re-radiated.

Ground plane spacing was also minimized. Antennas held over ground planes require at least $\lambda/4$ spacing at the lowest operating frequency such that image currents created by the ground plane do not cancel the radiation of the antenna. The required spacing for the measured cutoff frequency of 1.3 GHz is approximately 5.6 cm in free space, and 1.8 cm on the Rogers material. The high dielectric constant Rogers material enabled size miniaturization and also lengthened the electrical distance from the spiral element to the

ground plane, at the cost of reduced radiation efficiency. At a spacing of 0.5cm, a profile 3.7 times thinner than that theoretically required is achieved.

Figure 28 shows the measured VSWR plot for the spiral antenna, indicating a good impedance bandwidth for the entire UWB frequency range, only raising above the VSWR = 2 limit twice throughout the UWB frequency band.

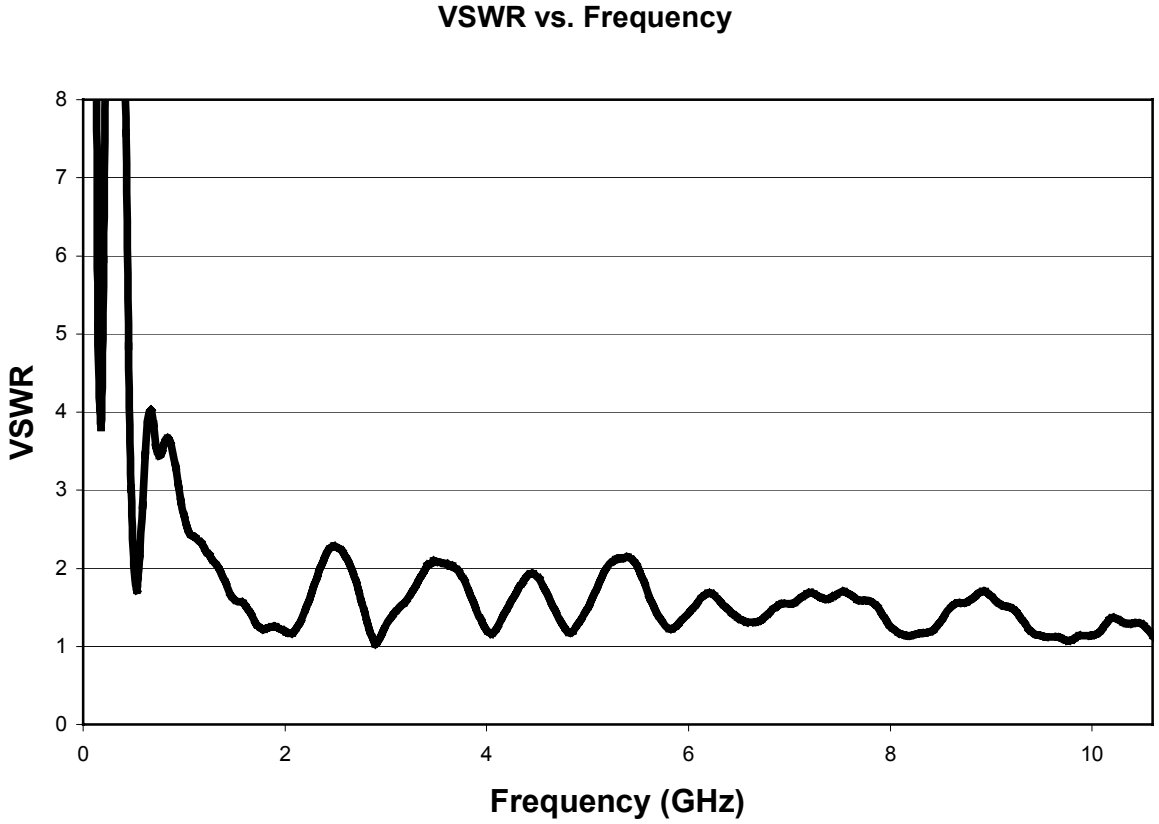

Figure 28. Measured VSWR vs. Frequency plot for the Equiangular Spiral Slot Patch Antenna.

While the frequency results indicate that the impedance bandwidth is adequate, a time domain plot is required to determine how well the spiral guides a UWB pulse to the antenna receive terminals. Figure 29 illustrates the time domain receive vs. transmit pulse for the spiral antenna.

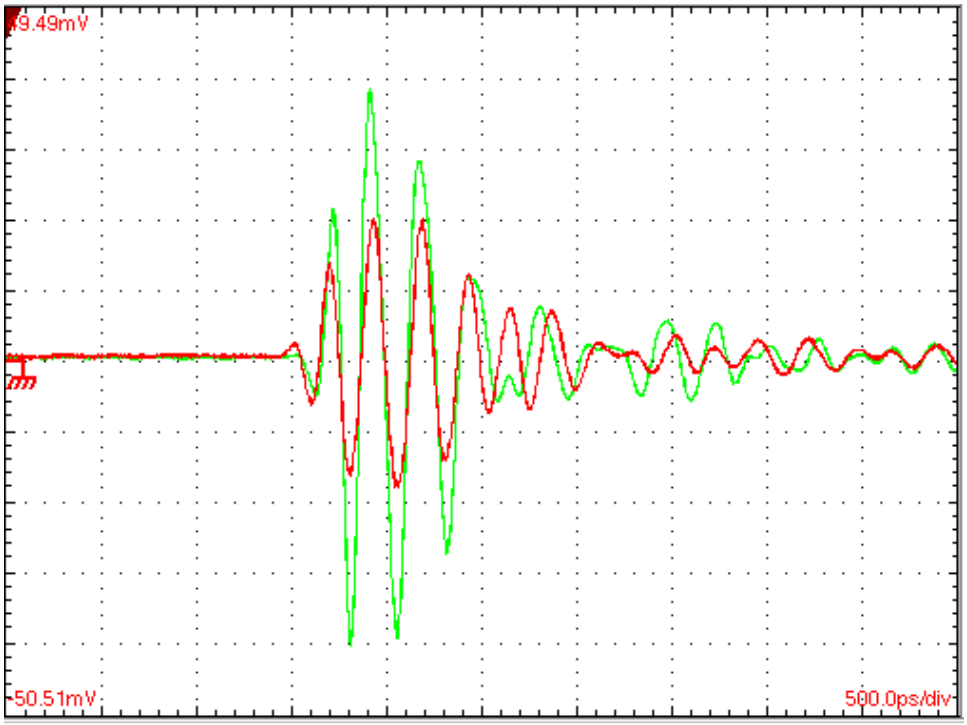

Figure 29. Time Domain Pulse. Received Pulse from spiral antenna superimposed on transmitted pulse. Transmit pulse is green, and receive pulse is red.

Comparing this plot with that of Figure 22, it can be observed that while the pulse shape is retained relatively well with the exception of ringing at the end of the receive signal, the pulse is attenuated significantly, which lead to a decrease in SNR (signal to noise ratio). The time domain plot above is displayed in units of 10mV/div while the plot of Figure 11 is displayed in units of 20mV/div in order to better observe the received pulse shape. Therefore, the maximum amplitude of the pulse is attenuated by approximately 75% from the maximum amplitude of the transmit pulse shown on the oscilloscope. The power spectrum of the transmitted pulse is indicated in Figure 17. As mentioned in Chapter 4, the transmit pulse was already attenuated by 30 dB when measured to account for the sensitivity of the receive oscilloscope. This generally accounts for the losses incurred during air transmission, given by the Friis transmission formula, which can be referenced in [9-11]. The attenuation in comparison to that of Figure 22 indicates low radiation efficiency as the result of resistive loading by absorptive material and resistive paint. Another contributor to the low radiation efficiency was likely the thick dielectric material, in which several losses could be incurred. While the thickness was necessary

for adequate bandwidth while operating over a ground plane, this is achieved at the cost of decreased radiation efficiency. This will be further discussed when radiation patterns from Lincoln Laboratory's mm wavelength anechoic chamber are presented.

4.2 Narrowband Monopole Antenna

Before approaching several other wideband antenna designs, a comparison to a simple narrowband wire antenna should be made. This will provide a clear perspective on the effect of impedance mismatch and phase nonlinearity on the time domain pulse. A narrowband monopole achieves its first resonant frequency at multiples of $\lambda/4$, and a narrowband dipole achieves resonance at multiples of $\lambda/2$. Multiple resonances occur at odd harmonics of the fundamental resonant frequency.

A narrowband wire monopole antenna was built in order to observe comparative effects on pulse reception in the time domain, and also impedance bandwidth characteristics. A picture of this wire antenna is shown in Figure 30.

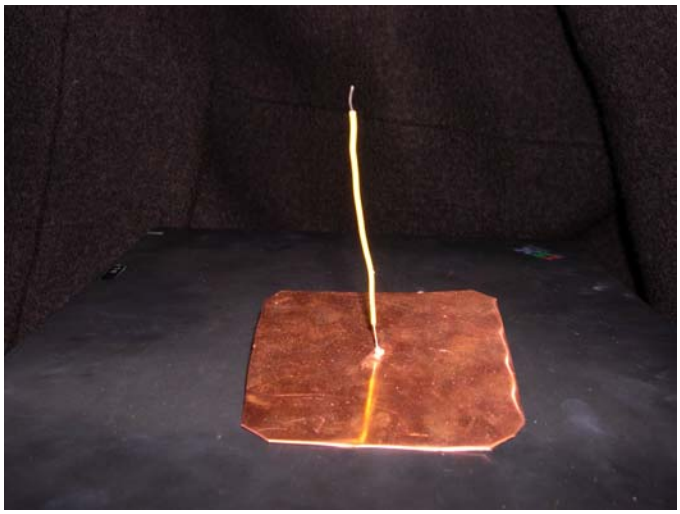

Figure 30. Picture of narrowband wire antenna.

This monopole antenna is one of the most basic and most fundamentally understood antennas theoretically and practically, and was fabricated simply for comparative purposes. It can be observed in Figure 31 that the impedance bandwidth of this wire antenna does not achieve the VSWR = 2 specification throughout the UWB frequency range, nor does it achieve this requirement except for at the very narrow frequency ranges at approximately 2.2, 4, 5.5, 7, 8.7 and 10.2 GHz. With a length of approximately 9.5 cm, this antenna achieves its fundamental resonance at a frequency with $\frac{\lambda}{4} = 9.5cm.$ Given $\frac{c}{f} = \lambda$, the fundamental frequency of the antenna can be found by: $\frac{c}{.095 * 4} =$ .790 GHz. This antenna will theoretically achieve harmonic resonances at odd multiples of the fundamental frequency, or at 2.37 GHz, 3.9 GHz, 5.5 GHz, 7.1 GHz, 8.6 GHz, and so on. Inspection of the VSWR plot leads to the conclusion that the theoretical resonant frequencies are very close to the measured resonant frequencies. The reason that the odd multiples of the fundamental frequencies achieve resonance can be understood when considering the impedance characteristics of a Smith chart. One revolution about the Smith Chart entails a revolution of $\frac{\lambda}{2}$, whereby a full revolution entails that the same input impedance will be found at values of 0, $\frac{\lambda}{2}$, $\frac{3\lambda}{2}$, $\frac{4\lambda}{2}$, and so on. Resonance occurs at a particular antenna input impedance, typically 50Ω. Then, theoretically, if the fundamental resonance occurs at $\frac{\lambda}{4}$, the next harmonic will be found $\frac{\lambda}{2}$ away, or $\frac{3\lambda}{4}$, and the next harmonic will be at $\frac{5\lambda}{4}$, and so on. Therefore, the quarter wavelength monopole achieves resonance at its fundamental frequency, and other odd harmonics of that fundamental frequency. More information can be found about Smith charts in [9-11].

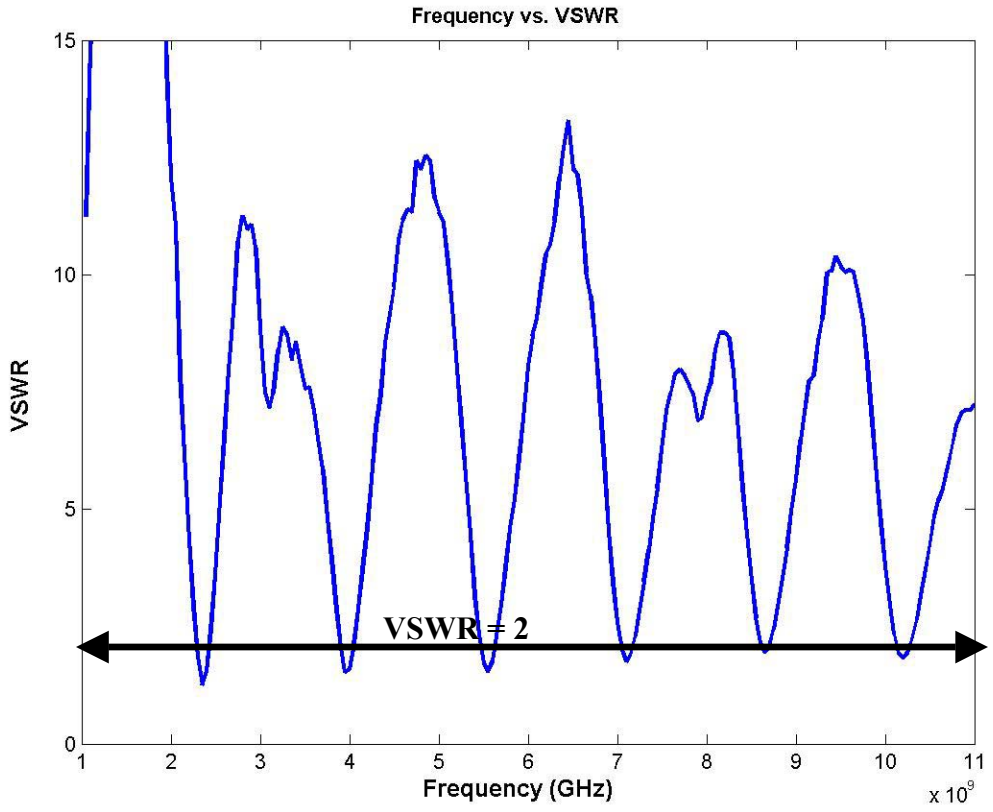

Figure 31. Measured VSWR vs. Frequency for Narrowband Wire Antenna.

The phase of this antenna shown in Figure 31 exhibits several very sharp resonances at each of the frequencies mentioned previously. Sharp 180° phase shifts are clearly indicative of these resonant points. The phase plot of the horn antenna (Figure 20) compared with that of the monopole wire antenna demonstrates that the phase of the horn antenna exhibits a more linear characteristic throughout the frequency range.

Comparison of the group delay plot (Figure 33) with that of the horn antenna (Figure 21) is slightly counterintuitive in that the group delay plot of the wire antenna seems to be more constant than that of the horn antenna, with less noise throughout the bandwidth. However, it is important to consider that the frequency values for which the group delay appears constant for the wire antenna are the values for which the antenna is maximally mismatched. These ranges should not be considered in the group delay plot, as the impedance mismatch between the resonant points is so sizeable, most of the signal

incident at the antenna terminals will be reflected back and forth between the antenna feed line and the antenna terminals, the received pulse will be attenuated and distorted.

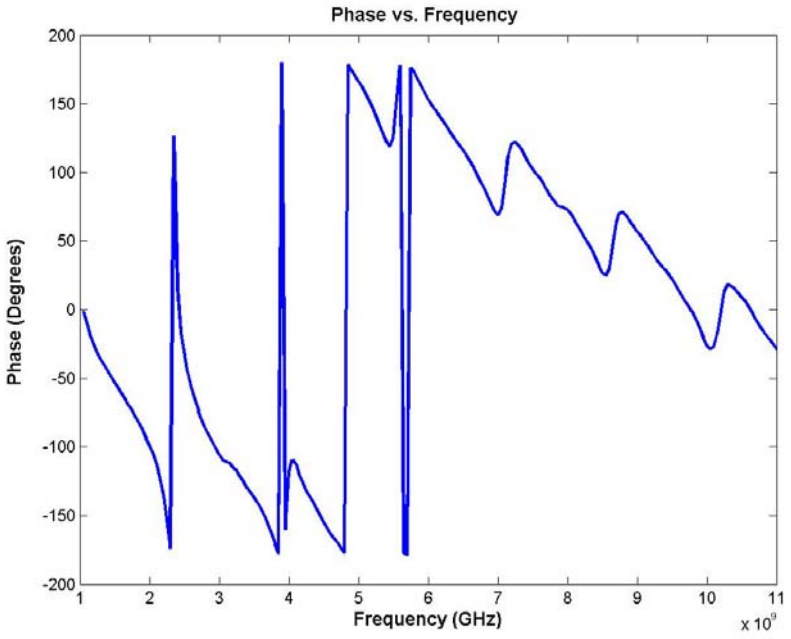

Figure 32. Measured Phase vs. Frequency for Narrowband Wire Antenna.

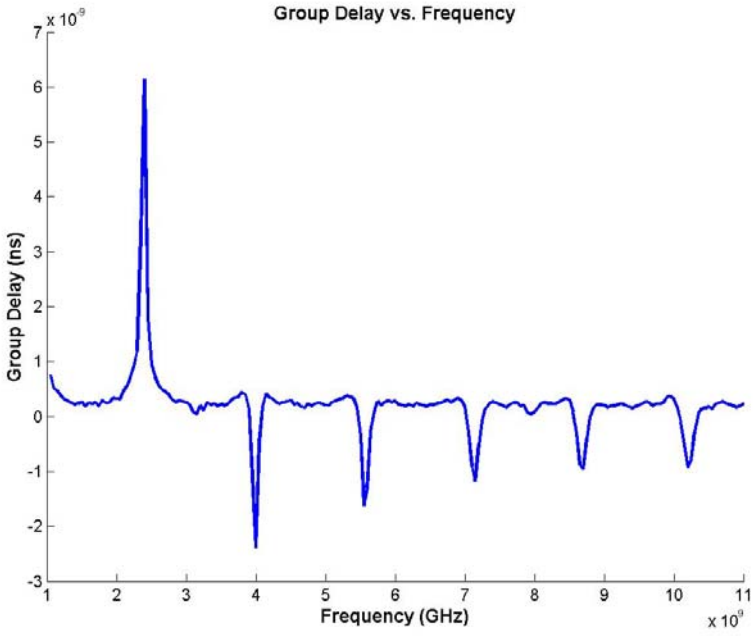

Figure 33. Group Delay vs. Frequency for the Narrowband Wire Antenna.

The important point to be made is that group delay is a relevant metric to be considered for the frequency ranges that achieve a sufficient impedance match of VSWR < 2. For frequency ranges through which the impedance is not impedance matched, group delay should not be considered.

The time domain plot of the received pulse superimposed over the transmitted pulse for the narrowband monopole antenna is shown in Figure 34. This plot is comparable to the time domain plots of the pulses for the horn antenna and the spiral antenna in that it is measured with 500 ps/div and 10mV/div. The received pulse of the wire antenna shows a great deal of distortion, in that the pulse information is lost within the noise of the signal.

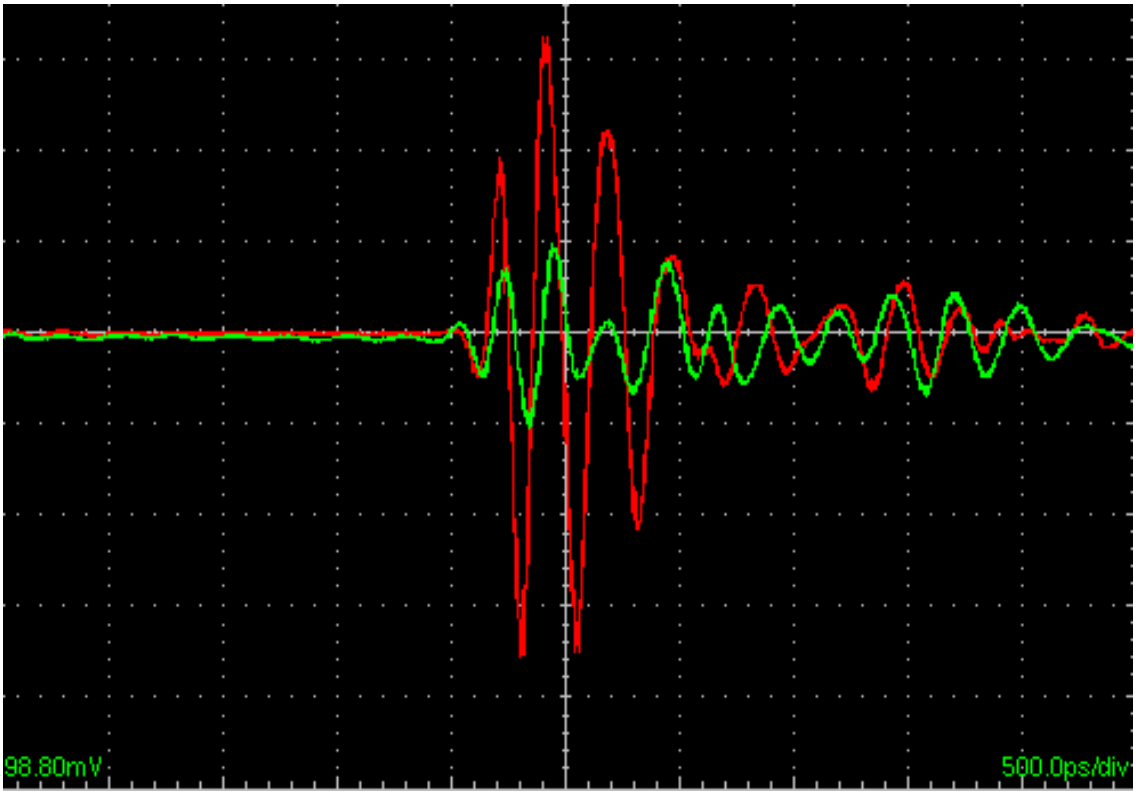

Figure 34. Time Domain plot of wire antenna received pulse superimposed over transmitted pulse. Transmit pulse is red, and receive pulse is green.

4.3 Diamond Dipole Antenna

The diamond dipole antenna configuration follows from theory that thickening a dipole increases its impedance bandwidth. Time Domain, Inc. proposed the use of these antennas for transmitting and receiving gaussian impulse waveforms in 2001 [12]. As described in Chapter 2, thickening a dipole spreads the energy throughout the dipole, therefore lowering its resonant Q value. Thin dipoles are analyzed theoretically under the assumption that all of the energy of the dipole is located within a few wire radii of the antenna. If this assumption holds true (as it does for thin wire antennas), a TEM transmission line approximation can be applied to the analysis of these antennas. However, this assumption breaks down as the antenna thickness is increased. Also, it becomes much harder theoretically to solve Maxwell's equations for more complex shapes. Simulation tools and empirical results attest to the claim that thickening a wire antenna increases its bandwidth.

4.3.1 . Sharp-Edged Wire Diamond Dipole

Another theory that lead to the development of the diamond dipole configuration is that antennas in a loop configuration with sharp corners at the edges provide current nulls at the edges, which leads to lower standing wavelength ratios (SWR) at antiresonant frequencies. This therefore leads to broader bandwidth. [9,10] The sharp edge wire diamond dipole configuration, pictured at the right of Figure 11, was simulated along with three other configurations including a solid version of the wire diamond dipole, a wire diamond dipole incorporating curved edges, and a solid diamond dipole incorporating curved edges.

While the sharp-edged wire diamond dipole of Figure 11 was simulated to achieve an impedance bandwidth of approximately 500 MHZ, from 2.9 GHz to 3.4 GHz, the other configurations yielded over twice the bandwidth. Therefore, the sharp-edged wire

diamond dipole was not fabricated. Figure 35 shows the three other variations of the diamond dipole antenna including a solid sharp-edge dipole, a wire curved-edge dipole, and a solid curved-edge dipole.

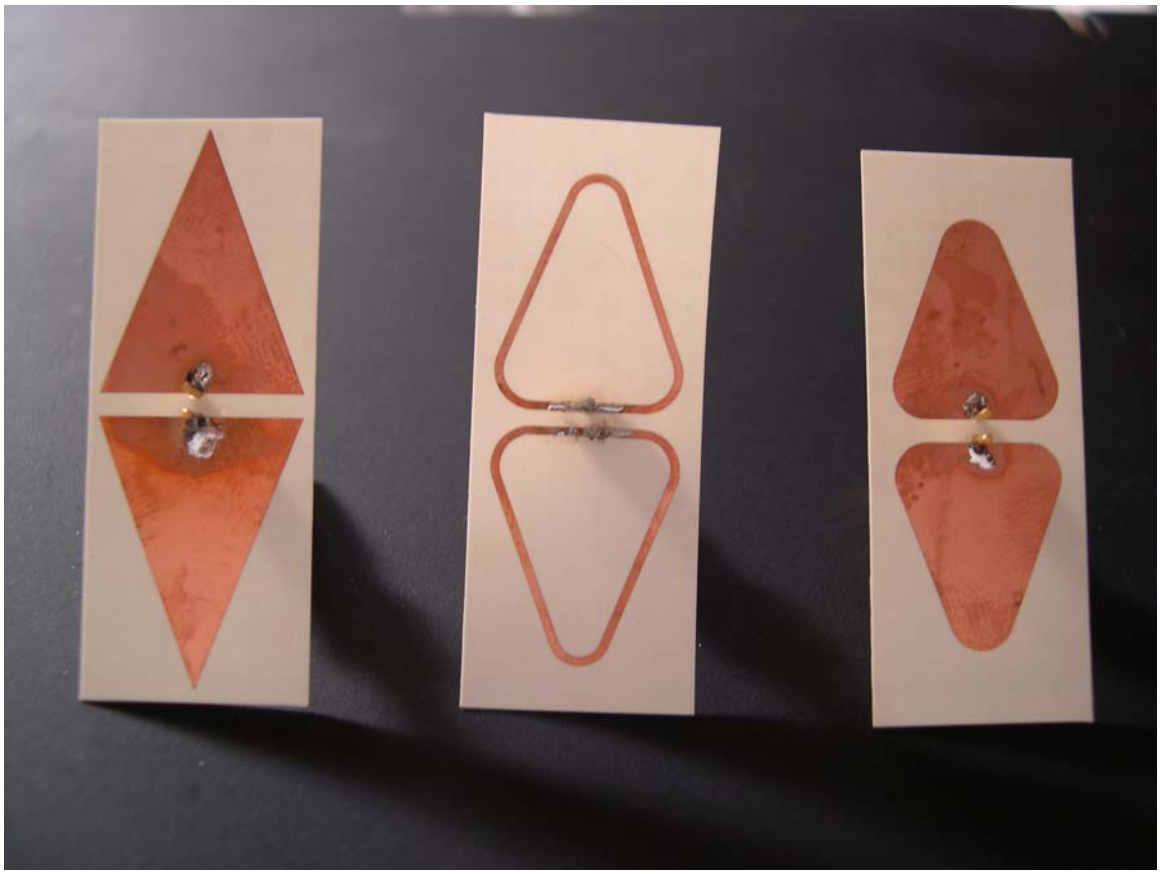

Figure 35. Three configurations of a diamond dipole antenna [12] including a solid sharp-edge dipole, a wire curved-edge diamond dipole and a solid curved-edge diamond dipole.

4.3.2 Solid Sharp Edge Diamond Dipole

The leftmost antenna, the solid sharp-edge dipole, follows from the theory that adding sharp corners to a thick dipole antenna adds current nulls at antiresonant frequencies. If the height of this antenna (at 0.774") is equated with the height of a thin λ/2 dipole, an operating frequency of 3.8 GHz and bandwidth of approximately 100 MHz would be expected. This antenna achieved ten times the amount of bandwidth expected of a linear dipole of the same height, at 1.18 GHz of bandwidth, operating from approximately 4-5

GHz. The measured VSWR result can be observed in Figure 36. The antenna likely achieves a resonant frequency higher than that expected because the current path can travel out along the shorter edges of the antenna, rather than being confined to the full length of the λ/4 thin wires which make up the λ/2 dipole.

4.3.3 Curved Wire Diamond Dipole

The middle antenna, the wire curved-edge diamond dipole, incorporates curvature, which allows for smoother impedance transition. The wire antenna shown in the middle of the figure attains a slightly higher bandwidth at a lower operating frequency. The reason for its lower operating frequency is that the effective current path from the antenna feed to the end of the antenna was lengthened. The bandwidth achieved for this antenna was 1.24 GHz from 3.2 to 4.54 GHz. It should be noted that the fractional bandwidth of this antenna is 33%, while the fractional bandwidth of the sharp-edge solid dipole is 26%, when the center frequencies are taken into account. It should be noted that the simulated fractional bandwidth of the sharp-edge wire dipole was only 15%.

4.3.4 Curved Solid Diamond Dipole

The rightmost antenna, the solid curved-edge dipole, achieves the largest bandwidth of the three configurations, with 2.9 GHz of bandwidth from 4.5 – 7.4 GHz. This corresponds to a 49% bandwidth for its center frequency. This antenna is apparently the optimal configuration of the diamond dipole in that it exploits the "thick dipole" theory, while also easing the impedance variation by incorporating a curved surface. Analysis of these results leads to the conclusion that the pulse is much more easily guided by a smooth, tapered variation in shape rather than sharp corners, which cause scattering and a non-uniform variation in input impedance. The solid-curved dipole operates at a higher frequency than the wire curved dipole and the solid sharp edge dipole because its edges are blended with a relatively large radius (0.100"), which makes it shorter and therefore compatible with higher frequencies and smaller wavelengths. Also, the current path from the feed point to the ends of the antenna is shortened from that of the wire-curved dipole.

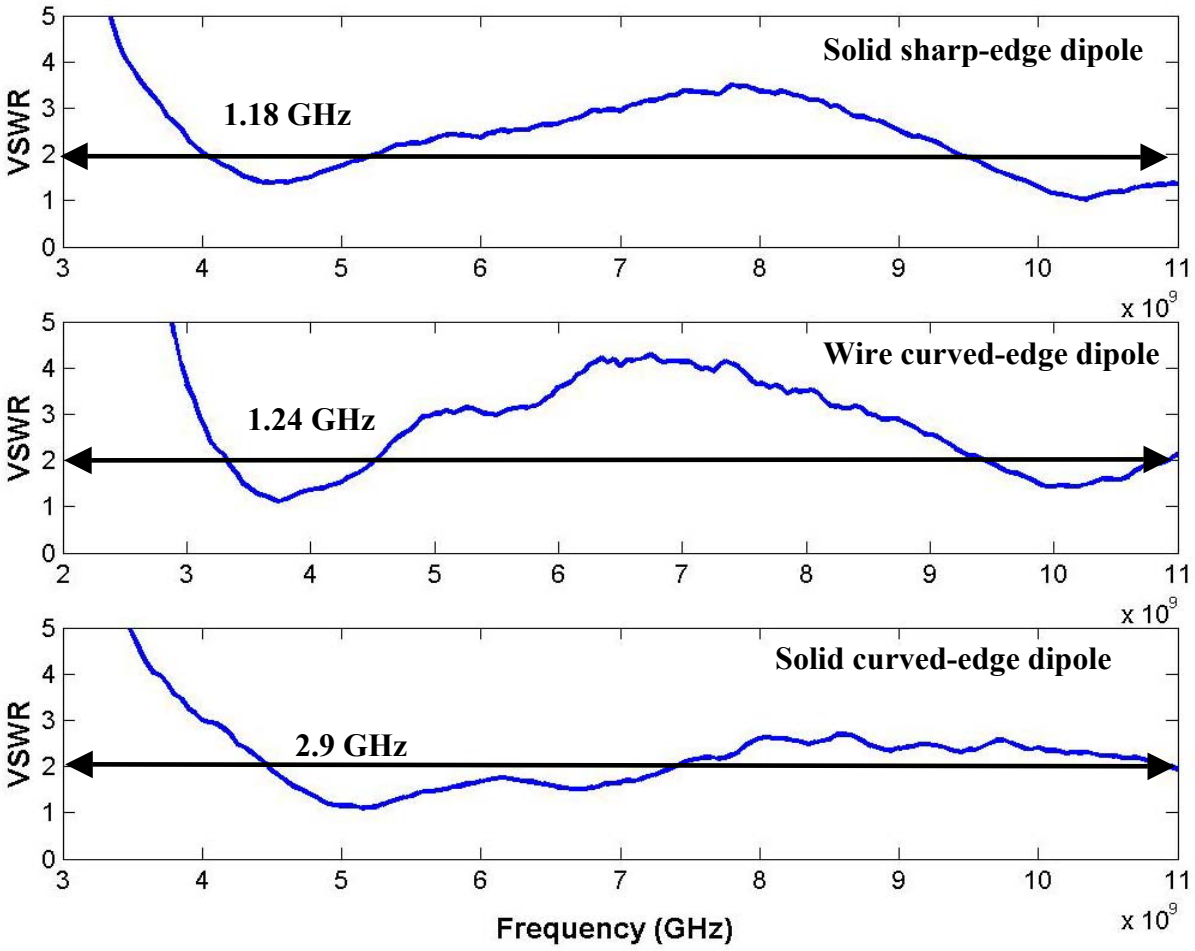

Figure 36. VSWR plots for Diamond Dipole Configurations.

4.4 Circular Disc Monopole Antenna

One of the strongest contenders in terms of impedance bandwidth and radiation efficiency is the circular disc monopole (CDM), initially proposed by Kumar and Ray in 2003 and in 1998 [23, 24]. This achieves very high radiation efficiency and impedance matching capability in that the initial 50 ohm impedance match is made at the feed, and the pulse is guided from the feedpoint along the circular radiator by the tapered clearance from the ground plane. This enables very little variation in impedance. Also, the resonant modes of the circular resonator are characterized by the roots of the Bessel function rather than sine or cosine functions that tend to describe the fields of rectangular

resonators [23,24]. This results in the resonant modes being much more closely spaced than those of other antenna configurations, which leads to less variation in impedance bandwidth. Figure 37 shows a photograph of a circular disc monopole designed, simulated and fabricated at MIT.

4.4.1 Design

In this research, a CDM is designed with a radius of 2.54cm and a ground plane 7.6cm x 7.6cm, the theoretical lower end frequency is given by [24]

$$f = \frac{c}{\lambda} = \frac{30 \times .24}{L + r} GHz \qquad \text{Equation 25}$$

Where L = disc height (cm), and r =equivalent radius given by $2\pi rl = \pi r^2$. The equivalent radius is derived by equating the planar disc area with that of a cylindrical wire (monopole) of height L. For this particular configuration, the parameters L and r were set to 2b and a/4, respectively [24]. The theoretical lower frequency is 1.28 GHz, and the measured lower frequency value is 1.45 GHz. Properties of this antenna including circular polarization, demonstrable wide bandwidth, easy construction and high radiation efficiency make it an interesting candidate to study pulse reception properties. High radiation efficiency is attained because the disc radiates in the absence of lossy dielectric, which tends to attenuate the radiation efficiency.

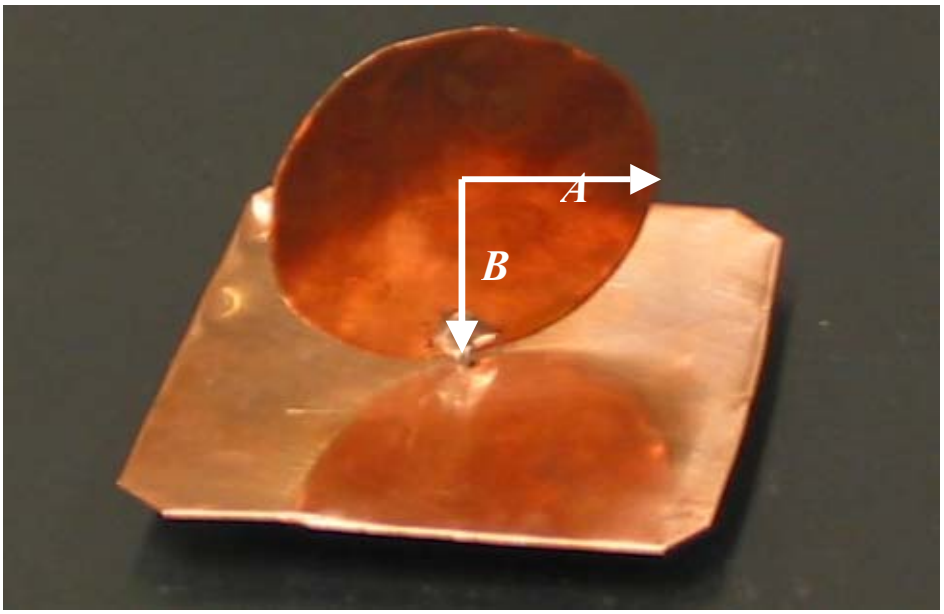

Figure 37. Circular Disc Monopole.

This antenna topology was easily constructed with a feed point distance of 39.4 mils from the antenna to the ground plane, suspended by the center conductor of an SMA connector.

4.4.2 CDM Results

Excellent impedance bandwidth can be observed in the VSWR plot of Figure 38, which indicates that not only does the antenna match the impedance requirements; the antenna exceeds the minimum specification in that it achieves a VSWR ≤ 1.5 throughout the UWB frequency range. This corresponds to less than 4% of the power reflected at the antenna terminals due to reflections from impedance mismatch. This is calculated by using the equation for VSWR as described in chapter 2:

$$\text{VSWR} = \frac{1+|\Gamma|}{1-|\Gamma|}$$

With this equation, $|\Gamma|$ can be solved. For the case of the CDM the reflection coefficient Γ attained a value of less than 0.2 throughout the UWB spectrum. Considering power

reflection measurements, the power delivered to the antenna is proportional to $(1-|\Gamma|^2)$, or 96%.

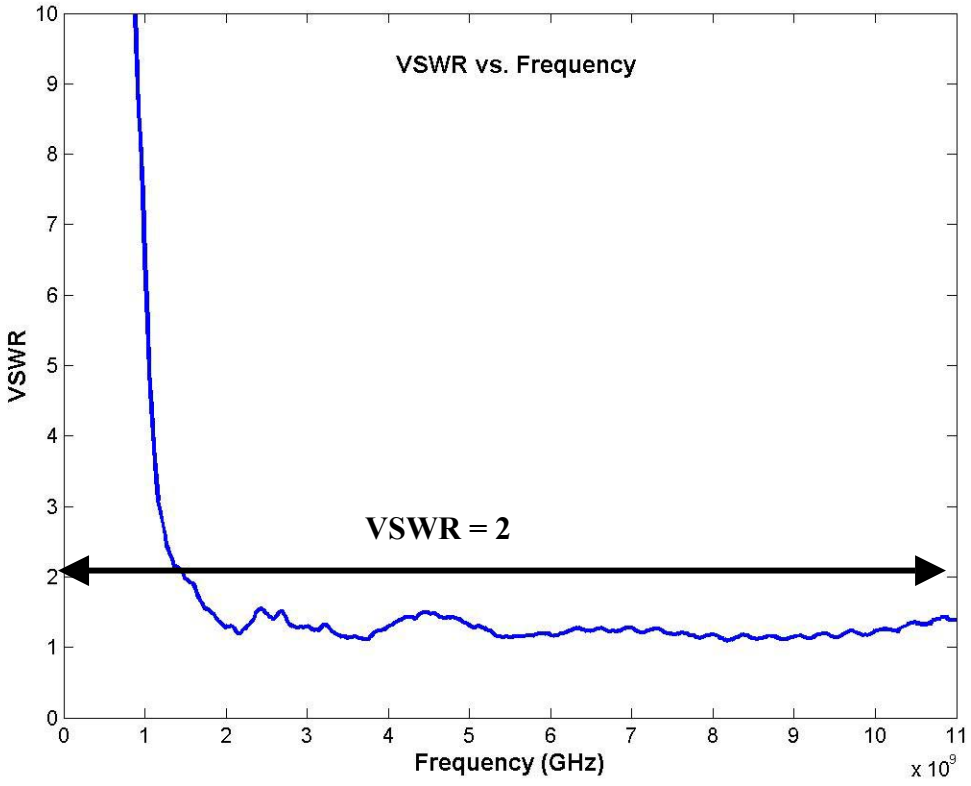

Figure 38. VSWR plot for the CDM.

Given that the CDM achieves excellent impedance bandwidth and also high radiation efficiency, it is natural to expect its impulse reception quality to be strong. Figure 39 illustrates the time domain received pulse superimposed over the transmit pulse. This plot, consistent with the other time domain plots presented, was measured with 500ps/div and 10mV/div. The red pulse represents the transmit pulse, and the green pulse represents the receive pulse.

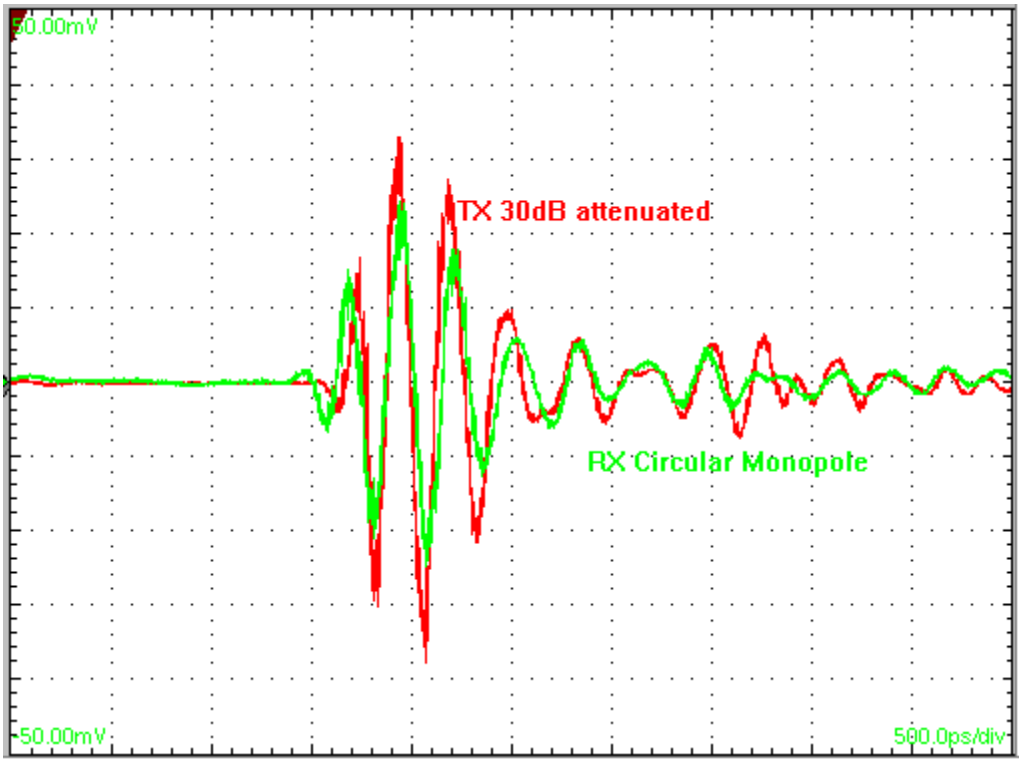

Figure 39. Time Domain pulse characteristics of CDM. Transmit pulse (red) vs. Receive pulse (green).

Figure 39 shows very little distortion from the transmitted pulse to the received pulse. Again, this time domain measurement was taken at 500ps/div and 10mV/div. The received pulse taken at the terminals of the circular monopole antenna is superimposed over the transmitted pulse, which is red. This indicates near linear phase and near constant group delay. This can also be observed by the impedance bandwidth, which is even throughout the frequency spectrum.

While the CDM clearly has excellent impedance bandwidth, good radiation efficiency and time domain characteristics, the caveat to this antenna is its physical profile. Similar to the double ridged waveguide horn antenna, which has exceptional impedance characteristics and impulse transmission and reception qualities, its obtrusive physical profile renders it incompatible with portable electronic devices and integrated circuits.

4.5 Single Ended and Differential Elliptical Monopole Antennas (SEA and DEA)

4.5.1 Designs

Keeping in mind the strengths of the circular disc monopole antenna including impedance bandwidth, radiation efficiency and time domain characteristics, this research shows that tapering the clearance from the ground plane to the radiating disc such that it is coplanar with the antenna actually yields very similar results to the CDM. This enables tapering similar to that of a vivaldi antenna, which also achieves wideband and nearly frequency independent properties [25]. Pictures of single ended and differential elliptical antenna (SEA and DEA) configurations are shown in Figure 40, Figure 41 and Figure 42. In fact, the same equation used to define the fundamental lower end operating frequency of the CDM, equation 37, can be used to determine a value close to that of the planar single ended and differential elliptical monopole antennas (SEA and DEA). This equation is again presented below for reference:

$$f = \frac{c}{\lambda} = \frac{30 \times .24}{L + r} GHz$$

Adjustment for ellipticity is achieved by defining L = 2*y radius (cm) and r = (x radius)/4 (cm).

The equivalent radius is derived by equating the planar disc area with that of a cylindrical wire (monopole) of height L. This equation has been applied to the DEA and SEA in this research for quite accurate results in design, simulation and measurements.

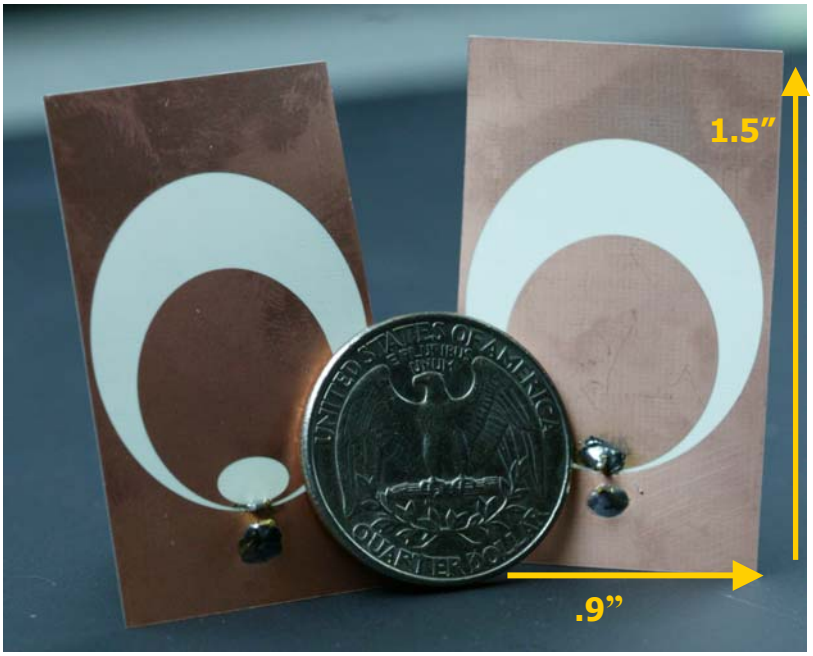

Figure 40. Single Ended Elliptical Monopole Antennas.

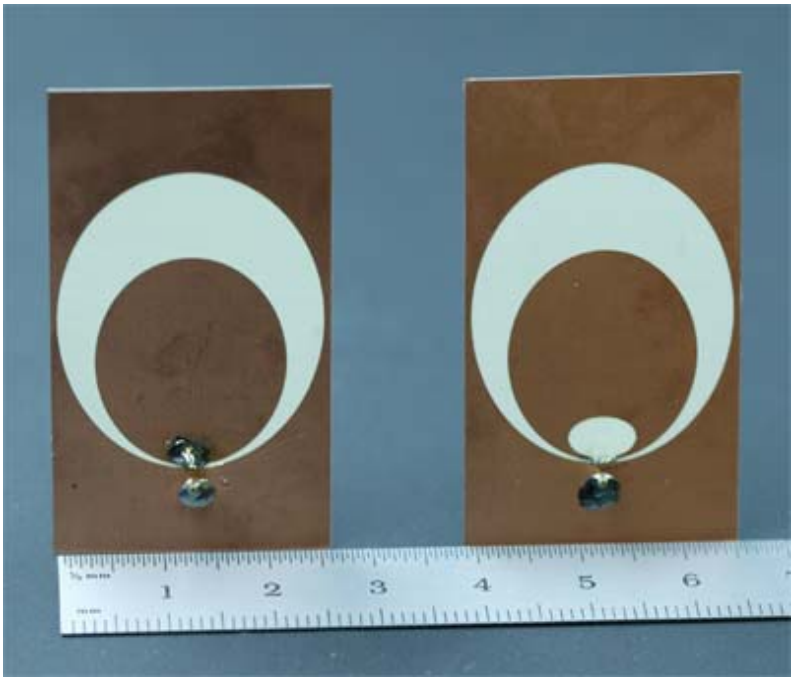

Figure 41. Single Ended Elliptical Monopole Antennas, measured in cm for size demonstration.

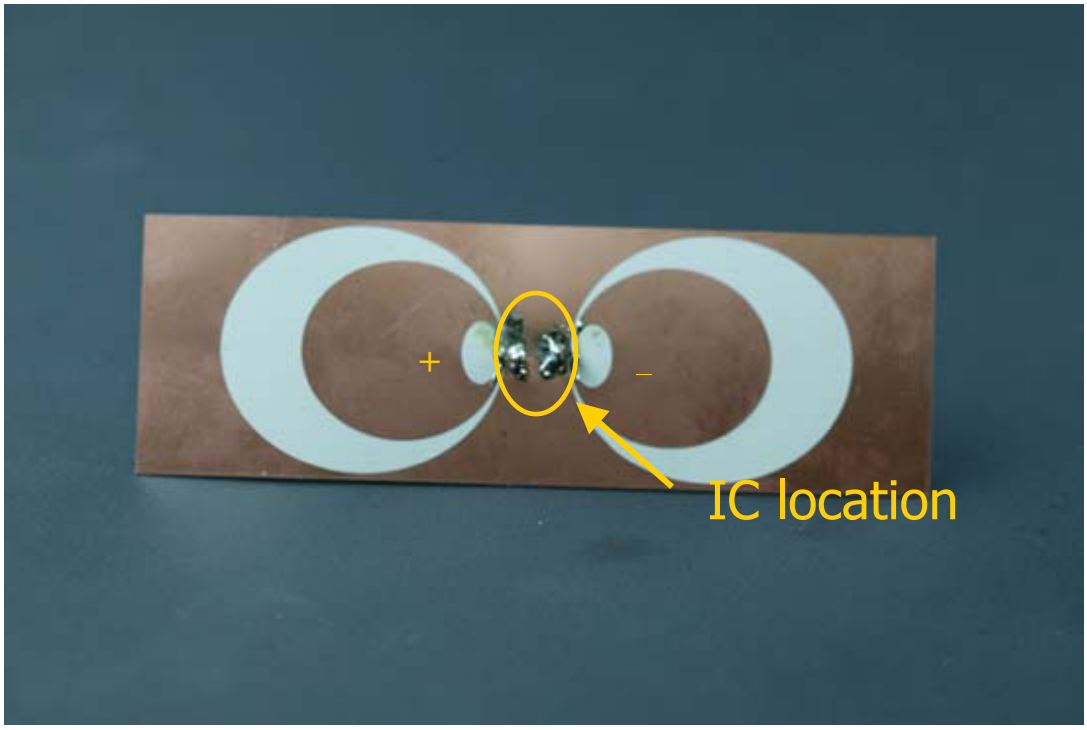

Figure 42. Differential Elliptical Antenna.

The single ended antennas shown in Figures 48 and 49 stand 0.9” wide and 1.5” tall, with a thickness of 0.004”. Their compact planar profile renders them compatible with portable electronics and integrated circuits. The design allows for an integrated circuit to be downbonded to the ground plane of the antenna (which is tapered about the inner elliptical antenna), with bondwire extending to the feedpoint of the antenna, at the center and bottom of the elliptical disc.

The horizontal elliptical slot cutout near the feed in the rightmost antenna of Figure 40, the leftmost antenna of Figure 41, and both terminals of the differential antenna, are known as antenna loads. Antenna loading has been practiced for several years in narrowband antenna research including microstrip patch antennas in order to lower the operating frequency of an antenna by increasing the length of the current path through it, therefore enabling size reduction of the antenna. Here, the antenna load achieves a similar effect in that the cutout near the antenna feed effectively lengthens the current path about the elliptical disc, therefore slightly lowering the fundamental frequency of the

antenna. This enables size reduction of the antenna, and will be discussed further with regard to results.

The differential antenna, shown in Figure 42, allows for the integrated circuit to be housed within the common ground plane of the positive and negative terminals of the antenna, with bondwire extending to the positive and negative terminals of the antenna. There are several benefits to using a fully differential antenna. A differential antenna allows for a fully differential system from front to back. This eases the design complexity for the RF front end of the UWB radio in that the single ended to differential converter is not required in the front-end design. Also, this would decrease the overall noise figure that would have been increased by the single ended to differential converter. There are tradeoffs to this design, as well. First of all, each feedpoint requires a sufficient impedance match such that mismatch between the positive and negative terminal is minimized. If one antenna terminal becomes detuned, pulse distortion will be present at one terminal, but not the other. Careful consideration must be taken in matching the lengths of the wires such that there is no delay mismatch between the terminals.

The key intuition behind the SEA and DEA designs is the understanding of the bandwidth effects at various higher modes within a circular resonator such as a CDM. The roots of the derivative of the Bessel function characterize these closely spaced modes [24]. Since the antenna distance from the ground plane consistently increases symmetrically from the antenna feed, the impedance change from one resonant mode to another resonant mode is very small, and therefore enables a very large bandwidth from the fundamental resonant frequency on through much higher frequencies. The designs presented here differ from that of a CDM in that they are coplanar with their ground planes rather than perpendicular, and they are printed on dielectric substrate. As such, they have tapered clearance area from the ground plane, which increases fringing capacitance and therefore may cause a slight decrease in the fundamental frequency. This has been indicated in simulation.

Each antenna was designed and simulated using CST Microwave Studio. They were fabricated on RO4350B material, e_r=3.36, tanδ = 0.0037, and thickness = 0.004". This very thin, low loss, low dielectric constant material was chosen because it incurred the least amount of losses, absorbing the least amount of signal. This maximized radiation efficiency.

Impedance matching was achieved with MMCX to SMA adapters at the feed, located at the bottom center of the ellipse. In simulation, the distance from the ground plane to the radiating ellipse was adjusted to achieve the closest match to 50 ohms. Better impedance matching for the bandwidth was generally achieved with closer placement of the radiating ellipse to the ground plane; however, the optimal match was achieved at approximately 0.010". In the designs presented, the radiating ellipse was placed 0.005" from the ground plane at the Unloaded SEA feed, and 0.010" from the Loaded SEA and DEA feeds. It was found that slightly increasing the ellipticity ratio (ie. ratio of y-axis value to x-axis value) enabled a better impedance match with an increase in directivity. However, once the ellipticity ratio reached 1.3-1.4, the bandwidth of the antenna deteriorated. These results were similar to that observed in [23] for the circular disc monopole. A plausible explanation for this is that as the ellipticity of the antenna increases, the antenna begins to resemble a structure closer to a narrowband monopole. The energy becomes more concentrated toward the center of the antenna, thereby attaining a higher Q resonance and hence, losing bandwidth.

The radiating ellipse of each design had an x-radius of 0.360" and a y-radius of 0.405" with a total clearance ellipse of x-radius 0.500" and y-radius 0.575". The horizontal elliptical slot load placed in the DEA and Loaded SEA had an x-radius of 0.130" and a y-radius of 0.080". This slot cutout is that pictured in the rightmost antenna of Figure 40, the leftmost antenna of Figure 41, and both positive and negative antenna terminals of Figure 42. The slot was placed .010" from the feed point in the SEA and 0.005" from the feed point in the DEA.

4.5.2 Results

The frequency effects for each of these locations are not negligible, as can be seen in Figure 43, which illustrates the VSWR plots for each of the antennas presented. The lower end theoretical frequency (VSWR ≤ 2) for a CDM of this size is 3.15 GHz. Simulations of a CDM of these dimensions were in agreement with theory (achieving a lower end frequency of 3.13 GHz). The measured lower end frequencies of the antennas presented in this paper were 3.2 GHz for the Loaded SEA, 3.15 GHz for the Unloaded SEA and 2.85 GHz for the DEA. This further solidifies the argument that the CDM equation can be used in designing the planar elliptical antennas. The DEA seems to have a slight advantage in achieving better impedance matching throughout the UWB frequency range.

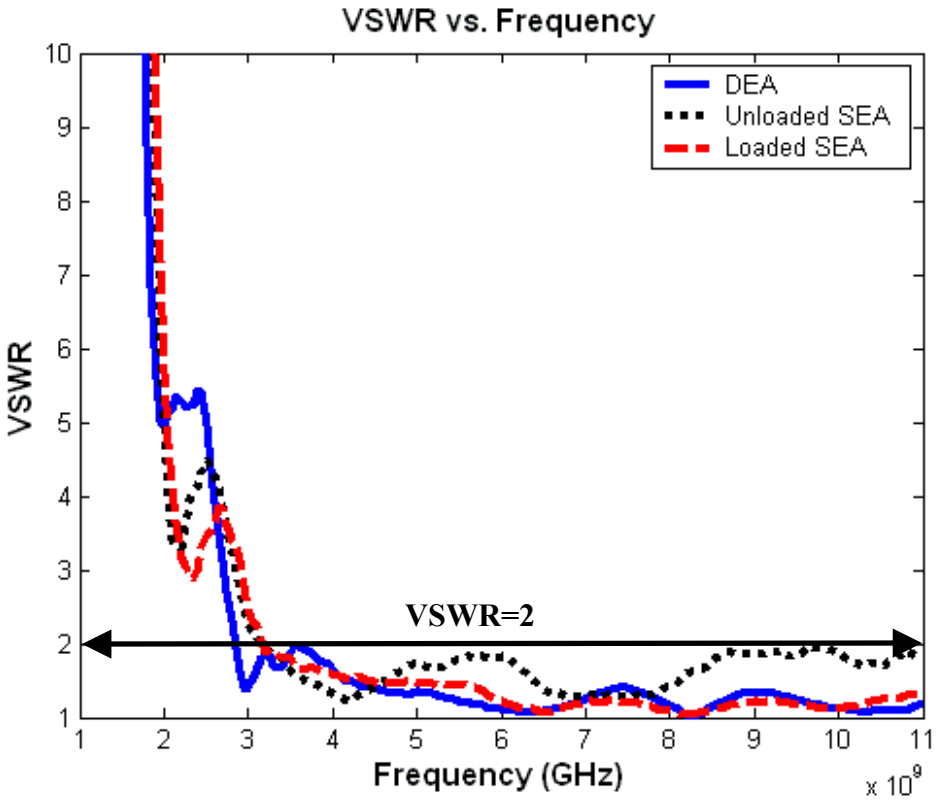

Figure 43. Measured VSWR vs. Frequency for Elliptical Monopole Antennas.

Although the Loaded SEA and DEA both incorporated elliptical cutouts near the feed, the DEA exhibited the lower fundamental operating frequency as expected, while the Loaded SEA did not. It should be noted that the distance from the feed to the horizontal elliptical cutout in the DEA was half of the distance as in the Loaded SEA, This therefore entails some discrepancy in the results. Also, the difference in frequency results should be a testament to achieving an appropriate impedance match directly at the feed. Several parasitic effects such as parasitic inductance in the solder at the feed and placement location of the MMCX adapter at the feed can alter the performance of each antenna.

Despite slight differences in the fundamental lower end operating frequency, the Loaded SEA and DEA antennas show very similar frequency characteristics throughout the rest of the UWB frequency band. The Loaded SEA and DEA achieve better matching characteristics in that from 4 GHz and higher, the VSWR achieved is less than 1.5, which corresponds to less than 4% of power loss due to reflections at the terminals, similar to the CDM. Another conclusion that can be derived about the horizontal elliptical slot load is that it improves impedance matching throughout the frequency band.

It is also important to compare the phase and group delay to that of the double ridged waveguide horn antenna in Figure 20 and Figure 21. The phase of the DEA, Loaded SEA and Unloaded SEA are shown in Figure 44. The group delay is shown in Figure 45.

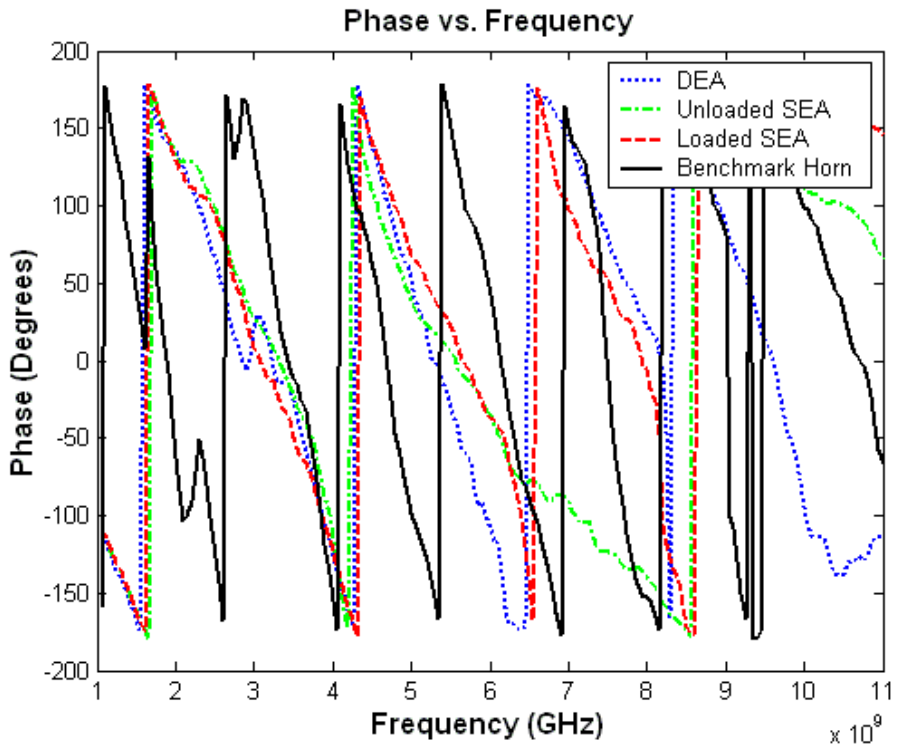

Figure 44. Measured Phase vs. Frequency for Elliptical Antennas and Benchmark Horn Antenna.

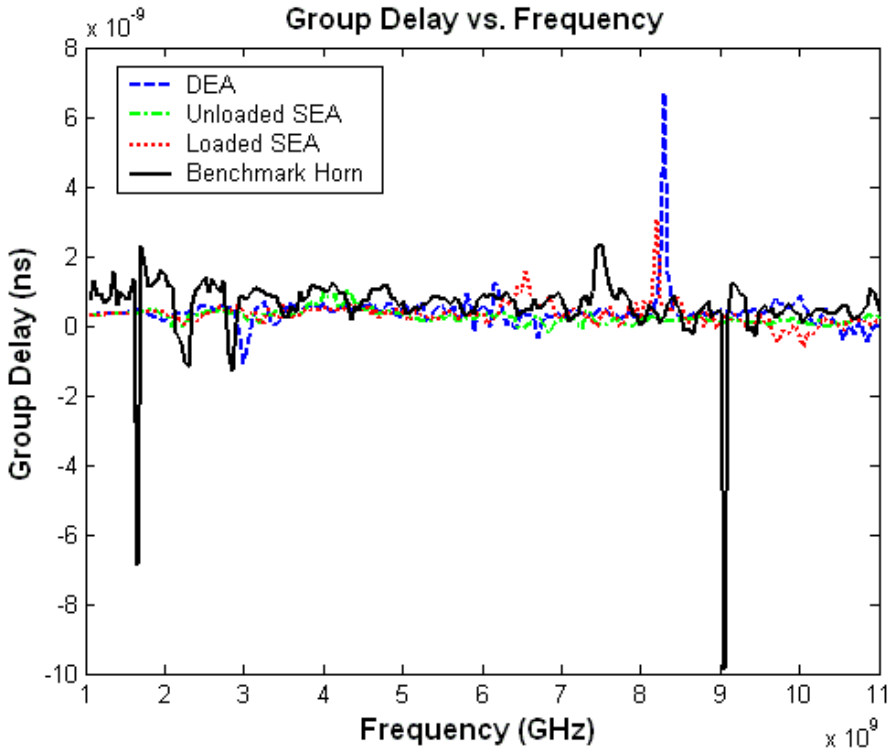

Figure 45. Measured Group Delay for Elliptical Monopole Antennas and Benchmark Horn Antenna.

The phase and group delay of the benchmark horn antenna are plotted along with the phase and group delay for the DEA, Loaded SEA and Unloaded SEA. While the phase plot indicates that while there is a general linear characteristic, it is hard to discern the quality of the elliptical antennas compared to the horn antenna. When comparing the group delay, however, the three elliptical antennas show a slightly more constant characteristic than that of the horn antenna.

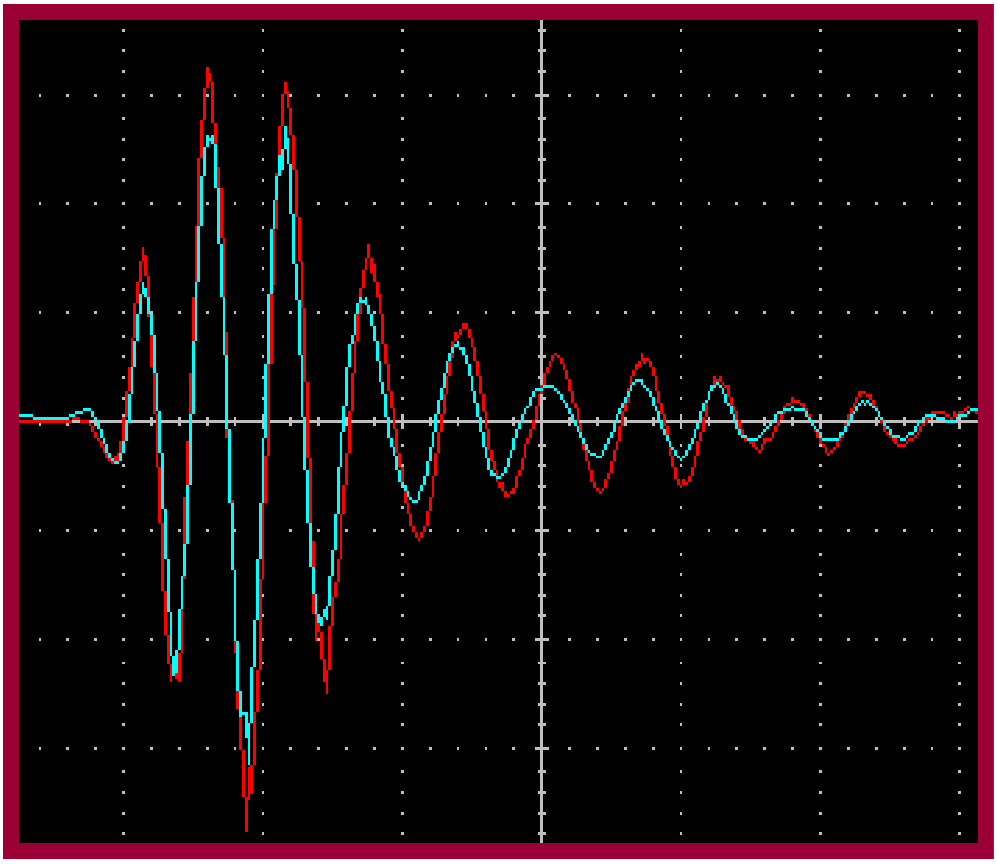

Figure 46. Received pulse (blue) over Transmit pulse (red) for Loaded SEA.

Figure 46 illustrates the transmitted pulse from the horn antenna superimposed on the received pulse for the Loaded SEA. Pulse reception measurement was similar for the Unloaded SEA and the DEA, conducted in a typical multipath lab environment with reception distance approximately 1m. Each measurement was taken on a timescale of 500 ps/div, with a voltage scale of 10 mV/div. By the theory of reciprocity, it can be inferred that each antenna transmits the same way it receives.

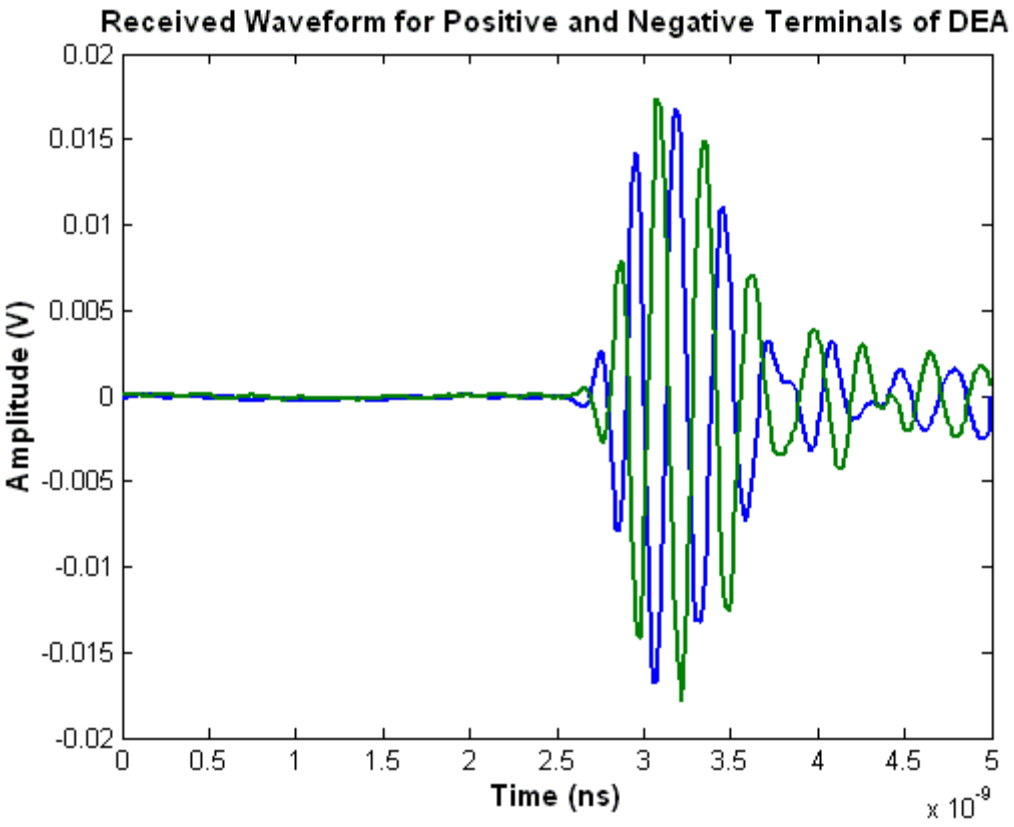

Figure 47. Pulse Measurement for DEA. Measured at Positive and Negative Terminals.

The received pulse from the loaded single ended elliptical monopole antenna (Loaded SEA) shows very little pulse distortion from transmit to receive, indicating an excellent impedance bandwidth and near constant group delay. High radiation efficiency is indicated by the low level of attenuation, and will be further analyzed when the radiation patterns from the anechoic chambers are presented. Similar results were shown for the DEA and the Unloaded SEA.

Since the receive pulse characteristics were similar for the differential elliptical antenna, the time domain measurement presented for the DEA is the simultaneous measurement of the received pulses at the positive and negative terminals. This plot is shown in Figure 47.

The time domain plot of Figure 47 exhibits the positive and negative pulses measured on separate channels simultaneously at the positive and negative terminals of the differential antenna. This qualitatively implies that if the antenna attains an adequate impedance match at each point of the differential feed, a truly complementary characteristic can be achieved in the differential antenna. While several issues must be resolved before incorporating this antenna into an RF front end design, such as parasitic inductance from bondwires, lengths of bondwires from the differential LNA to the input terminals and circuit architecture that would enable delay matching, this structure gives initial insight into the possibilities for fully differential design.

In order to better display the amount of difference in pulse shapes in terms of amplitude and phase for the positive and negative terminals, the absolute value of these pulses are plotted in Figure 48.

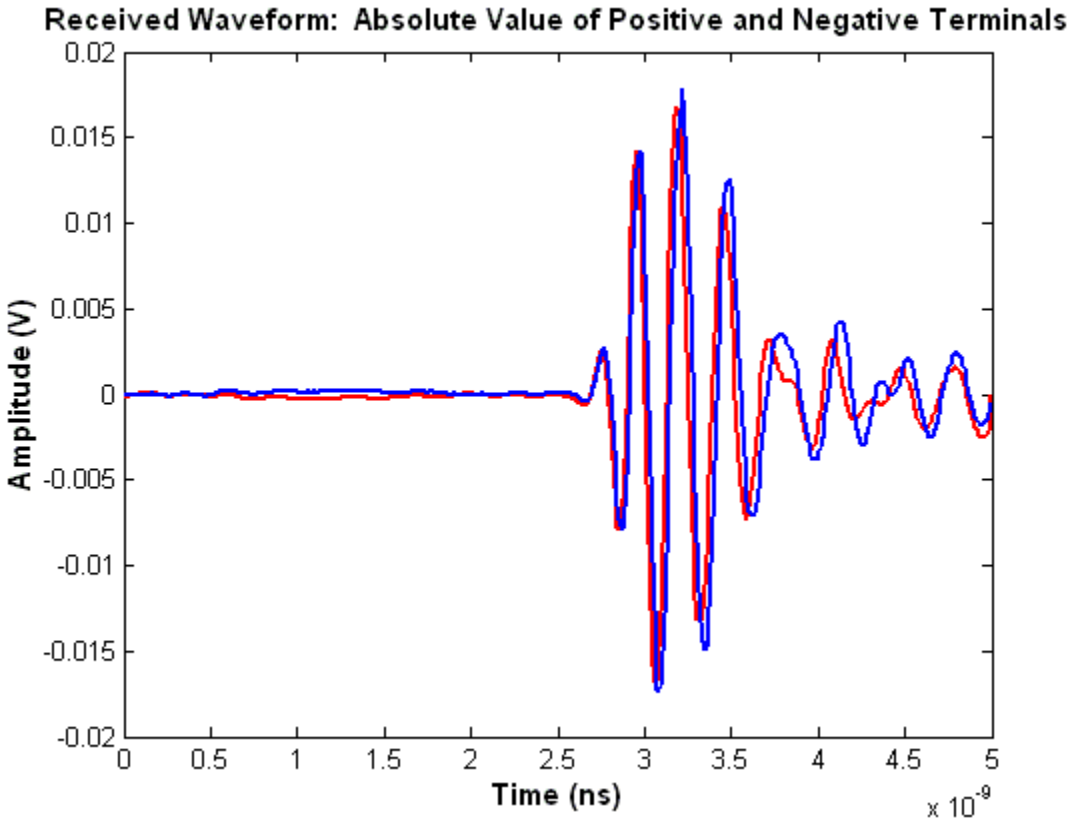

Figure 48. Absolute value of received pulse from positive and negative terminals for the DEA.

Figure 48 makes clear that there is very little difference in the received pulse amplitude from the positive to negative terminals. The worst case amplitude deviation is 2mV. There is a slight phase variation in that the negative terminal (red pulse) exhibits a worst case time offset of 50 ps. These measurements were taken at line of sight with respect to a benchmark horn transmitter. While amplitude and phase variations increase for non LOS measurements, further testing on a differential front end integrated circuit will be required to determine the feasibility of this antenna.

4.6 Anechoic Chamber Results

Some of these antennas were characterized in MIT's Lincoln Laboratory mm wavelength anechoic chamber in order to determine radiation patterns, maximum gain values, half power beamwidth and radiation efficiency. Figure 49 shows pictures of the mm wavelength anechoic chamber, courtesy of Lincoln Laboratory.

Figure 49. Photos of mm wavelength anechoic chambers. Courtesy David Bruno, Lincoln Laboratory.

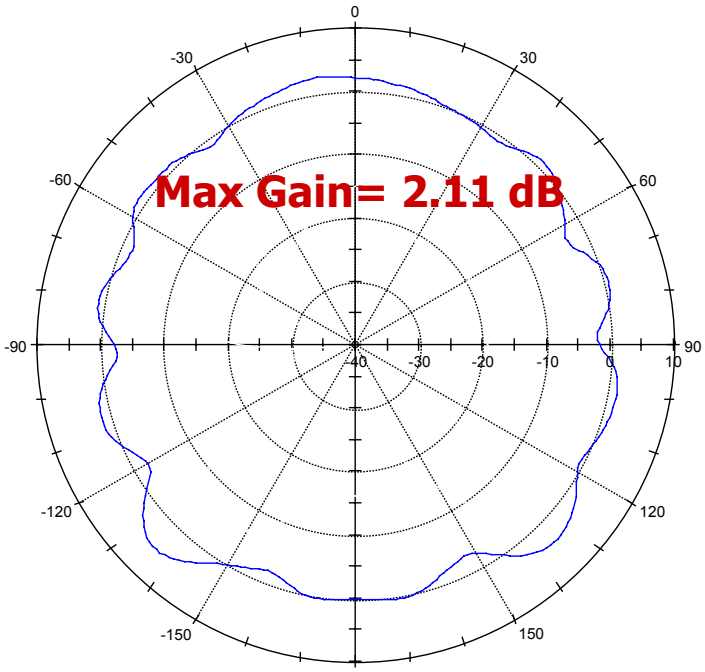

Figure 50. Azimuth Radiation Pattern for Loaded SEA at 4 GHz.

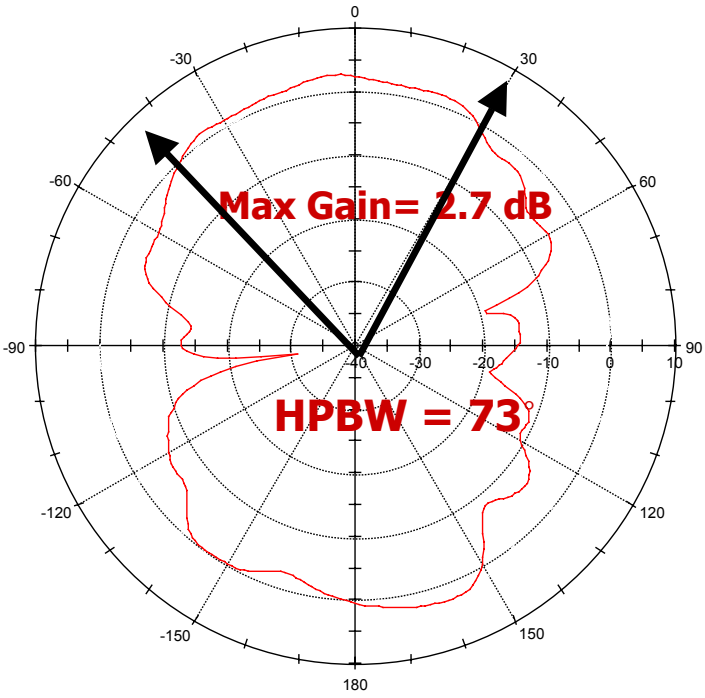

Figure 51. Elevation Radiation Pattern for Loaded SEA at 4 GHz.

Chamber measurements are made by placing the antenna under test at one end of the chamber, while placing a standard gain horn antenna at the other end of the room (the placement occurs in the window shown at the picture on the right). Two principle plane measurements, azimuth and elevation, were taken at several frequencies, including 3.5, 4, 5, 7, 9 and 10 GHz. Considering spherical coordinates, an azimuth plane measurement indicates rotation in the xy plane with the theta measurement held constant and rotating the antenna in the phi direction.

An elevation plane measurement indicates rotation through the x-y plane with the phi measurement held constant and rotating the antenna in the theta direction. These measurements are plotted on polar plots, with 0° indicating the direct LOS path. Usually, these measurements will be taken with two polarization orientations. One measurement is taken with the standard gain horn oriented such that it is vertically polarized, and another measurement is taken with the standard gain horn horizontally polarized. The orthogonal polarizations are achieved simply by rotating the standard gain horn antenna by 90°. One polarization orientation constitutes co-polarization with the antenna under test (AUT) such that received power is maximal, and the orthogonal polarization constitutes cross-polarization such that the received power is minimal. Chamber measurements were conducted on the single ended and differential elliptical monopole antennas as well as the equiangular spiral slot patch antenna.

4.6.1 Single Ended and Differential Elliptical Antennas

Anechoic chamber patterns were measured with vertical and horizontal polarization for frequencies 3.5 GHz, 4 GHz, 5 GHz, 7GHz, 9GHz and 10 GHz. and Figure 51 show azimuth and elevation plane measurements for the Loaded SEA antenna at 4 GHz to determine the half power beamwidth and gain at the lower end operating frequencies. The azimuth pattern is similar to that of a dipole, but slightly more directive. The maximum gain occurs at the front and back of the antenna, with 2.11 dB of gain at the front and 0 dB at the back. The sides exhibit a slight minimum from the maximum

points, in that they achieve gains of approximately –2 dB. This is consistent with the CST Microwave Studio simulation. The elevation pattern also indicates a similarity to that of a half wavelength dipole. Slightly more directivity is observed in the elevation plane, and nulls occur at the top and bottom of the antenna. The maximum gain is 2.7 dB, and the 3 dB points occur at 29° and –44 ° for a total HPBW (half power beamwidth) of 73° in the elevation plane.

While it is hard to visualize a three dimensional radiation pattern from two orthogonal plane patterns plotted on two dimensional polar plots, a CST Microwave Studio simulation of the 3D radiation pattern at 4 GHz is shown in
Figure 52 to better illustrate the direction of radiated power from the Loaded SEA.

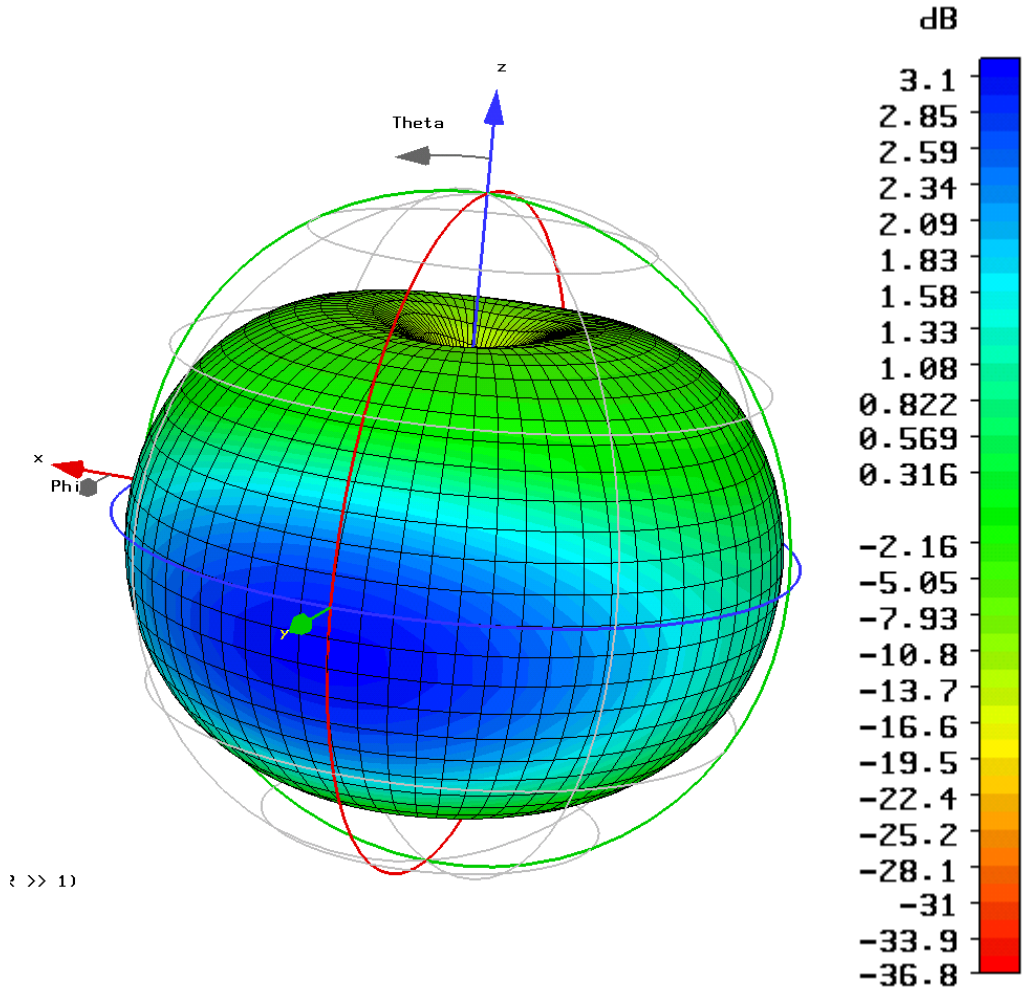

Figure 52. Simulated 3-D Radiation Pattern for the Loaded SEA. Simulated in CST Microwave Studio.

Measured results for this antenna include a half power beamwidth of 73°, indicating a near omnidirectional radiation pattern. The antenna radiation efficiency is approximately 90%, which is a great value considering most commercial antennas achieve an efficiency of 50-60%. This measurement was taken by estimating the directivity of the antenna given the HPBW [9-11]:

$$\Omega_A = \frac{32400}{\theta_1 \theta_2} \ , \ D_{\max} = \frac{4\pi}{\Omega_A} \ , \ e_{rad} = \frac{G}{D}$$

The DEA HPBW was approximately 70˚, with a max gain of 2.5 dBi, and an estimated efficiency of 93%. Several other radiation patterns have been measured for this antenna at frequencies 3.5 GHz, 4 GHz, 5 GHz, 7 GHz, 9 GHz and 10 GHz, for vertical and horizontal polarization, to gain an understanding of how the antenna operates throughout the UWB bandwidth. It was found that the radiation pattern is nearly omnidirectional for frequencies 3.5 GHz to 7 GHz, and co-polarized for vertical polarization. However, as frequencies increase to the second mode of resonance above 7 GHz, the antenna becomes more directive and exhibits a different mode of radiation. This is indicated by the radiation plots measured at 9 and 10 GHz, co-polarized in elevation for vertical polarization. The azimuth plane exhibits elements of horizontal and vertical polarization. It was found that the antenna exhibited more elements of vertical polarization than horizontal polarization, which would be expected, given that the elliptical radiator is vertically oriented.

The differential antenna was also measured for each frequency and polarization in the two principle planes. Each of these radiation patterns can be referred to in Appendix B.

4.6.2 Spiral Equiangular Slot Patch Antenna

Radiation patterns were also taken for the spiral equiangular slot patch antenna at each of the aforementioned frequencies. The plots in red indicate the elevation plane measurement, and the plots in blue indicate the azimuth plane measurements. Figure 53 shows the radiation pattern for the spiral antenna taken at 3.5 GHz. The elevation and azimuth plane measurements are shown in the same plot. This measurement was taken with the standard gain horn oriented for vertical polarization. However, since the spiral antenna achieves circular wave polarization, the vertical component is approximately equal to the horizontal component. The plots taken with vertical polarization and horizontal polarization should look similar. This is indicated in the vertical polarization radiation pattern plot that can be found in Appendix B. All of the radiation patterns for the spiral antenna can be seen in Appendix B.

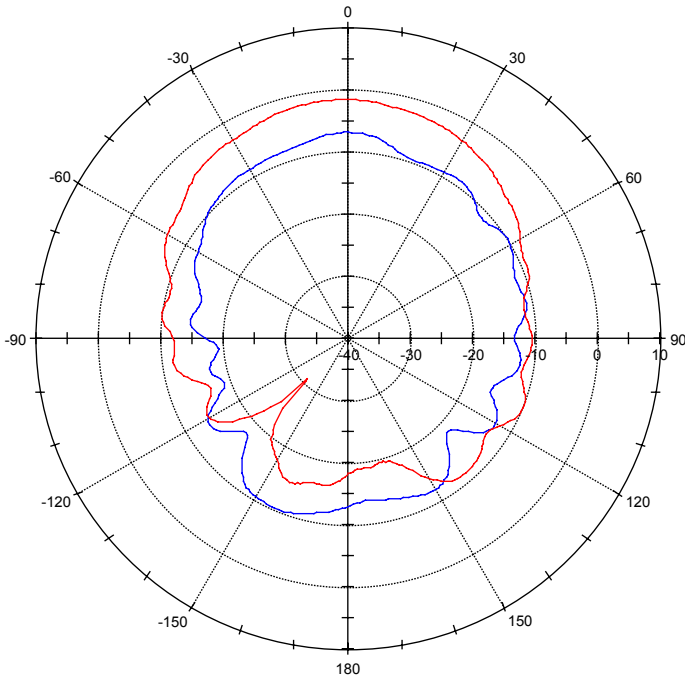

Figure 53. Radiation pattern for Spiral Equiangular Slot Patch Antenna. Azimuth measurement shown in Blue, Elevation measurement shown in Red.

Figure 53 indicates that the shape of the antenna radiation pattern is typical of what would be expected (ie. maximum radiation at zero degrees, and minimum radiation and nulls at the back). The gain is lower than 0 dBi at most points throughout the radiation pattern, indicating poor radiation efficiency. This was mentioned in 4.1, affirmed by the attenuated time domain plot and caused by the thick dielectric and RF absorbent material. The half power beamwidth measured is approximately 60°, indicating higher directivity for the spiral than that of the elliptical antennas, and an efficiency of approximately 56%.

4.6.3 Summary of Antenna Results

Several antennas were designed, simulated, fabricated and characterized, including a spiral equiangular slot patch antenna, a narrowband wire antenna for comparative purposes, diamond dipole antennas, a circular disc monopole antenna, and single ended and differential elliptical monopole antennas. Tradeoffs were considered for all of the

antenna topologies, indicating that the strongest contender for UWB integrated circuit compatibility was the tapered clearance elliptical monopole antenna design.

While the spiral equiangular slot patch antenna achieved an acceptable impedance match to 50Ω, the required tradeoff was the use of RF absorbent material in order to absorb reflections that traveled from the ends of the spiral arms back toward the feed terminals of the antenna. These reflections harmed the impedance bandwidth, which otherwise would have impaired the operation of the antenna if the RF absorber had not mitigated the problem. The use of the RF absorber attenuated the radiation efficiency for the spiral antenna. Another contributor to the attenuated radiation efficiency was the thick dielectric in between the ground plane and the spiral. While this thickness was required for sufficient impedance bandwidth operation due to ground effects, the tradeoff of the increased dielectric loading was again reduced radiation efficiency. The reduced radiation efficiency was exhibited in the gain patterns measured at Lincoln Laboratory, rendering the spiral antenna a weaker contender for use with UWB.

The narrowband monopole antenna was designed purely for comparative purposes, and to make the argument clear that a wideband antenna is necessary for limited distortion UWB pulse transmission. The VSWR bandwidth shown indicated that the antenna was sufficiently impedance matched at a few specific narrow frequency ranges throughout the UWB bandwidth, and maximally mismatched elsewhere. The received pulse measured against the transmitted pulse demonstrated that the pulse could not be discerned among the noise, clearly indicating that for optimal reception, a wideband matched antenna (such as the benchmark horn antenna used in the UWB discrete system) is necessary.

Next, the diamond dipole topology was investigated, which was initially proposed by Time Domain, Inc. for UWB applications. The diamond dipole antennas achieved a planar profile and high radiation efficiency, albeit reduced bandwidth. The intuitive observations made in comparing each diamond dipole topology were advantageous in

that clearly the best bandwidth configuration incorporated curvature, which provided for a smooth impedance transition for the current path through the antenna. This curvature limited scattering and reflections throughout the band, which enabled a better impedance bandwidth.

The conclusions made from the diamond dipole transition well into the analysis of the circular disc monopole, which is essentially a circular disc that radiates in free space over a ground plane. This, therefore, incorporates curvature and tapered clearance from the ground plane throughout the entire antenna topology. This enables a 50 ohm impedance match to be made directly at the feed. From the feedpoint, the pulse is guided along the circular antenna by the tapered clearance from the ground plane such that minimum impedance variation is achieved. Since the circular radiator has resonant modes determined by the roots of the derivative of the Bessel function, which are more closely spaced than that of a rectangular resonator, the impedance bandwidth incorporates less impedance variation throughout the bandwidth. While the CDM achieved excellent impedance bandwidth and radiation efficiency, the caveat to the design is that the profile is obtrusive and not compatible with portable electronic devices.

Keeping in mind the strengths of the CDM, this research draws clear parallels to the results of the CDM and an elliptical monopole antenna design which tapers the ground plane about the circular radiator such that it is coplanar with the antenna. The results achieved with this design exhibited very similar impedance bandwidth and time domain results to that of the CDM. In fact, the equation which governs the fundamental lower operating frequency of the CDM can actually be used in this topology as well for very accurate results. A differential version of this antenna was also designed such that it incorporated a common ground plane in between positive and negative antenna terminals. The packaging scheme is such that the integrated circuit can be housed in the common ground plane with bondwire extending from the positive and negative terminals of the antenna. The benefits to the differential design are a reduction in noise figure and ease of design complexity in the RF front end circuit, as the single ended to differential converter

will not be necessary. The tradeoffs to this differential design are that the differential feed must be carefully designed such that accurate impedance matches are made at both the positive and negative terminals of the antenna. Slight differences in the bondwire feed could result in mismatch. However, both the differential and single ended designs yielded excellent results with respect to bandwidth, efficiency, time domain pulse reception, phase and group delay when compared with the benchmark double ridged waveguide horn antenna. If the differential antenna topology is packaged carefully with the IC, matched results with regard to complementary pulses can be obtained.

Finally, radiation patterns were observed for the single ended and differential elliptical monopole antenna designs, as well as the spiral antenna design. It was confirmed that the single ended and differential elliptical antenna designs achieved a nearly omnidirectional radiation pattern, with increasing directivity for increasing frequency. The patterns at 9 and 10 GHz indicate a different resonant mode, which exhibits a different radiation pattern characteristic and increased directivity. An intuitive explanation for this phenomenon is that at these higher frequencies, the wavelengths are much smaller, and as a result, the antenna effective aperture is larger and therefore more directive. The radiation pattern shapes for the spiral antenna are as expected, with maximum radiation at the front of the antenna, achieving approximately a 60° HPBW. Nulls at the back end of the spiral antenna are due to the back ground plane.

Given all of the tradeoffs discussed for the several UWB antennas designed, the single ended and differential elliptical monopole antennas are the strongest contenders for use with UWB integrated circuits and portable electronics. Given the planar profile, high radiation efficiency, broad radiation pattern and wide impedance bandwidth, the design achieves all of the necessary UWB specifications. Future work will include further investigation of packaging considerations including bondwire simulation and ground effects, as well as frequency notching for the in-band 802.11a interferer.

The table below summarizes all simulated and measured results for the key metrics considered in UWB antenna design. Where the results specified are simulated values, they were not measured because of time constraints at Lincoln Laboratory.

ANTENNA RESULTS SUMMARY TABLE

Antenna	VSWR Bandwidth	Radiation Pattern	Max Gain (~ 4 GHz)	Efficiency	HPBW	Physical Profile
Benchmark Horn	1-18 GHz	Directive	9 dBi (4GHz)	High (commercial antenna, not specified in manual)	40 °	Large (9.6"x 11")
Spiral Equiangular Slot Patch	1.6- +20Ghz	Semi- Directive	-1 dBi (4 GHz)	~56 %	60°	Planar, thick: Radius = 1"
Narrow Monopole	140 MHz (narrow bandwidth for harmonic and fundamental frequencies)	Semi-directive. Directivity caused by ground plane, increasing directivity with frequency	7.9 dBi (3.9 GHz), 4.3 dBi (fundamental freq. 0.7 GHz) (simulated)	93% (3.9 GHz) (simulated)	25.3°, two lobes (3.9 Ghz) (simulated)	Non-planar, operates above a ground plane.
Diamond Dipole (solid curved)	4.5- 7.4 GHz	Near Omnidirectional	2.23 dBi (4 Ghz, simulated)	96% (4 GHz, simulated)	81.0 ° (4 GHz, simulated)	Planar (.65" x 1.65")
Circular Disc Monopole	1.2 – 12.5 GHz	Semi-Directive. Directivity caused by operation over ground plane.	5.7 dBi (4 GHz, simulated)	96% (4 GHz, simulated)	63.4° (4 GHz, simulated)	Non-planar, 1" radius, operation over 3" x 3" ground plane
Single Ended Elliptical Antenna (SEA)	3.1 – 17.5 GHz	Near Omnidirectional	2.7 dBi (4 GHz)	~90% (4 GHz)	73° (4 GHz)	Planar (.9" x 1.5")
Differential Elliptical Antenna	2.9 – 19.3 GHz	Near Omnidirectional	2.5 dBi (4 GHz)	~93% (4 GHz)	73° (4 GHz)	Planar (.9" x 2.5")

CHAPTER

5

CONCLUSIONS AND GUIDELINES FOR FUTURE WORK

5.1 Conclusions

In this research, a comprehensive study of UWB antennas including design, simulation, testing and characterization is presented. Fundamental considerations in narrowband antenna design were outlined, with emphasis on the extra constraints placed on antenna design by Ultra Wideband operation. Several parameters were taken into account in analyzing strengths and weaknesses in potential antenna designs including impedance bandwidth, phase, group delay, radiation pattern, directivity and gain, radiation efficiency and physical profile.

In addition, a discrete system modeled after a design by Intel Labs was implemented in order to test UWB antenna designs against a commercial benchmark antenna, qualitatively assessing the linearity of UWB pulse reception. The benchmark antenna was a double ridged waveguide horn antenna, rated from 1-18 GHz with excellent impulse transmission and reception characteristics. Measurements of group delay, phase and impedance bandwidth were taken on this antenna and compared against potential UWB antenna designs.

Several UWB antennas were designed, simulated, tested and characterized at MIT, as summarized in 4.6.3, including a spiral equiangular slot patch antenna, several variations of the diamond dipole topology, a circular disc monopole, and single ended and differential elliptical monopole antennas, which were designed by tapering a ground plane about an elliptical antenna such that it was coplanar with the antenna, enabling a

planar profile. The last designs were found to achieve very similar results to that of the circular disc monopole antenna, which has been noted for its very wide impedance bandwidth [23,24]. Taking into account the tradeoffs of each antenna topology, the single ended and differential elliptical monopole antennas faired the best, with excellent impedance bandwidth and impulse reception characteristics, high radiation efficiency, a nearly omnidirectional radiation pattern for frequencies from 3.1-8 GHz and a small, compact, planar profile. Further characterization was performed at Lincoln Laboratories, where radiation patterns were taken at 3.5, 4, 5, 7, 9 and 10 GHz for the single ended and differential elliptical monopole antennas and the spiral antenna. These radiation patterns are included in Appendix B, and are discussed in section 4.6. The radiation patterns indicated a nearly omnidirectional pattern with a half power beamwidth of 73° at 4 GHz for the single ended elliptical monopole antenna. This trend is similar throughout the UWB bandwidth except at the higher frequencies of 9 and 10 GHz, where the antenna enters a different mode of radiation and exhibits higher directivity and gain. This result was evident in simulation, as well. The radiation patterns for the spiral antenna indicated reduced radiation efficiency and increased directivity. The HPBW measured for the spiral antenna was approximately 60° at 4 GHz. The directivity tended to increase for increasing frequency, as well.

The results and discussion presented in this research should provide an intuitive perspective on fundamental requirements of antennas with regard to UWB, design of UWB antennas, and testing and characterization of a UWB antenna. The single ended and differential elliptical monopole antennas should also provide a potential solution to UWB systems requiring a low profile, planar, highly efficient UWB antenna that is compatible with UWB integrated circuits.

5.2 Future Work

Future work with regard to UWB antenna design includes packaging considerations, simulation and ground effects. Frequency notching for the 802.11a interferer band occurring at 5.15-5.35 GHz and 5.725-5.825 GHz will also be considered with regard to antenna design.

APPENDIX A

Matlab Script for Power Density Spectrum. Written by Raul Blazquez-Fernandez.

```
% 1.- Spectrum of a gaussian pulse. Generate the signal.
sigma = 0.9640e-9; % Sigma in seconds.
frame = 10e-9;     % Time between two consecutive pulses in s.
center = 5e-9;     % Center of the pulse in the frame in s.

% You need to change t_s to the right value.
t_s = 5000e-12/2000;      % Sampling time in s.
iter = 100;        % Number of bits used for the periodogram.
longitud = 512;   % Number of carriers used in the periodogram.
freq = 2e9;        % Carrier in hz.
trials = 100; % Number of trials to average the periodogram.
Psignal_aux = zeros(257,1);
template=importdata('tx_4000_500ps.txt');

for kk1 = 1:trials,
   kk1,
   bits = sign(randn(1,iter)); % A sequence of bits that we are going to transmit.
% Take into acount that the transmitted signal in a realistic condition is random... bits transmitted are random.
    outline = template*bits; % This one generates a matrix in which each column is a template (with the sign associated to a different bit)
    signal = outline(:);      % This one generates a long vector with the columns one after the other. It looks like a modulated signal.
   [Psignal,Freqs] = periodogram(signal,hamming(length(signal)),longitud,1/t_s);
    Psignal_aux = Psignal + Psignal_aux;
end
periodogram_averaged = Psignal_aux/trials;

benchmark = 10*log10(periodogram_averaged);
```

```
figure, plot(Freqs,benchmark), grid on,

first_trial = benchmark - 10*log10(Zo) + 90;
figure, plot(Freqs, first_trial)
```

APPENDIX B

See Radiation patterns for the single ended elliptical monopole antenna, differential elliptical monopole antenna and spiral equiangular slot patch antenna on the following pages.

Radiation Patterns for Single Ended Elliptical Monopole Antenna

Red = Elevation Pattern, Blue = Azimuth

Measurements 1-6: Standard Gain Horn oriented for Vertical Polarization. Co-polarized for azimuth plane measurement. Horizontally polarized for elevation plane measurement, which indicates cross-polarization.
Measurements 7-12: Std. Gain Horn oriented for Horizontal Polarization. Cross-polarized for azimuth plane measurement. Vertically polarized for elevation plane measurement, which indicates co-polarization.

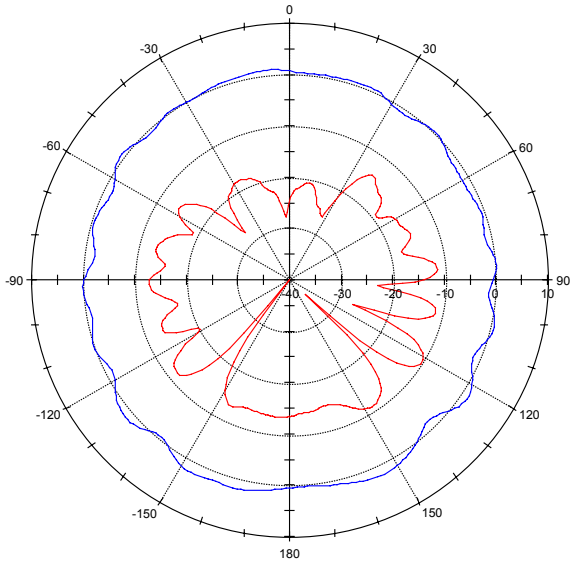

1. 3.5 GHz

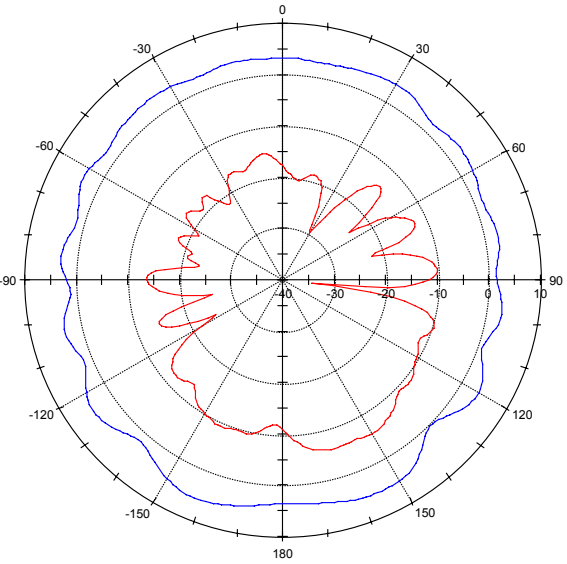

2. 4 GHz

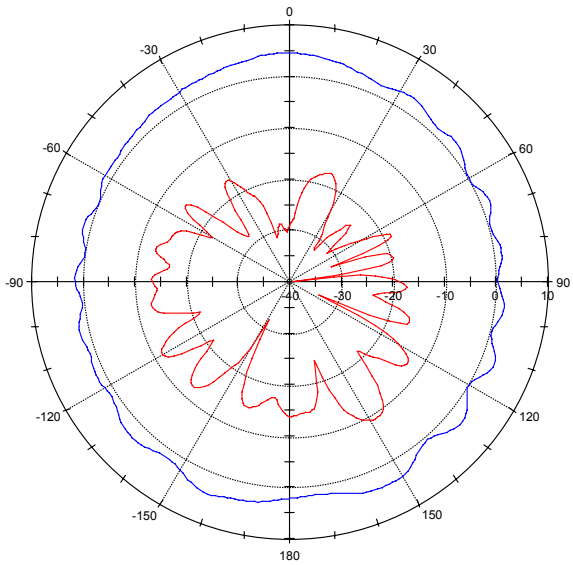

3. 5 GHz

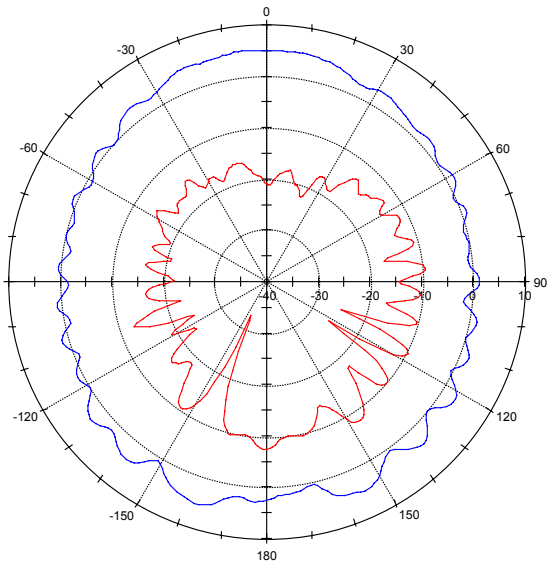

4. 7 GHz

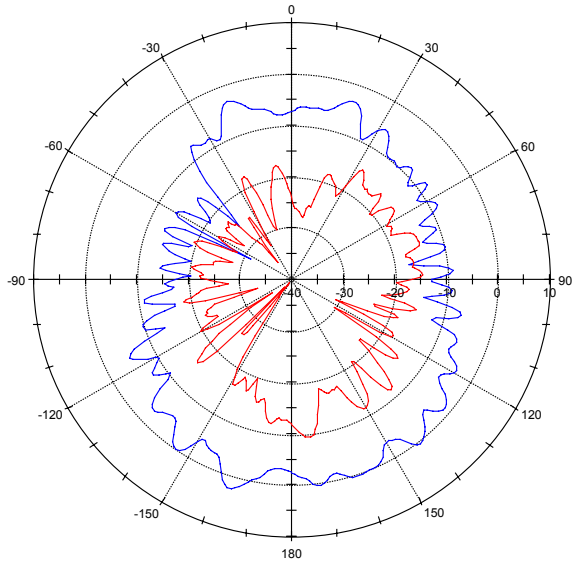

5. 9 GHz

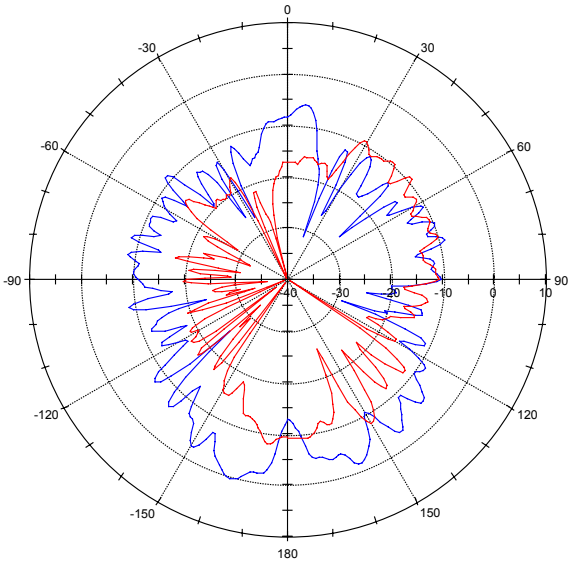

6. 10 GHz

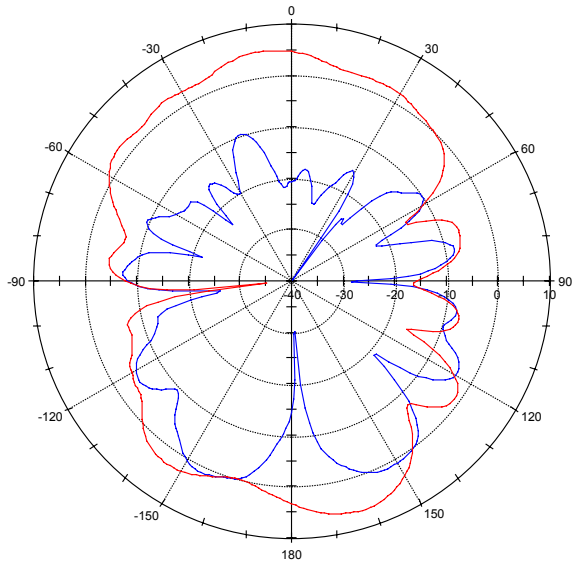

7. 3.5 GHz

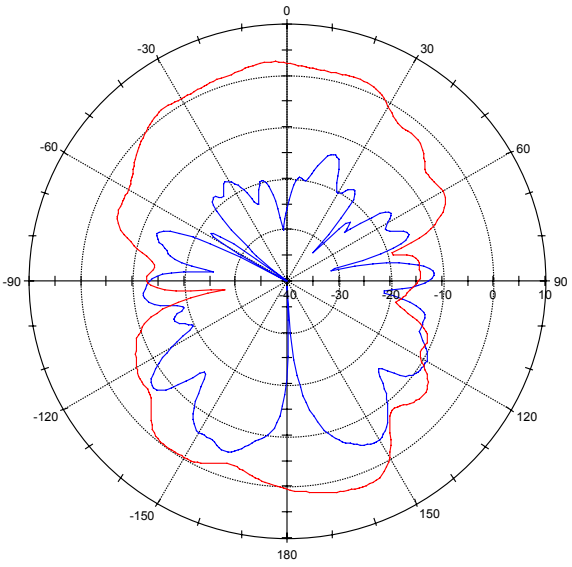

8. 4 GHz

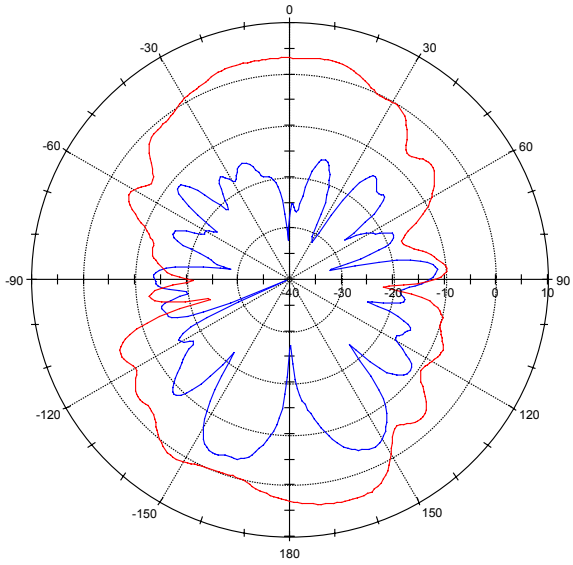

9. 5 GHz

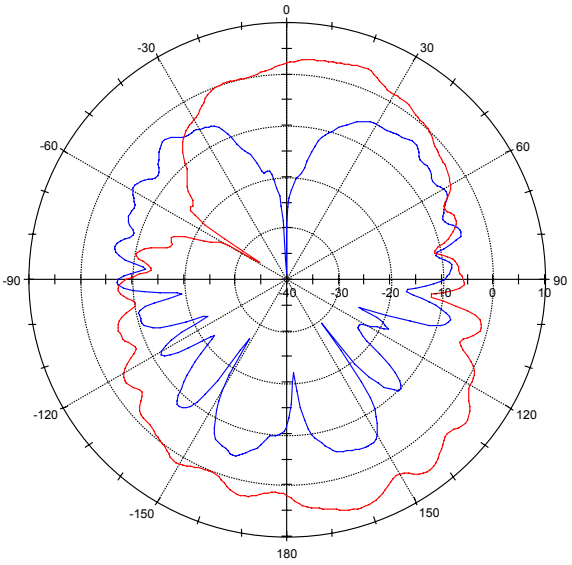

10. 7 GHz

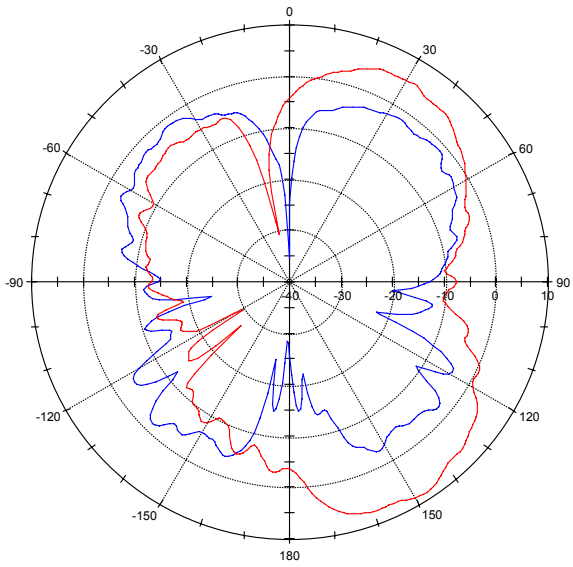

11. 9 GHz

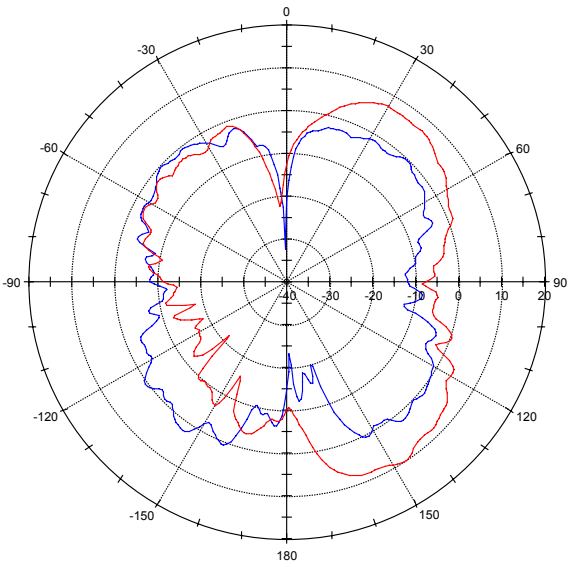

12. 10 GHz

Radiation Patterns for Differential Elliptical Antenna

Red = Elevation, Blue = Azimuth.
Measurements 1-6: Standard Gain Horn Vertical Polarization. Co-polarized for azimuth plane measurement, cross-polarized for elevation plane measurement.
Measurements 7-12: Std. Gain Horn Horizontal Polarization. Co-polarized for elevation plane measurements, cross-polarized for azimuth plane measurement.

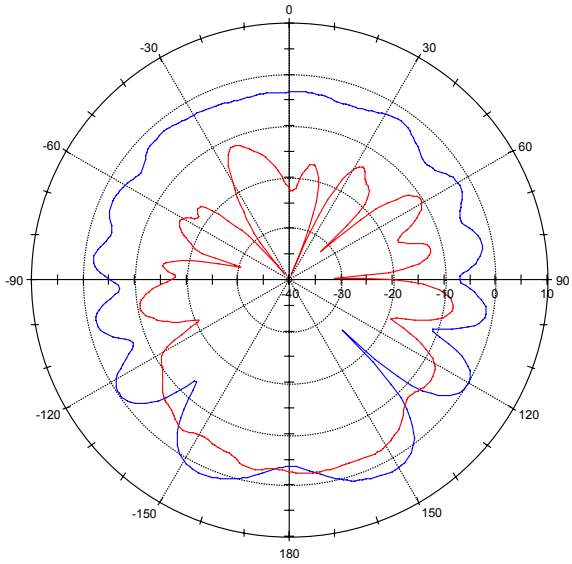

1. 3.5 GHz

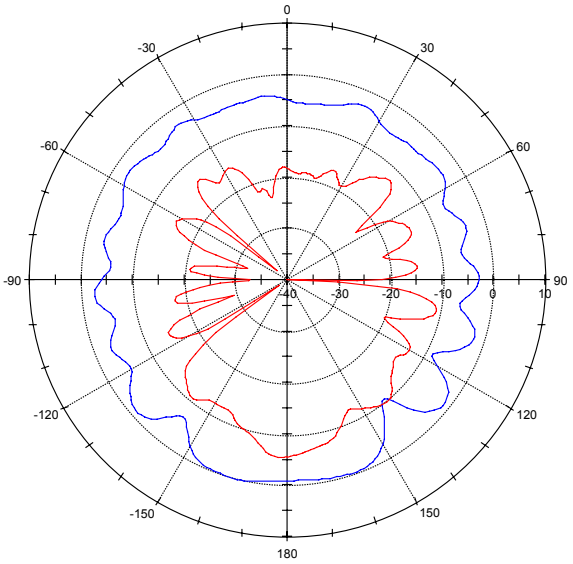

2. 4 GHz

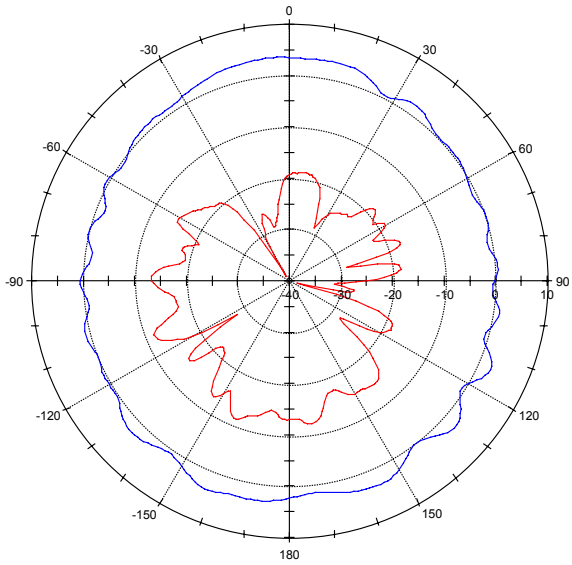

3. 5 GHz

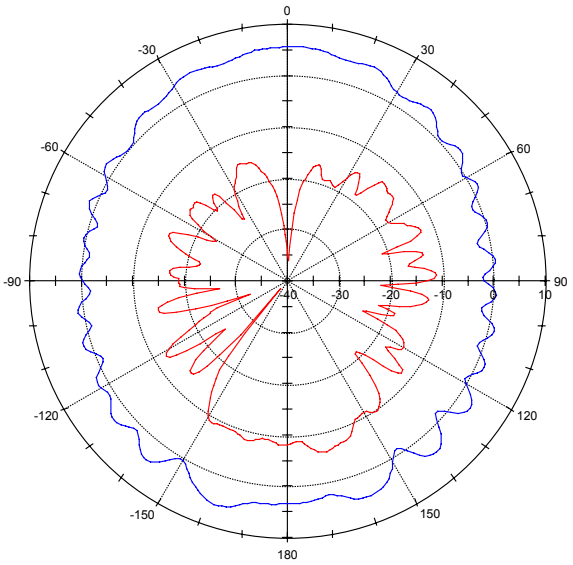

4. 7 GHz

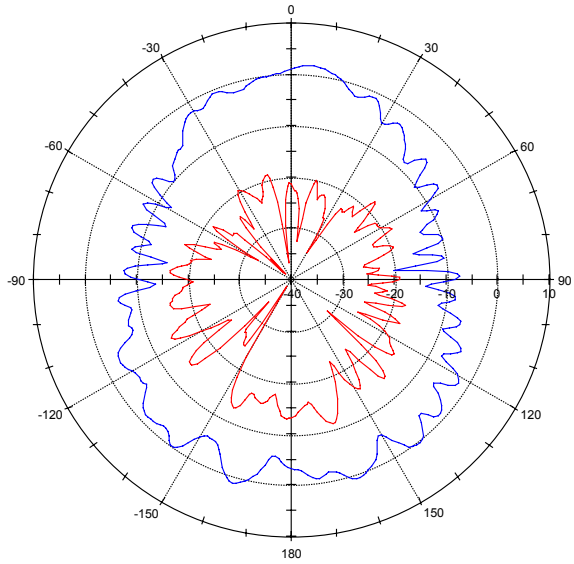

5. 9 GHz

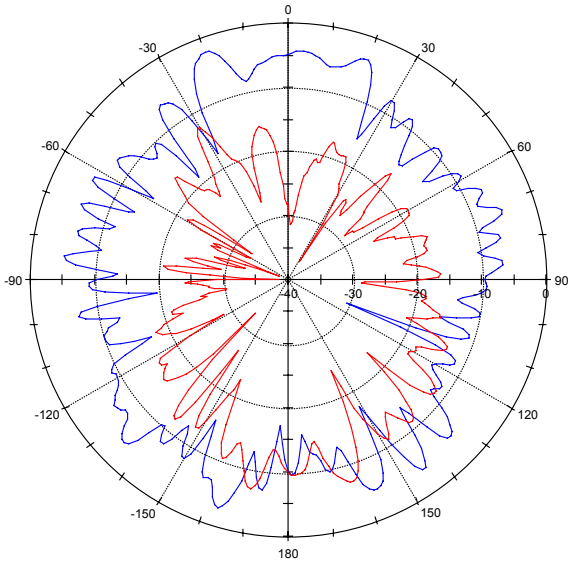

6. 10 GHz

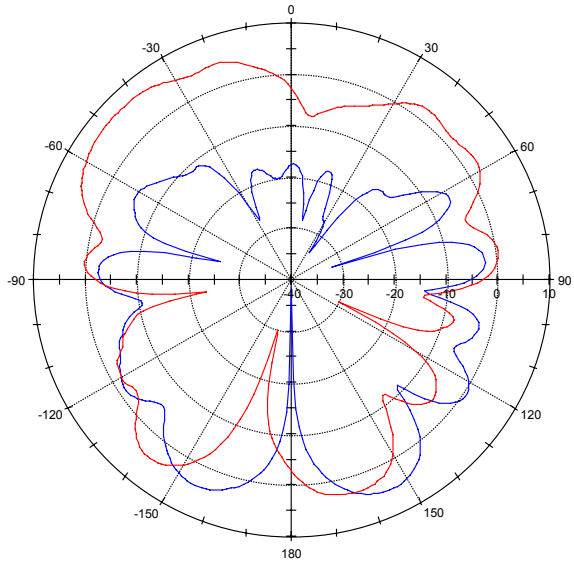

7. 3.5 GHz

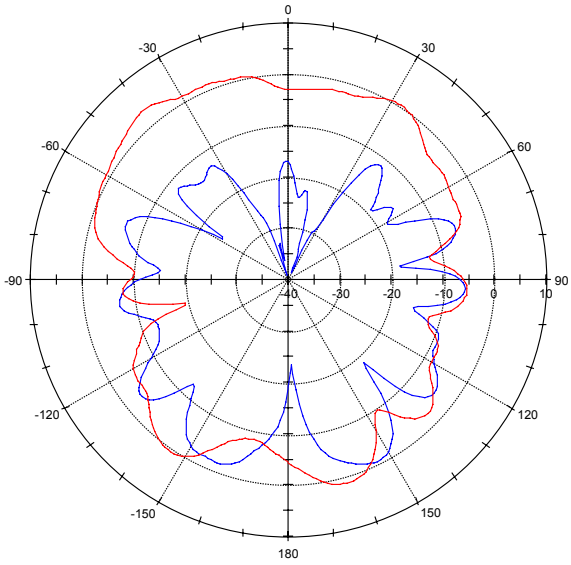

8. 4 GHz

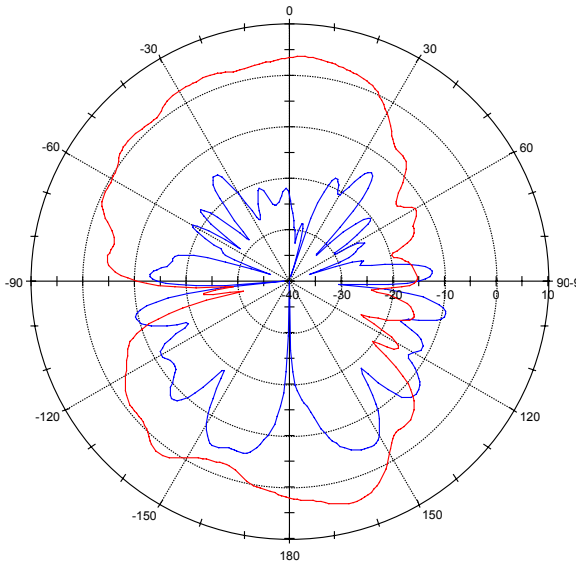

9. 5 GHz

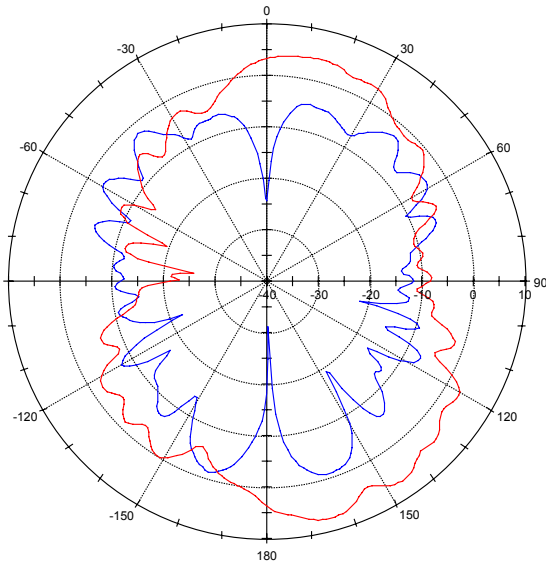

10. 7 GHz

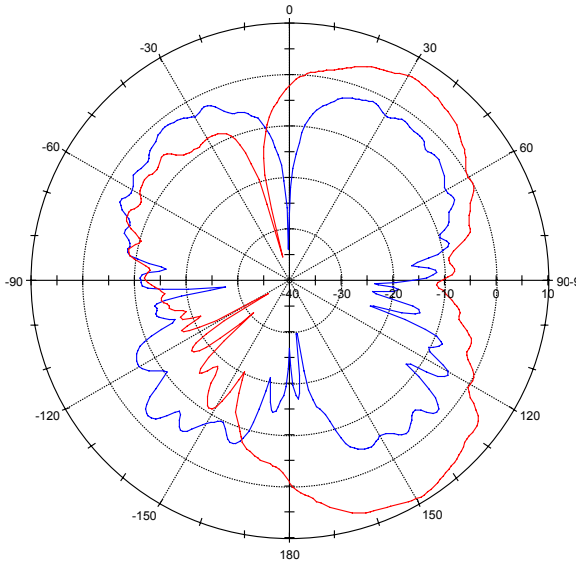

11. 9 GHz

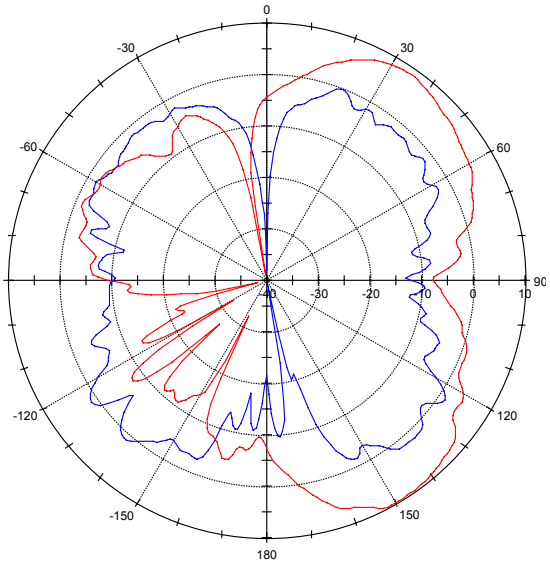

12. 10 GHz

Radiation Patterns for Spiral Equiangular Slot Patch Antenna

Red = Elevation, Blue = Azimuth.
Measurements 1-6: Standard Gain Horn Vertical Polarization.
Measurements 7-12: Std. Gain Horn Horizontal Polarization.

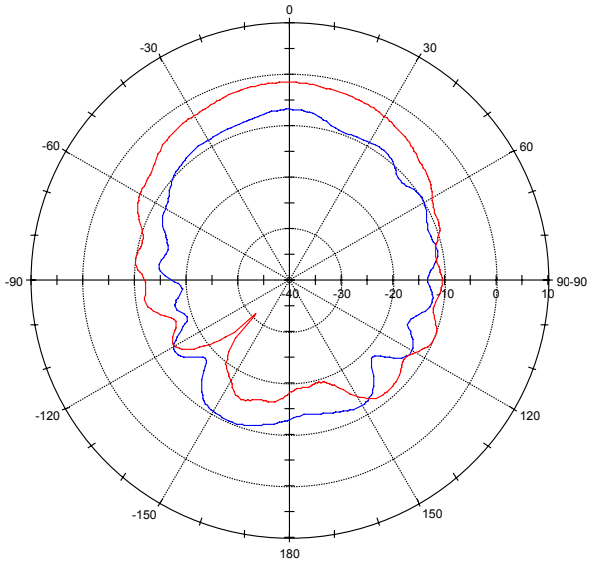

1. 3.5 GHz

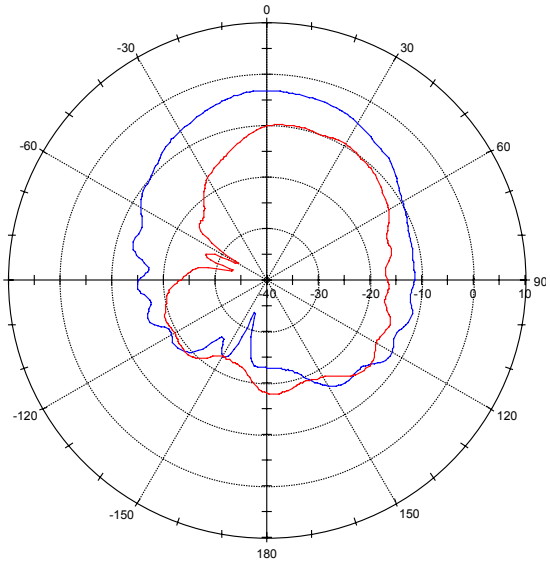

2. 4 GHz

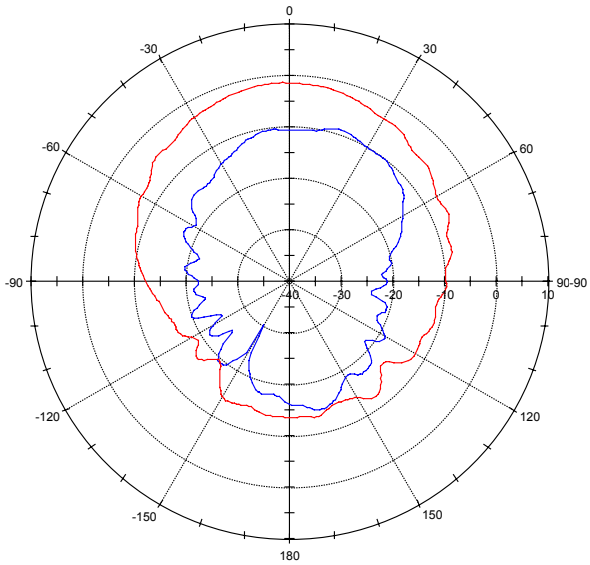

3. 5 GHz

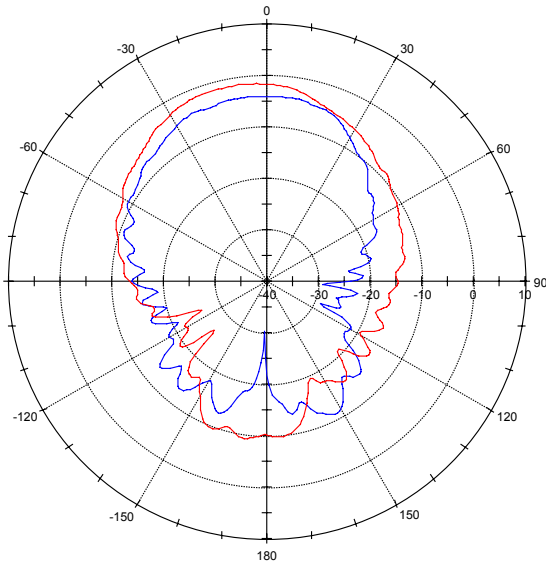

4. 7 GHz

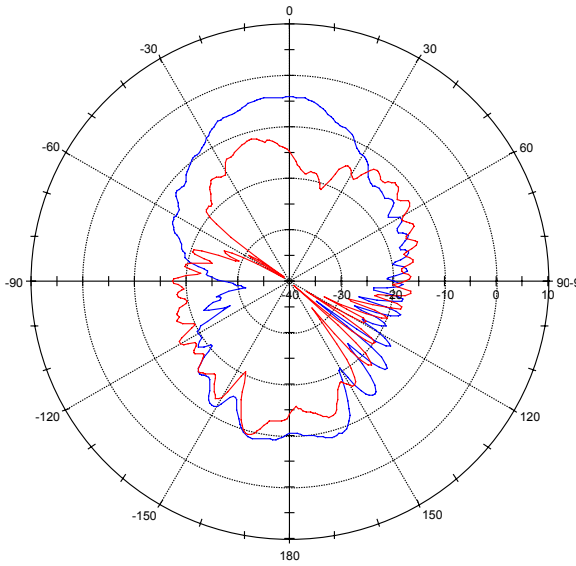

5. 9 GHz

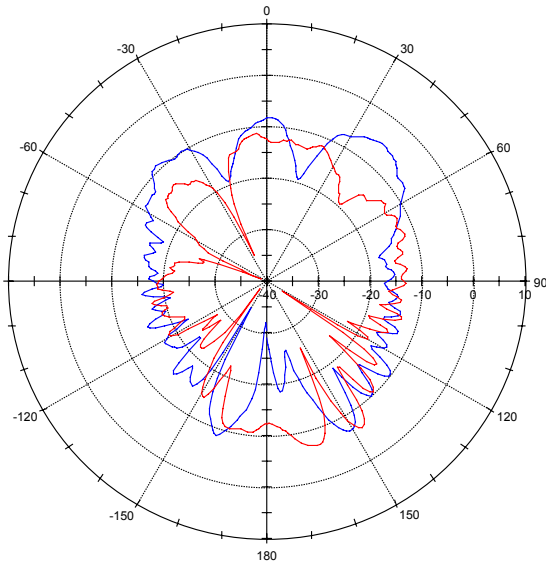

6. 10 GHz

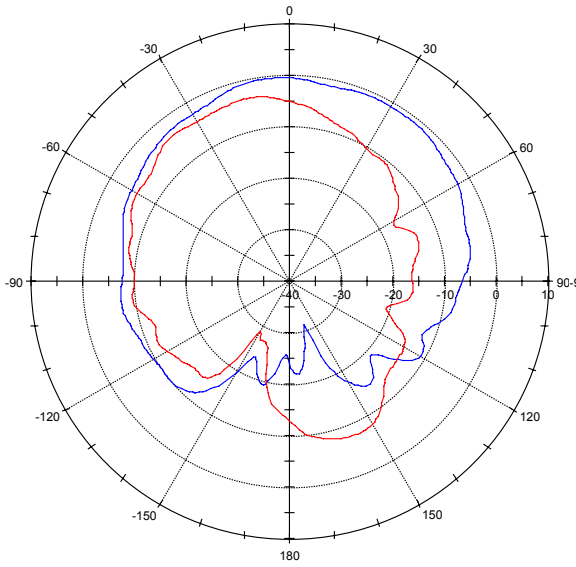

7. 3.5 GHz

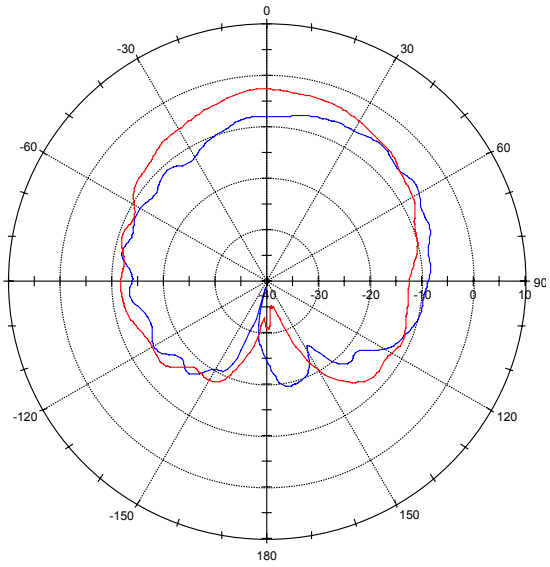

8. 4 GHz

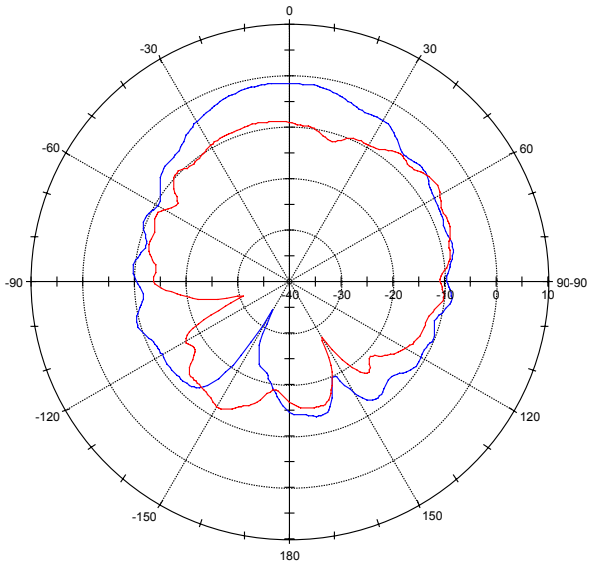

9. 5 GHz

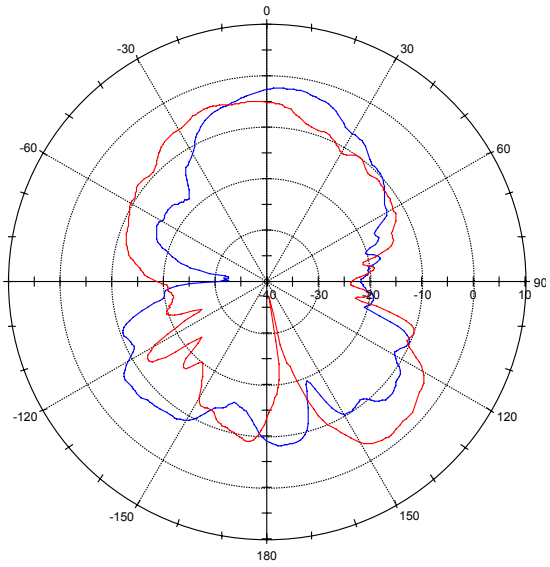

10. 7 GHz

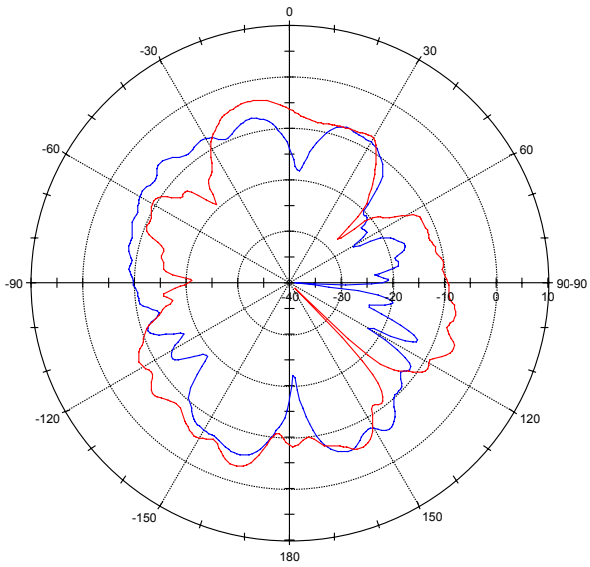

11. 9 GHz

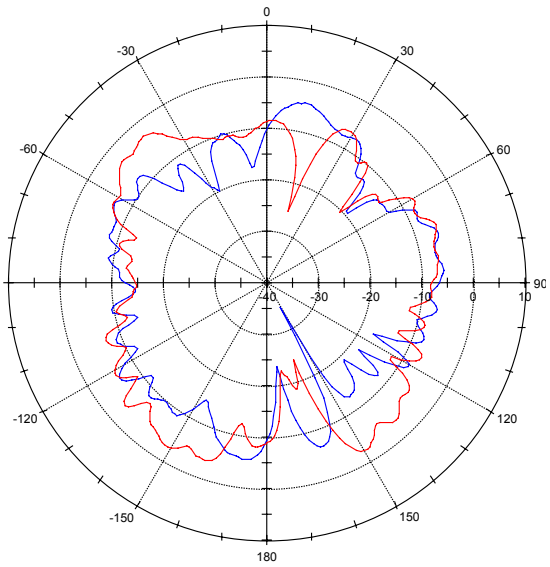

12. 10 GHz

REFERENCES

[1] First Report and Order (FCC 02-48). Action by the Commission February 14, 2002. New Public Safety Applications and Broadband internet access among uses envisioned by FCC authorization of Ultra-Wideband Technology

[2] John S. Belrose. The Sounds of a Spark Transmitter: Telegraphy and Telephony. Adventures in CyberSound.

[3] Dr. Robert J. Fontana. A Brief History of UWB Communications. Multispectrum Solutions, Inc.

[4] V. H. Rumsey, "Frequency Independent Antennas," 1957 IRE National Convention Record, pt. 1, pp. 114-118.

[5] J.D. Dyson, "The Unidirectional Equiangular Spiral Antenna," *IRE Trans. Antennas Propagat.,* Vol. AP-7, pp. 329-334, October 1959.

[6] Ross, G.F., 1968, A time domain criterion for the design of wideband radiating elements, IEEE Trans. Antennas Propagat., Vol. 16, No. 3, p. 355.

[7] Dr. Tarance W. Barrett. History of Ultra Wideband (UWB) Radar & Communications: Pioneers and Innovators

[8] *IEEE Transactions on Antennas and Propagation,* Vols. AP-17, No. 3, May 1969; Vol. AP-22, No. 1, January 1974; and Vol. AP-31, No. 6, Part II, November 1983.

[9] C.A. Balanis, *Antenna Theory and Analysis,* 2nd ed., Wiley, New York, 1997.

[10] Stutzman, *Antenna Theory and Design,* 2nd ed., Wiley, New York, 1998.

[11] D. M. Pozar, *Microwave and RF Design of Wireless System,* Wiley, New York, 2001.

[12] Hans Gregory Schantz, Larry Fullerton, "The Diamond Dipole: A Gaussian Impulse Antenna", *IEEE Antennas and Propagation Society International Symposium,* Boston, MA, July 2001.

[13] G. Pochanin, "Large Current Radiator for the Short Electromagnetic Pulses Radiation," Ultra-Wideband, Short-Pulse Electromagnetics 4, New York: Kluwer Academic/Plenum Publishers, 1999), pp. 149-155.

[14] J. A. Kong, *Electromagnetic Wave Theory,* EMW Publishing, Cambridge, 2000.

[15] Green, Evan R., Manny, Ben. "Ultra Wideband: A Disruptive RF Technology," *Intel Developer Conference,* February 28, 2002.

[16] K. Siwiak, "Ultra Wide Band Signal Simulations Using FDTD Method", The Third IEEE Workshop on Wireless Local Area Networks, September 15, 2001

[17] Paulino, N, "Design of a Spiral-Mode Microstrip Antenna and Matching Circuitry for Ultra-Wide-Band Receivers," *IEEE International Symposium on Circuits and Systems,* vol. 3, 2002.

[18] Liu, Bosui, A.M. Ferendeci, "Broadband Spiral Antennas with Thin Dielectric Substrates", *IEEE Radio and Wireless Conference, 2002 (RAWCON 2002),* August 2002.

[19] Asfar, M.N., Wang, Yong, Hanvi, D., "A New Wideband Cavity-Backed Spiral Antenna", IEEE *Antennas and Propagation Society International Symposium,* Vol. 4, July 2001

[20] Thaysen, J., Jakobsen, K.B., Appel-Hansen, J., "Characterization and Optimization of a Coplanar Waveguide Fed Logarithmic Spiral Antenna", *IEEE Antennas and Propagation for Wireless Communications Conference,* November 2000.

[21] K. Kunz and R.J. Luebbers, *The Finite Difference Time Domain Method for Electromagnetics*, CRC Press Inc., 1993

[22] J. Want, V. Tripp, "Design of Multioctave Spiral-Mode Microstrip Antennas", *IEEE Transactions on Antennas and Propagation,* Vol. 39, No. 3, March 1991.

[23] G. Kumar, K.P. Ray, *Broadband Microstrip Antennas*, Artech House, Inc., Boston, 2003.

[24] Agrawall N. P. ,Kumar G.,Ray. K.P., "Wideband planar monopole antennas", IEEE Transactions on Antennas and Propagation, vol. AP-46(2),pp.294-295 ,1998.

[25] P. J. Gibson, "The Vivaldi Aerial," in Proc. 9th Eur. Microwave Conf., Brighton, U.K., Sept. 1979, pp. 101-105.